UNIVERSITY OF CALIFORNIA SAN DIEGO

Electrochemical glucose biosensors for non-invasive glucose monitoring

A dissertation submitted in partial satisfaction of the requirements for the degree

Doctor of Philosophy

in

Nanoengineering

by

Ernesto De La Paz Andres

Committee in charge:

Professor Joseph Wang, Chair
Professor Jinhye Bae
Professor Gert Cauwenberghs
Professor Tse Nga Ng
Professor Sheng Xu

2022

The dissertation of Ernesto De La Paz Andres is approved, and it is acceptable in quality and form for publication on microfilm and electronically.

University of California San Diego

2022

DEDICATION

This dissertation is dedicated to my family, friends, and co-workers.

TABLE OF CONTENTS

LIST OF FIGURES

ACKNOWLEDGMENTS

I would like to acknowledge Professor Joseph Wang for his constant support as faculty advisor and the chair of my comiteee. Through the valuable guidance and suggestions he provided along my Ph.D. I would also like to acknowledge my coworkers for their friendship, help and support.

Chapter 2, in full, is a reprint of the material as it appears in G. Bolat, E. De la Paz, N. F. Azeredo, M. Kartolo, J. Kim, A. N. de Loyola e Silva, R. Rueda, C. Brown, L. Angnes, J. Wang, J. R. Sempionatto, Wearable soft electrochemical microfluidic device integrated with iontophoresis for sweat biosensing. *Analytical and Bioanalytical Chemistry*. **414**, 5411–5421 (2022).

Chapter 3, in full, is a reprint of the material as it appears in E. De la Paz, A. Barfidokht, S. Rios, C. Brown, E. Chao, J. Wang, Extended Noninvasive Glucose Monitoring in the Interstitial Fluid Using an Epidermal Biosensing Patch. *Analytical Chemistry*. **93**, 12767–12775 (2021). The dissertation author was the primary author of this paper.

Chapter 4, in full, is a reprint of the material as it appears in J. R. Sempionatto, M. Lin, L. Yin, E. De la paz, K. Pei, T. Sonsa-ard, A. N. de Loyola Silva, A. A. Khorshed, F. Zhang, N. Tostado, S. Xu, J. Wang, An epidermal patch for the simultaneous monitoring of haemodynamic and metabolic biomarkers. *Nature Biomedical Engineering*. **5**, 737–748 (2021).

VITA

2016 Bachelor of science, Tijuana Institute of Technology

2019 Master of Science, University of California San Diego

2022 Doctor of Philosophy, University of California San Diego

SELECTED PUBLICATIONS

1. G. Bolat, E. De la Paz, N. F. Azeredo, M. Kartolo, J. Kim, A. N. de Loyola e Silva, R. Rueda, C. Brown, L. Angnes, J. Wang, J. R. Sempionatto, Wearable soft electrochemical microfluidic device integrated with iontophoresis for sweat biosensing. *Analytical and Bioanalytical Chemistry*. **414**, 5411–5421 (2022).

2. E. De la Paz, A. Barfidokht, S. Rios, C. Brown, E. Chao, J. Wang, Extended Noninvasive Glucose Monitoring in the Interstitial Fluid Using an Epidermal Biosensing Patch. *Analytical Chemistry*. **93**, 12767–12775 (2021).

3. J. R. Sempionatto, M. Lin, L. Yin, E. De la paz, K. Pei, T. Sonsa-ard, A. N. de Loyola Silva, A. A. Khorshed, F. Zhang, N. Tostado, S. Xu, J. Wang, An epidermal patch for the simultaneous monitoring of haemodynamic and metabolic biomarkers. *Nature Biomedical Engineering*. **5**, 737–748 (2021).

ABSTRACT OF THE DISSERTATION

Electrochemical glucose biosensors for non-invasive glucose monitoring

By

Ernesto De La Paz Andres

Doctor of Philosophy in Nanoengineering

University of California San Diego, 2022

Professor Joseph Wang, Chair

With the continuous growth in the field of glucose monitoring devices, non-invasive glucose monitoring devices integrating electrochemical glucose biosensors represent an attractive alternative to replace the gold standard self-monitoring of blood glucose or minimally invasive procedures. The first approach rely upon repetitive finger pricking to collect blood samples to quantify glucose levels, leading to discomfort from patients that require blood analysis, while minimally invasive procedures make use of skin penetrating approaches to collect glucose from an alternative biofluid. Non-invasive devices offer the unique capability of quantifying glucose levels without the need of penetrating the skin tissue to collect the sample.

In this dissertation, the non-invasive monitoring of glucose will be demonstrated in three different wearable sensing platforms using iontophoresis as a non-invasive biofluid collection

method coupled with electrochemical glucose sensing. The first platform delivered sweat-stimulating agents through the skin of volunteers using iontophoresis to enable sweat secretion. Sweat samples were then collected by a microfluidic platform that integrated a glucose biosensor. In the second platform, an adhesive patch that coupled an iontophoretic system and a glucose biosensor enabled glucose monitoring from the interstitial fluid for up to 8 and 4 hrs on healthy individuals and diabetic subjects respectively. In the last platform, the capability of performing glucose monitoring alongside multiple biomarkers of interest such as blood pressure, lactate, caffeine, and alcohol was demonstrated through different daily activities that involved exercise, food, and alcohol intake. Before human evaluation, each sensing modality was tested in terms of its sensing capability, stability, and selectivity toward the specific analyte of interest. During on-body operation, the results obtained from each sensing modality were validated by using commercial gold standard devices. Further data analysis implies the potential application of such devices as the next generation non-invasive platforms toward point-of-care operation.

Chapter 1. Introduction

1.1 Wearable non-invasive glucose monitoring devices

The concept of wearable technologies is not only oriented to the fabrication of smartwatches but also to any class of device capable to be incorporated into the human anatomy. Researchers all over the world have been trying incorporate in such technologies the capability of quantifying key metabolites and electrolytes responsible for some of the chronic diseases present in the human body. For instance, the assessment of glucose levels on individuals could enable a better control in glucose levels on patients with diabetes. By definition, diabetes is a disease caused by irregular levels of blood glucose in the body due to a deficiency of insulin production or use by the body. During glucose regulation after food intake, insulin is realsed to induce glucose uptake by the cells, muscles and also to store glucose through a process known as glycogenesis[1,2].

However, in some scenarios, the insulin production is not enough leaving still high blood glucose values in the blood which leads to diabetes type 1, which is caused by the low release of insulin. Whenever insulin is still produced by is not used properly (which means there is resistance made by the insulin) this is better know as diabetes type 2. Between diabetes type 1 and 2, type 2 is more commonly present with approximatelt 85% of the total population of people with diabetes[3,4].

One of the most well-known technologies used for glucose monitoring is the biosensor. By definition, a biosensor is composed of a bioreceptor that can be a protein, enzyme, amino acid, or cells, which the analyte of interest (e.g., glucose) has specificity to. The interaction between receptor and analyte is translated to a transducer as an electrochemical, optical, or physical signal. This signal is taken and amplified and displayed in a monitor as a current, intensity, and other factors[5].

Given that the amount of glucose is the analyte that we desire to measure. This can be done in the different types of biofluids present in the human body (e.g., blood, sweat, interstitial fluid, tears, saliva, and urine). The quantification of glucose in different biofluids has been demonstrated in platforms consisting of wearable patches[6], microneedles[7], mouthguards[8], microfluidics[9] and cathethers[10]. Despite their potential application as continoue glucose monitoring platforms, some of these technologies rely on invasive procedures that require penetrating the skin to access the biofluid of interest.

In this dissertation, the fabrication of non-invasive wearable platforms for the quantification of glucose levels will be highlighted in three different chapters. In the first chapter, the monitoring of glucose will be assessed through the fabrication of a soft, wearable microfluidc platform that performs develiry of a FDA approved molecule to induce sweat perspiration through iontophoresis. The sweat generated through this chemical stimulation will relocate inside the microfluidic device, where a glucose sensor enabled the sensing of glucose levels before and after food consumptions.

In the second chapter, the extended performance of a adhesive patch containing a glucose sensor and a reverse iontophoresis system for interstitial fluid collection will be discussed. The platform was evaluated in healthy individuals for a period of 8 hrs. In addition, the device was tested in a clinical trial, where type 1 and type 2 diabetic patients worn the device.

In the last chapter, the integration of multiple sensing modalities alongside glucose sensing in to a flexible patch will be discussed. Lactate, caffeine, alcohol and blood pressure sensors were included to the wearable patch. The influence of regular activities performed on a daily basis (e.g., food intake, caffeine intake, excersice and alcohol intake) and their effect on blood pressure will be discussed.

1.2 References

1. U. Alam, O. Asghar, S. Azmi, R. A. Malik, General aspects of diabetes mellitus. *Diabetes and the Nervous System*. **126**, 211–222 (2014).

2. P. V. Röder, B. Wu, Y. Liu, W. Han, Pancreatic regulation of glucose homeostasis. *Experimental & Molecular Medicine*. **48**, 1–19 (2016).

3. A. Salsali, M. Nathan, A Review of Types 1 and 2 Diabetes Mellitus and Their Treatment with Insulin. *American Journal of Therapeutics*. **13**, 349–361 (2006).

4. N. G. Forouhi, N. J. Wareham, Epidemiology of diabetes. *Medicine*. **38**, 602–606 (2010).

5. N. Bhalla, P. Jolly, N. Formisano, P. Estrela, Introduction to biosensors. *Essays In Biochemistry*. **60**, 1–8 (2016).

6. A. J. Bandodkar, W. Jia, C. Yardımcı, X. Wang, J. Ramirez, J. Wang, Tattoo-Based Noninvasive Glucose Monitoring: A Proof-of-Concept Study. *Analytical Chemistry*. **87**, 394–398 (2014).

7. F. Tehrani, H. Teymourian, B. Wuerstle, J. Kavner, R. Patel, A. Furmidge, R. Aghavali, H. Hosseini-Toudeshki, C. Brown, F. Zhang, K. Mahato, Z. Li, A. Barfidokht, L. Yin, P. Warren, N. Huang, Z. Patel, P. P. Mercier, J. Wang, An integrated wearable microneedle array for the continuous monitoring of multiple biomarkers in interstitial fluid. *Nature Biomedical Engineering*, 1–11 (2022).

8. T. Arakawa, K. Tomoto, H. Nitta, K. Toma, S. Takeuchi, T. Sekita, S. Minakuchi, K. Mitsubayashi, A Wearable Cellulose Acetate-Coated Mouthguard Biosensor for In Vivo Salivary Glucose Measurement. *Analytical Chemistry*. **92**, 12201–12207 (2020).

9. A. Martín, J. Kim, J. F. Kurniawan, J. R. Sempionatto, J. R. Moreto, G. Tang, A. S. Campbell, A. Shin, M. Y. Lee, X. Liu, J. Wang, Epidermal Microfluidic Electrochemical Detection System: Enhanced Sweat Sampling and Metabolite Detection. *ACS Sensors*. **2**, 1860–1868 (2017).

10. B. Nacht, C. Larndorfer, S. Sax, S. M. Borisov, M. Hajnsek, F. Sinner, E. J. W. List-Kratochvil, I. Klimant, Integrated catheter system for continuous glucose measurement and simultaneous insulin infusion. *Biosensors and Bioelectronics*. **64**, 102–110 (2015).

Chapter 2. Wearable soft electrochemical microfluidic device integrated with iontophoresis for sweat biosensing

2.1 Introduction

Wearable systems for monitoring health status in real-time are strongly desirable[1-6]. Recent innovative technologies have been developed to meet this goal generating considerable progress in the field of non-invasive wearable platforms based on sweat analysis as a diagnostic tool[1,3,7]. Efforts made on the fabrication of soft epidermal microfluidic devices for sweat collection had greatly improved sweat sensing performance[8–12]. Conformal elastomeric polydimethylsiloxane (PDMS)-based microfluidic devices hold major advantages for wearable applications due to their skin-mimicking features (soft, flexible, skin compatible etc.), being largely used for collection and analysis of sweat[13–16]. Most sweat analyses performed by this microfluidic technology rely either on the convenient battery-free colorimetric, sensing[1,1317–21], or in the combination of this system with electrochemical sensors[16,22]. The recent combination of wearable microfluidic devices with electrochemical biosensors has brought new capabilities to epidermal sweat monitoring, such as the efficient biofluid replenishment over the sensor that prevents mixing of old and new sweat, providing reliable, continuous, and real-time detection of analytes[16,20,22–24].

Although the introduction of electrochemical sensors in wearable microfluidic systems represents a major advance for sweat analysis, most of the epidermal sweat microfluidic platforms rely on extensive exercising for sweat generation[10,22,24–27]. Recently in one study, a hydrogel-based sensor pad was reported for continuous passive extraction of sweat and designed for in-situ potentiometric sensing of Cl^- ions in sweat. The touchpad fully integrated sensor was capable of extracting sweat non-invasively without requiring any external activities to induce perspiration[28]. Moreover an alternative fluidic system was developed to collect latent sweat in the fingertip overcoming the need of exercising[29]. Sweat from fingertips has shown to be very promising for monitoring biomarkers and harvesting energy[30–36]; however, further research is needed to develop a reliable wearable fingertip sensing platform. Currently, stimulated sweat is the most appropriate approach for sweat analysis in resting state. For this, FDA approved (US Food and Drug Administration) drug delivery protocols based on iontophoresis (IP) mechanism is largely used[23,37–39].

Analysis of extracted sweat induced by an iontophoretic drug-delivery system offers significant advantages in non-invasive monitoring, such as short sampling time, enough sample volume, controlled sweat flow, and decreased motion artifact when compared with measurements during exercising[5,12,38,40]. The use of iontophoretic delivery of cholinergic agonist drugs for stimulated sweat in combination with fluidic platform has been previously demonstrated by using a two-step system where sweat is first stimulated followed by the transfer of the fluidic device to the stimulated site for further collection and quantification[41–43], and by using absorbent/wicking materials for passive sweat collection on the iontophoretically stimulated area[23,40]. To the best of our knowledge, exercise-free drug induced perspiration analysis based on electrochemical soft epidermal microfluidic systems with specifically designed iontophoretic electrodes incorporating simultaneous sweat induction, collection and detection capabilities has never been addressed[9,10,44].

Herein, we propose and demonstrate, for the first time, the fabrication of a wearable single step platform for simultaneous sweat stimulation and detection by combining merits of iontophoresis, microfluidics, and electrochemical quantification. This was realized using a skin conformal silicone rubber polydimethylsiloxane (PDMS) integrated with soft lithography- and screen-printed based sensors. Sweat was directly stimulated in the microfluidic inlet and transported toward the sensor surface by the PDMS inlet channels. The iontophoretic gel was physically separated from the sweat collection area by placing the IP electrode around a PDMS cylindrical inlet "pillar" (**Figure 2.1.1B**). The pressure of the stimulated sweat was enough to pump it vertically through the inlet toward the PDMS channel without any dilution in the iontophoretic gel. Glucose was chosen as a proof-of-concept model target analyte for the iontophoretic-fluidic application. High blood glucose levels are taken as an indicator of diabetes type 1 or 2; therefore, their continuous monitoring is essential to control such levels in the body[40,45,46]. Glucose readings were taken before and after food consumption, the resulting sweat glucose values were validated against a commercial finger stick glucometer, presenting a good correlation for all tested subjects as demonstrated in previous publications[32,47]. This approach opens new opportunities for sweat monitoring beyond the fields of sports and into the healthcare and wellness areas.

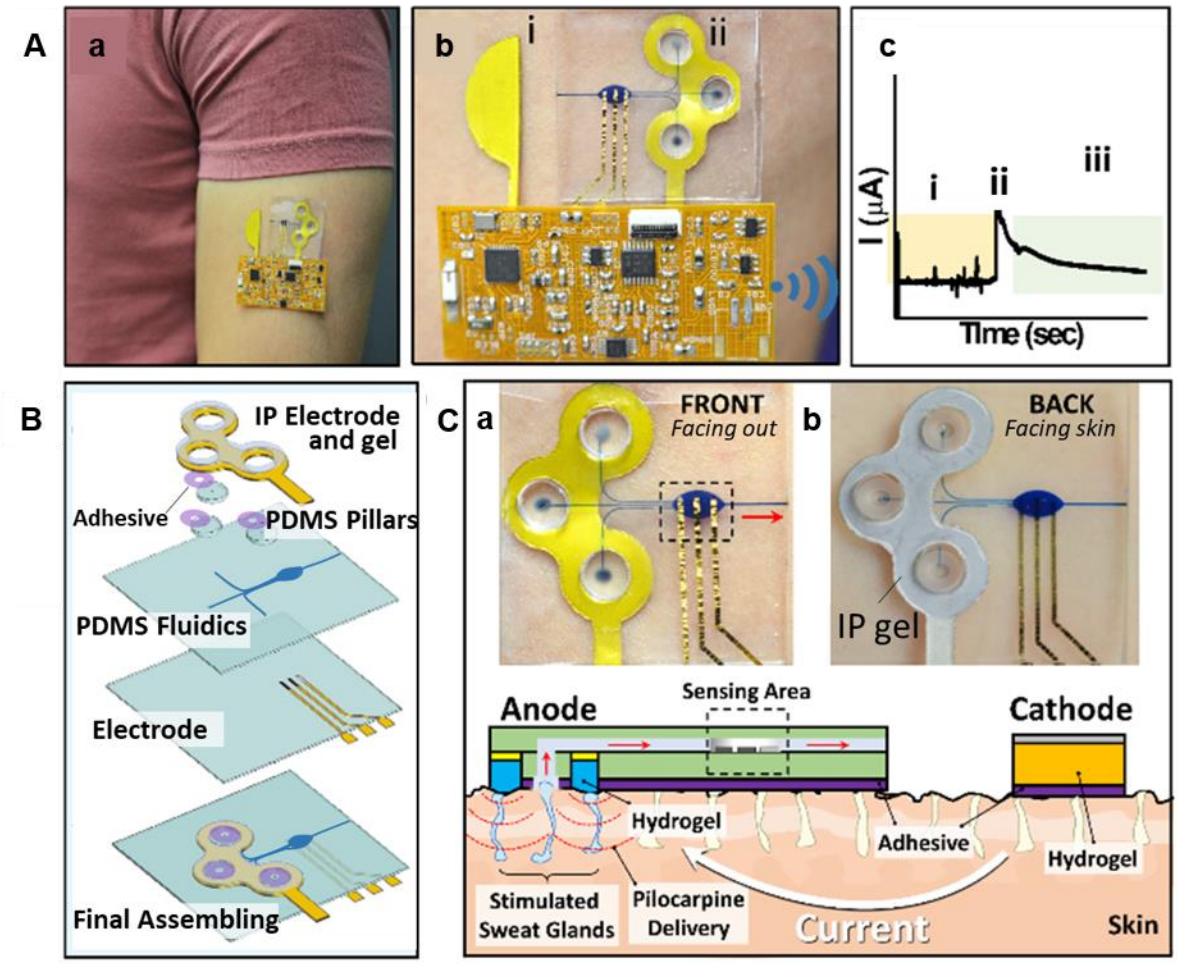

Figure 2.1.1 Concept of the non-invasive microfluidic device.
A) Depiction of fluidic device with electrochemical sensor placed on the volunteer's arm. (b) IP fluidics system with electronic board capable of performing IP and wireless signal transmission **(i)** Cathode and **(ii)** anode. **(c)** Typical response of the IP fluidic device**: (i)** Initially zero current is measured during IP time due the absence of sweat**. (ii)** Sweat starts contacting the detector. **(iii)** Electrochemical response of the biosensor in the presence of sweat glucose. **B)** Schematic showing device's layers from top-down: Screen Printed Ag/AgCl IP electrode covered with iontophoretic gel, PDMS pillars for sweat collection and double-sided adhesive tape. PDMS with microfluidic features and final assembling showing the side which will be facing the skin. **C)** Iontophoresis schematics showing anode and cathode compartments for pilocarpine delivery and sweat generation. Agarose gel loaded with pilocarpine is drop casted on top of the IP electrode. After a current stimulation, pilocarpine is delivered by an iontophoretic current. Sweat is generated and collected in the inlet area in the PDMS micropillars, the collected sweat flows through the channels and is detected in the reservoir area. **(a)** Front view of the device showing flow direction, sensing area, back of the IP electrode (yellow) and back of the gold sputtered electrode. **(b)** Back view of the device showing screen-printed silver IP electrode with the golden sputtered electrode

2.2 Experimental

2.2.1 Chemicals and Instrumentation

Glucose oxidase (GOx) from Aspergillus Niger, Type X-S (EC 1.1.3.4), chitosan, bovine serum albumin (BSA), glutaraldehyde, potassium nitrate, potassium phosphate monobasic (KH_2PO_4), potassium phosphate dibasic (K_2HPO_4), ethanol, pilocarpine nitrate, D(+)-glucose, agarose type IV, poly(vinyl alcohol) (PVA, average molecular weight = 70 000–100 000), and acetic acid were obtained from Sigma Aldrich (St. Louis, MO). Poly(methyl methacrylate) (PMMA 950 A2, MicroChem, USA), Polydimethylsiloxane (PDMS) silicone (Dow Corning, Sylgard 184), polyimide (PI-2545, HD Microsystems, USA), 3 M Double Coated Medical Tape (#1522) (Maplewood, MN) were used for the microfluidic fabrication step. All reagents were used without further purification, deionized water was employed in all the solutions prepared. Conductive Prussian blue (PB) carbon ink (E3449) and silver/silver chloride ink (E2414) were obtained from Ercon Inc. (Wareham, MA). The electrochemical experiments were performed at room temperature using PGSTAT 101 from Metrohm Autolab (The Netherlands) type III PGSTAT302N (Metrohm) operated by NOVA software v 1.11.2) and a CH Instruments electrochemical analyzer (model 1232A, Austin, TX).

2.2.2 Device fabrication

The microfluidic silicon mold was fabricated according to previous work[22]; briefly, a silicon wafer was etched to generate a master with 100-μm-tall patterns. Next, a silicone layer of 500 μm (Dow Corning, Sylgard 184) was spin-casted onto the Si master yielding the PDMS fluidic layer. Subsequently, the pillar inlets, with 1 mm height, were transferred to the PDMS layer.

2.2.3 Fabrication and Chemical Modification of the Soft Electrochemical Biosensors

The soft electrodes were fabricated according to a previous publication[22]. Briefly, a 70 nm layer of PMMA was spin-casted onto a 4″ Si wafer to serve as a sacrificial layer. Subsequently, polyimide (PI-2545, HD Microsystems, USA) was spin casted to yield a 1.6μm film on the PMMA layer, followed by soft baking at 110 and 150 °C on a contact hot plate to remove volatile solvents, and then cured at 250 °C in a vacuum oven for 4h. Layers of Cr (550 nm) and Au (200 nm) were deposited by sputter coating (Denton Vacuum LLC, Discovery 635) and photolithography was used to pattern the sensors.

A second layer of the same polyimide thickness was placed on the sensor's interconnect and Reactive Ion Etching (Plasmalab Oxford P80) was used to etch the polyimide and define the layout of the array, exposing only the bonding pads and the sensors. The PMMA layer was then undercut with boiling acetone to enable the removal of the pattern from the Si wafer using a water-soluble PVA tape (3 M Company, Maplewood, MN). The exposed back surface of the electrode was then mounted on glass slides for deposition of Ti (6 nm)/SiO_2 (60 nm) by sputter coating (Denton Vacuum LLC, Discovery 635). A PDMS layer of 500 μm (Dow Corning, Sylgard 184) was spin casted onto a PMMA treated glass slide. The devices were then transferred onto the PDMS through formation of covalent bonds by condensation reactions between ozone (UVO) treated silicone and SiO_2 on the back side of the devices (**Figure 2.2.3.1**). The tape was dissolved with DI water. The devices were then ready for screen printing.

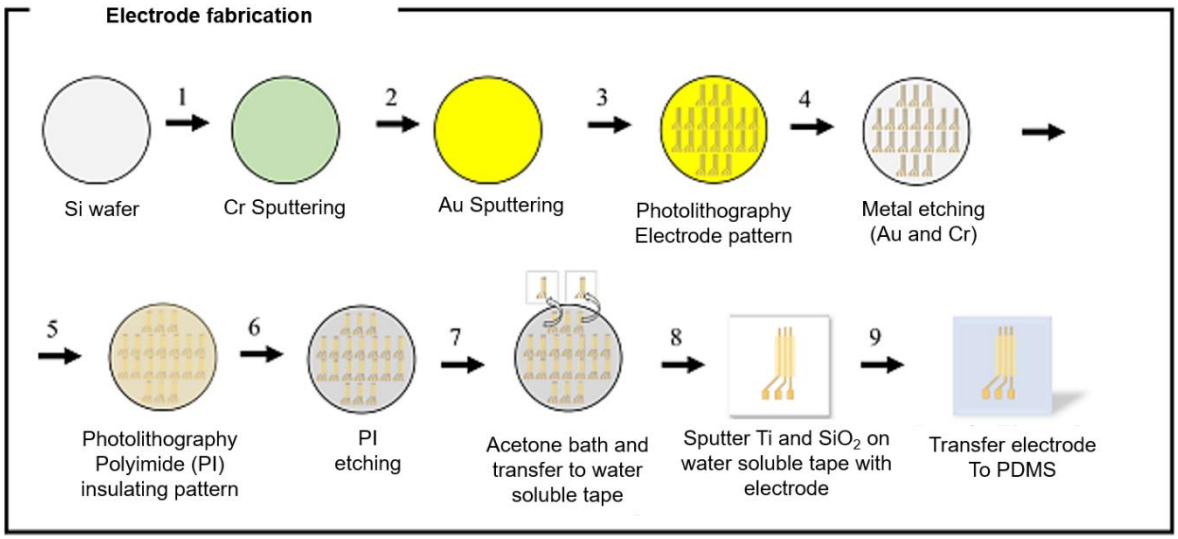

Figure 2.2.3.1 Fabrication steps for soft gold electrodes on PDMS.
A layer of PMMA was spin-casted onto a 4″ Si wafer to serve as a sacrificial layer. Subsequently, polyimide was spin casted on the PMMA film. Layers of Cr and Au were deposited by sputter coating, and photolithography was used to pattern the sensors and interconnect. A second layer of polyimide was placed on the sensor/interconnect and reactive ion etching was used to etch the polyimide and define the mesh layout of the array, exposing only the bonding pads and the sensors. The PMMA layer was then undercut with boiling acetone to enable the removal of the mesh from the Si wafer using a water-soluble PVA tape. The exposed back surface of the mesh was then mounted on glass slides for deposition of Ti (6 nm)/SiO2 by sputter coating. A PDMS layer was spin casted onto a PMMA glass slide. The devices were then transferred onto the PDMS through formation of covalent bonds by condensation reactions between ozone (UVO) treated silicone and SiO2 on the back side of the devices. The tape was then dissolved with DI water. The devices were then ready for screen printing.

The electrochemical sensors were patterned by screen-printing over the microfabricated gold collectors with two separate layers using Ag/AgCl ink as the reference electrode and Prussian blue conductive carbon ink as working and counter electrodes by operating an MPM-SPM semi-automatic screen printer (Speedline Technologies, Franklin, MA). The printed patterns were cured at 80 °C for 10 min in a convection oven. Following the printing process, the PB-carbon working electrode transducer was functionalized with the glucose recognition layer. Briefly, a glucose oxidase solution (40 mg/mL) was mixed with a chitosan solution (0.5 wt% in 0.1-M acetic acid) in a 1:1 v/v ratio. Subsequently, 1.0 μL of this solution was casted on the working electrode. Next, a 0.5-μL droplet of glutaraldehyde (5% in water) was applied on the modified surface. Finally, the enzyme modified glucose biosensor was dried at 4 °C overnight.

2.2.4 Fabrication of Flexible PDMS Microfluidic Channels and Multilayers

The microfluidic silicon mold was fabricated according to previous work[22]. Shortly, a 50 nm layer of Cr was deposited (Temescal BJD 1800) on a 4" silicon wafer to act as an etch mask. Next, photolithography was used to pattern the microfluidic channels and the unmasked portions were etched by Deep Reactive Ion Etching (Plasmalab Oxford P100), yielding 100 μm tall patterns. Depth measurements were performed using a Dektak 150 surface profiler (Veeco, Plainview, NY). Then, a 70 nm layer of poly(methyl methacrylate) (PMMA 950 A2, MicroChem, USA) was spin-casted onto the Si master, followed by soft baking at 180 °C. A silicone layer of 500 μm (Dow Corning, Sylgard 184) was then spin-casted onto the Si master to yield the final microfluidic pattern **(Figure 2.2.4.1**). Subsequently, for the pillar inlets, a flat PDMS (10:1) layer, of 1 mm height, was fabricated on a PMMA treated glass slide. A circular puncher of 5 mm diameter was used to produce a cylindrical pillar with 5 mm diameter and 1 mm heigh. The pillars were aligned and attached to the inlets of the microfluidic features, by casting a thin PDMS layer and curing at 120^{o}C (**Figure 2.2.4.2**). After attachment, the pillar and fluidic layers were punched together using a 700 μm mechanical puncher, to create the openings for sweat collection. Later, the resultant PDMS structure was exposed to UVO ozone (Jetline Co., Irvine, CA) at a gas flow rate of 3 sccm for 10 min (25^{o}C) to be bounded to a flat PDMS layer containing the electrode.

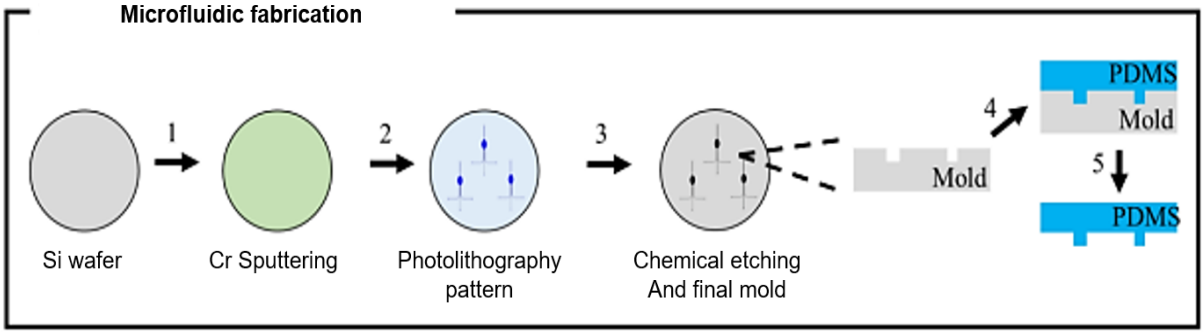

Figure 2.2.4.1 Fabrication of Si master for the PDMS fluidic features.
A 50 nm layer of Cr was deposited on a 4" silicon wafer to act as an etch mask. Next, photolithography was used to pattern the microfluidic channels and the unmasked portions were etched by deep reactive ion etching. Then, a layer of poly(methyl methacrylate) was spin-casted onto the Si master, followed by soft baking at 180 °C. Fınally, a silicone layer was then spin-casted onto the Si master to yield the microfluidic pattern.

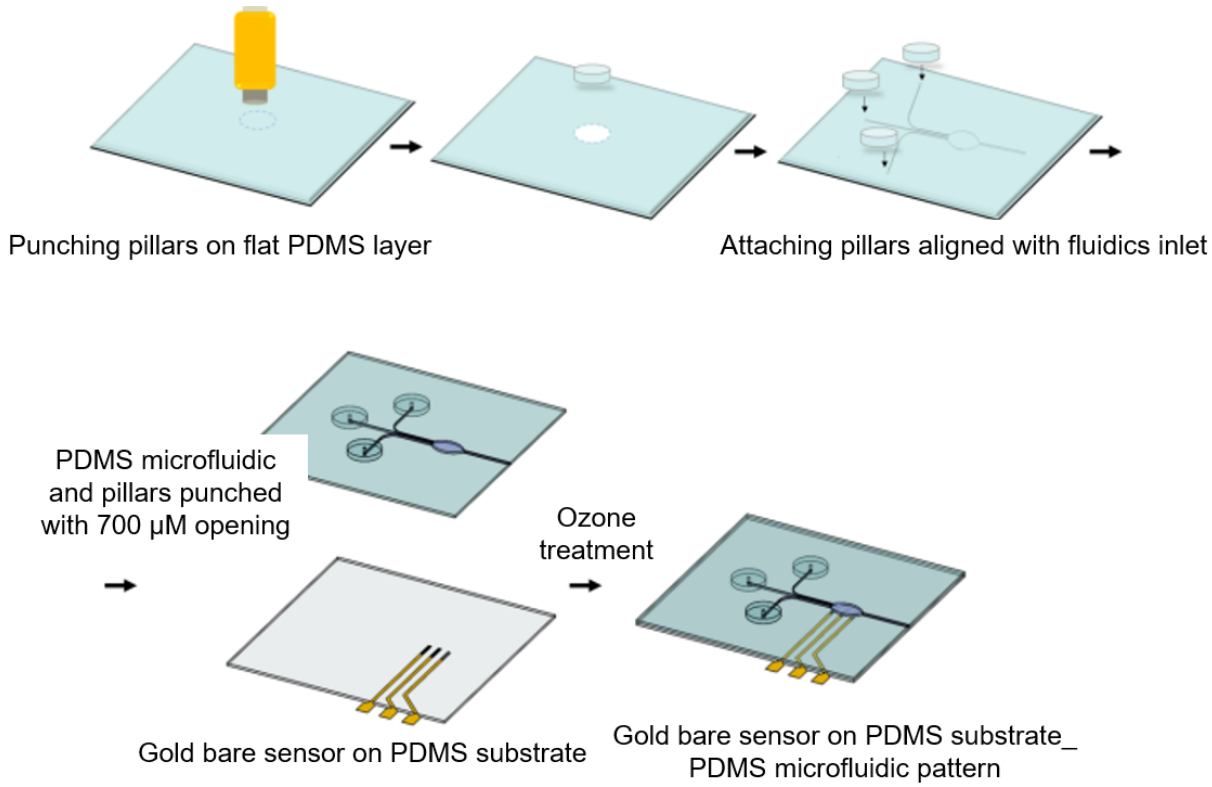

Figure 2.2.4.2 Fabrication of PDMS pillars and assembling to the PDMS fluidic layers.
For the fabrication of the pillar inlets, a flat PDMS layer was fabricated on a glass slide with its surface treated by PMMA. A metallic puncher was used to produce the cylindrical pillars. The pillars were aligned and attached to the inlets of the microfluidic features using uncured PDMS. After attachment, the pillar and fluidic layers were punched together using a 700 µm mechanical puncher, to create the openings for sweat collection. Later, the resultant PDMS structure was exposed to UVO ozone to be bound to the PDMS layer containing the electrode.

2.2.5 Iontophoretic electrode fabrication

The iontophoretic electrodes were designed with AutoCAD software (Autodesk, San Rafael, CA), and cut using a Cricut Explore Air Machine. First, a double layer of Ag/AgCl ink was screen printed on a polyimide substrate and cured at 80 ^{0}C for 10 min. After cured, the Ag/AgCl/polyimide- sheet was used as a substrate to cut the electrodes (**Figure 2.2.5.1**) using a premium fine point blade for better quality electrode resolution. After cut, the anode electrode was placed within the PDMS inlet pillars and covered with the anodic iontophoretic hydrogel (4% agarose gel containing 2% pilocarpine), while the cathode electrode was placed at 2.6 cm from the anode and covered with the cathodic hydrogel (PVA containing sodium nitrate). Detailed iontophoretic hydrogel composition and preparation will be discussed further.

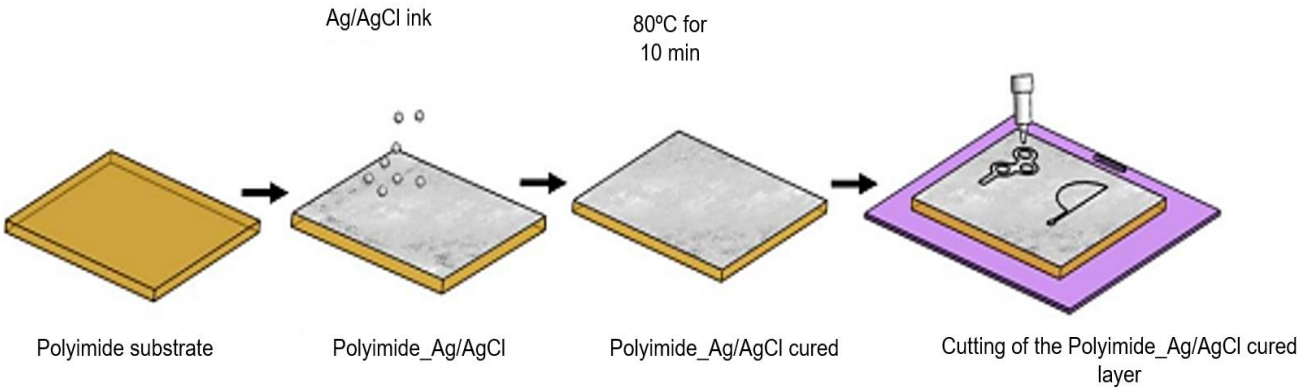

Figure 2.2.5.1 Fabrication of cathode electrodes on polyimide substrate.
The iontophoretic electrodes were designed and cut using a Cricut Explore Air Machine. First, a double layer of Ag/AgCl ink was screen printed on a polyimide substrate and cured at 80 0C for 10 min. After cured, the Ag/AgCl/polyimide- sheet was used as a substrate to cut the electrodes.

2.2.6 Assembling of the Microfluidic Device

The iontophoretic microfluidic device was composed of three main layers (**Figure 2.1.1B**). The first layer (1) was a thin PDMS layer with the electrochemical transducer screen printed labeled as “electrode”. The next layer (2) contained the microfluidic features coupled with the PDMS pillar inlets for sweat capture (“PDMS fluidics”). Finally, layer (3) defined as “IP electrode and gel” was composed by the screen-printed iontophoretic electrode containing the cholinergic agonist hydrogel. Prior coupling, dust from layers 1 and 2 was removed by a rigorous adhesion treatment using removable double-sided film tape (3M 667, Scotch^{TM}) until the polymeric layers were free of residue particles. After the cleaning step, layer 1 (facing electrochemical transducer), and layer 2 (facing microfluidic pattern) were exposed to an ozone treatment (25 °C for 7 min).

Subsequently, the layers were aligned and bonded and left to rest for 2 hours prior use. Iontophoretic electrodes were integrated to the final assembly by double sided medical tape (**Figure 2.2.6.1**). Cholinergic agonist component integration to the final system will be discussed in the next section.

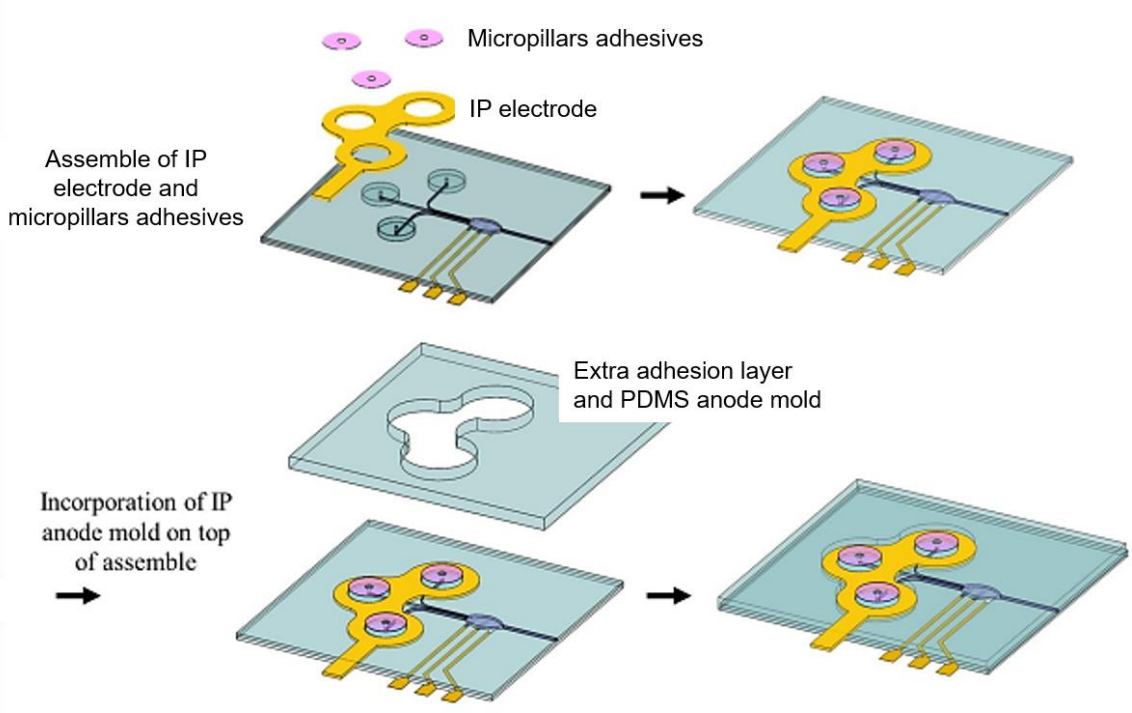

Figure 2.2.6.1 PDMS device assembling steps.
The iontophoretic microfluidic device was composed of the microfluidics pillar attached to the microfluidic features, which was bonded to the electrode layer (top row). Once the PDMS parts were assembled, the anode was placed on the device and an extra PDMS layer was used to improve the adhesion. Adhesive layer was also used on the pillars (bottom row).

2.2.7 Iontophoretic hydrogels fabrication

FDA-approved iontophoresis procedure was used to promote sweat stimulation by delivery of a cholinergic agonist drug (pilocarpine nitrate) into the skin by electro repulsion at the anode section. Iontophoretic electrodes were covered with two different hydrogel compositions, on the anode electrode, a hydrogel layer containing 4% agarose and 2% pilocarpine was used. Briefly, agarose hydrogel was prepared by dissolving the appropriate amount of agarose (4% w/v) in deionized water, heating and continuously stirring at 120 °C. After complete agarose dissolution, pilocarpine nitrate powder was added in the mixture to reach 2 % (w/v) pilocarpine in solution.

The solution was then cooled down to 60°C and 120 µL was casted on the electrode surface to form a uniform hydrogel layer covering the iontophoretic area. In the cathodic compartment, a polyvinyl alcohol (PVA) cryogel was used[38]. First, a 5.0 % w/v PVA solution was prepared in deionized water by heating the solution up to 180°C and then cooling it down to room temperature. After the temperature cooling step, the solution was placed in an ice bath (-3°C) followed by pH adjustment to pH 1.0 by adding small aliquots of 5 M Hydrochloric acid solution. Subsequently, an aliquot of 130 µL of glutaraldehyde was added to give a final concentration 50% w/v. The final mixture was then stirred for 1 min and 500 µL were poured into an ecoflex coin shaped mold (area per coin = 2.7 cm^2) and set in -20 °C freezer overnight (**Figure 2.2.7.1-2**). The resulting cryogels were removed from the mold by immersing the mold in deionized water for 30 min. To remove acid excess, cryogels were washed with water 6 times, later, the cryogels were then plunged in solution of 1% potassium nitrate for 1 h for further application. The iontophoresis protocol was optimized in terms of sweat volume generation and skin response to iontophoretic current. Sweat generation was achieved through pilocarpine delivery across the skin by applying an optimized electrical current density (~0.4 mA/cm^2) flowing from the anodic to the cathodic compartment for 10 min.

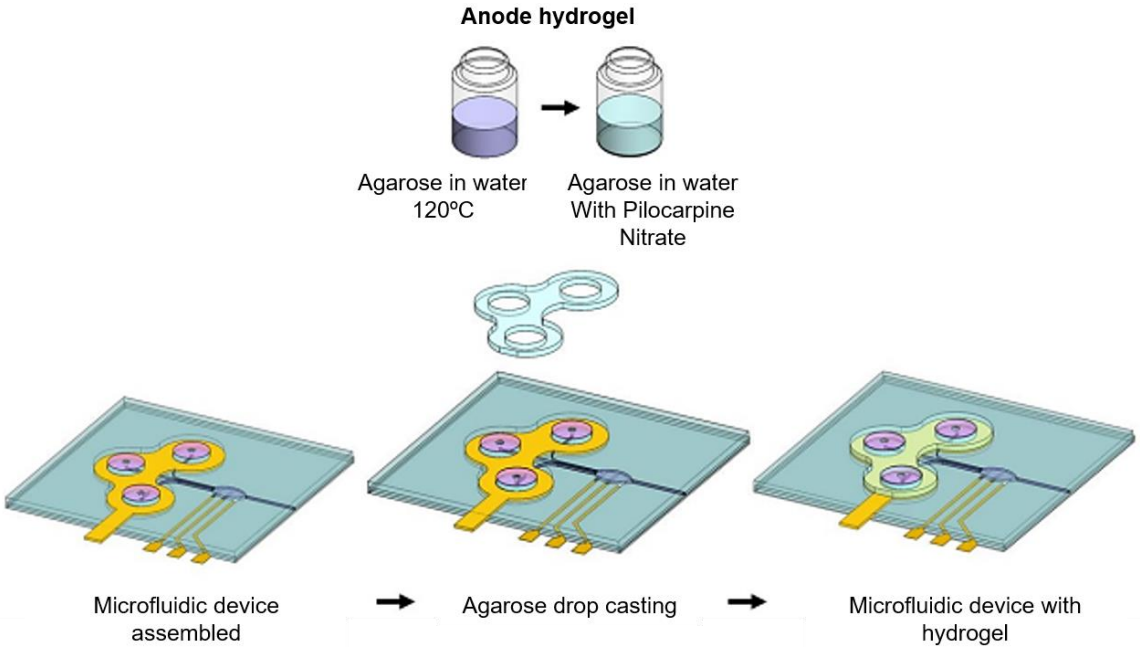

Figure 2.2.7.1. Agarose gel preparation and anode modification.
The agarose hydrogel was prepared by dissolving the appropriate amount of agarose (4% w/v) in deionized water, heating and continuously stirring at 120 °C. After complete agarose dissolution, pilocarpine nitrate powder was added in the mixture to get 2 % (w/v) pilocarpine in the solution. The solution was then cooled down to 60°C and 120 µL was casted on top of the surface to form a uniform hydrogel layer covering the iontophoretic area.

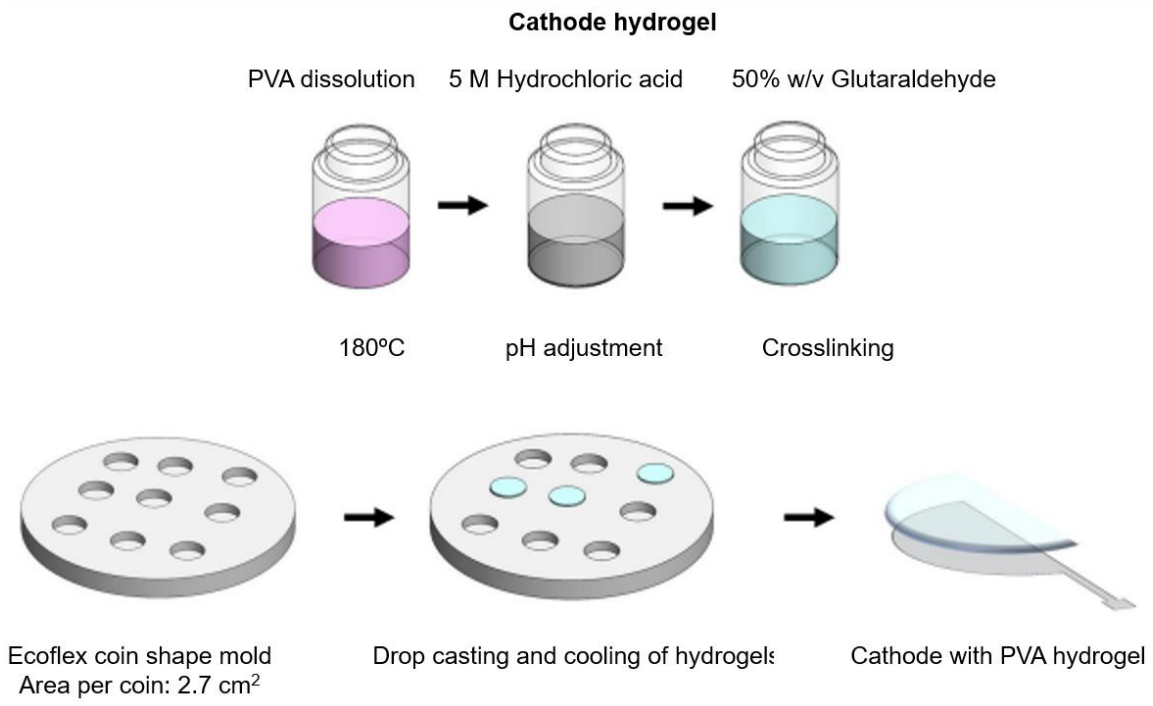

Figure 2.2.7.2. PVA gel preparation and cathode modification.
In the cathodic compartment, a polyvinyl alcohol (PVA) cryogel was used. First, a 5.0 % w/v PVA solution was prepared in deionized water by heating the solution up to 180°C and then cooling it down to room temperature. After the temperature cooling step, the solution was placed in an ice bath (-3°C) followed by pH adjustment to pH 1.0 by adding small aliquots of 5 M Hydrochloric acid solution. Subsequently, an aliquot of 130 µL of glutaraldehyde was added to give a final concentration 50% w/v. The final mixture was then stirred for 1 min and 500 µL were poured into an ecoflex coin shaped mold and set in -20 °C freezer overnight. The resulting cryogels were removed from the mold by immersing the mold in deionized water for 30 min.

2.2.8 Device Transfer and on-body real-time glucose monitoring

The device evaluation on human subjects was conducted in strict compliance following a protocol approved by the Institutional Review Board (IRB) at the University of California, San Diego. Nine healthy volunteers (with no prior medical history of diabetes) were recruited for on-body evaluation of the sensor platform before and after consumption of carbohydrate-rich food (the subjects were requested to arrive at the laboratory facility with 12h fasting state). The soft IP fluidic device was then transferred to the arm of the volunteers, previously cleaned with soap and sterile alcohol prep pads (MEDca^{TMz}). The microfluidic system was attached to the skin using a 3 M Double Coated Medical Tape attached to the PDMS pillars, the inner circle from the ring-shaped tape had 1 mm diameter which was aligned with the 700 µm inlets of the device. This ring tape defined the actual sweat collection area[22,26,48].

The outer circle diameter had 5 mm diameter (same diameter as the PDMS pillars). A PDMS layer, with the same thickness as the pillars, was used to improve the adhesion of the device to the skin (**Figure 2.2.8.1**). During the electroanalysis of sweat glucose, blood glucose levels were measured before and after meal using commercial fingerstick glucose strips (Accu-Chek Aviva Plus) to establish validation of the sensor performance. Subsequently, IP current was applied to the skin through cathode and anode iontophoretic electrodes for 10 min in order to promote sweat generation (at the anode) under a current density of 0.4 mA cm^{-2}. After the pilocarpine delivery, continuous amperometry was recorded at a constant reduction potential of − 0.2 V (vs Ag/AgCl). Steady-state amperometric pre/post-meal glucose current responses at 20 min were taken as sweat glucose values for further comparison and correlation.

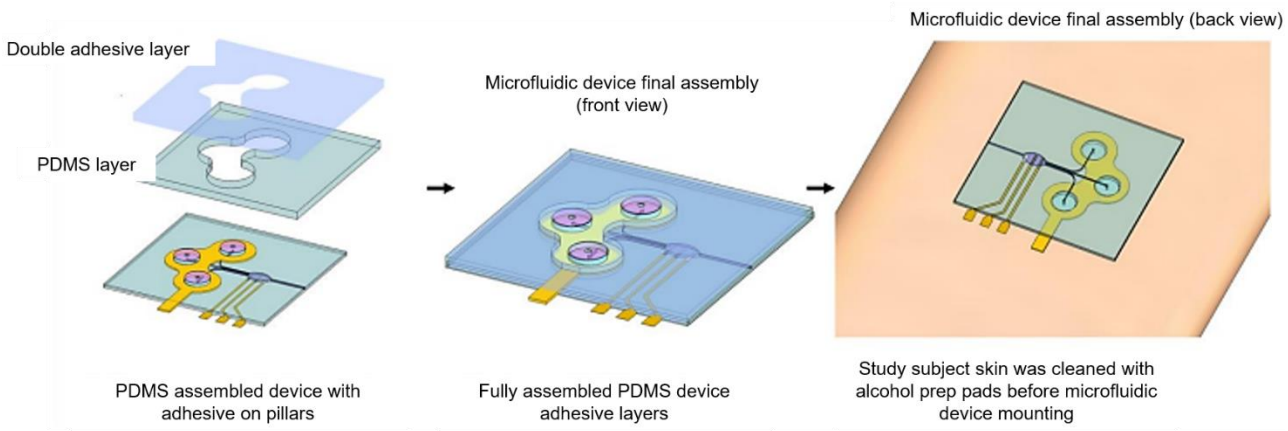

Figure 2.2.8.1. Medical tape assembling and on-body device transfer.
The device evaluation on human subjects was conducted in strict compliance following a protocol approved by the Institutional Review Board (IRB) at the University of California, San Diego. The soft IP fluidic device was transferred to the arm of the volunteers, previously cleaned with soap and sterile alcohol prep pads. The microfluidic system was attached to the skin using a Double Coated Medical Tape attached to the PDMS pillars. A PDMS layer, with the same thickness as the pillars, was used to improve the adhesion of the device to the skin

2.3 Results and discussion

2.3.1 Rationing for the epidermal microfluidic and IP electrode designs

The integration of sweat stimulants and sensing systems is a challenging task. Existing approaches rely on placing the sensor on the stimulated area, either in direct contact with the iontophoretic gels or at its proximity[23,37,38,40].

In both cases, there is a risk of mixing sweat with gels, and/or wicking material, causing dilution of the analytes and possible accumulation of old and new sweat. While analyte dilution can be corrected, the device is still limited to single time analysis. Thus, autonomous, single step, and efficient integration of the iontophoretic and biosensing systems, without cross-contamination, is strongly desirable. Here, we demonstrate a soft epidermal fluidic system capable of collecting stimulated sweat without any dilution or contamination with the stimulation system. The microfluidic design was optimized based on our previous work[22,26]. An oval-shape reservoir was adopted in the device due to the flow stagnation when using a circular chamber[22]. Because of the smaller reservoir dimensions (2 µL), the use of structural PDMS pillars was dismissed. The overall volume of the device (3.2 µL) was based on the total volume of stimulated sweat (each inlet collects ~7 µL). The number of inlets was further optimized based on iontophoretic parameters. The iontophoretic electrodes were designed to stimulate sweat around the inlet area of the epidermal fluidic device. In order to physically separate the iontophoretic gels from the sweat collection area, a PDMS structure, shaped as a pillar, was used as a barrier. Initially, the stimulated sweat flows vertically through the pillar further reaching the channels of the fluidic feature (**Figure 2.1.1**).

The sweat collection area was defined by the medical tape used for adhesion of PDMS devices to the skin. The PDMS pillar inlets need to be strongly attached to the skin in order to confine the area and build up pressure for the sweat flow. A ring-shaped medical tape was used to this end. Sweat collection area was formed by a 1 mm inner diameter circle, leaving a ring 2 mm wide for the skin adhesion. It was found that a larger sweat collection area implicates in more frequent leakage of sweat, preventing the flow of sweat towards the inner channels of the microfluidic device. The collected sweat was generated in the immediate proximity of the iontophoretic anode. Experimental optimization of the anodic electrode area showed that an anode 2 mm wide could generate enough sweat to reach the collection area. Smaller anode areas were not able to produce enough sweat. The sensor electrode size was optimized to fit in the microfluidic reservoir so the sweat signal could be measured once the chamber was filled. The iontophoretic cathode (140 mm^2) was designed to have approximately the same area of the anode (160 mm^2) to ensure comfort, with no burning sensation, during the sweat stimulation. The signal acquisition started right after sweat stimulation and its profile will be further discussed in the next sections.

2.3.2 Principle of IP integrated microfluidic epidermal biosensor

Prior to any collection or measurement, the microfluidic device was mounted on the volunteer's forearm. The forearm was selected for comfortable operation, and high density of sweat glands (108 glands/cm²) (**Figure 2.1.1A, a**)[13,49]. The complete device includes a flexible iontophoretic system with a screen-printed cathode (**Figure 2.1.1Ab, i**) and anode (**Figure 2.1.1Ab, ii**) for sweat stimulation by pilocarpine delivery. The PDMS microfluidic features consist of 3 inlets, aligned on the sweat sampling location, enabling the pumping of the simulated sweat through the microchannels towards the reservoir where the glucose biosensor, screen printed on lithography-based gold current collectors, is located. Then, sweat is driven to an outlet channel and replenished continuously. The miniaturized electronic board is attached to the sensors to acquire wireless electronic sweat glucose signal (**Figure 2.1.1A, b**).

During the iontophoresis process an electric current is applied (current density: 0.4 mA/cm^2). Pilocarpine loaded inside the agarose gel is delivered through the skin by electrostatic repulsion. Sweat is generated and captured in the inlet area located in the PDMS pillars, the collected sweat flows through the channels to the reservoir area. Typical amperometric response starts with obtaining a zero-current value in the first minutes (**Figure 2.1.1A, c, i**), and the response current values observed next, is an indicator of sweat in the reservoir (**Figure 2.1.1A, c, ii**). After complete reservoir filling, the current signal stabilizes obtaining a reliable electrochemical response corresponding to the redox reaction of hydrogen peroxide produced by the oxidation of glucose in sweat (**Figure 2.1.1A, c, iii)**. The design of the microfluidic platform includes (from top-down): screen printed Ag/AgCl IP electrodes, PDMS pillars for sweat collection, PDMS with microfluidic features and final assembling (**Figure 2.1.1B**). A front view of the device showing the flow direction and complete assembling on the skin (**Figure 2.1.1C, a**), and a back view showing anode and the sputtered golden electrode (**Figure 2.1.1C, b**) are also represented. Cross section schematics of the integrated device mounted on the skin illustrate the delivery of pilocarpine by means of current flow from the anode terminal to the cathode, followed by the stimulation of sweat glands and collection of samples after reaching the outer layer of the skin (**Figure 2.1.1C)**.

The mechanical stability of the IP integrated microfluidic sensor device was tested under various mechanical strains that may occur during on-body operation (**Figure 2.3.2.1A**). Application of subsequent bending (**Figure 2.3.2.1A, b**), stretching (**Figure 2.3.2.1A, c**), and twisting on the device (**Figure 2.3.2.1A, d**) caused no damage to PDMS structure (**Figure 2.3.2.1A, e**) demonstrating its flexible and stretchable features. Additionally, these deformation tests did not induce any apparent fracture or break on the sputtered/printed sensing and IP electrodes demonstrating the high mechanical resistance of the entire device. **Figure 2.3.2.1B** shows the view of the device that will be in contact with the skin. The inlets on the pillars looking upwards and the anodic electrode position can be clearly observed from this image (**Figure 2.3.2.1B, a**). Prior to transferring to the skin, a small droplet of a blue food dye was placed next to each inlet opening and left to dry. Upon sweating, the dry blue dye rehydrated, coloring the sweat. Next, the integrated microfluidic device is attached on the epidermis by medical adhesive (Outer diameter: 5mm, inner diameter: 1mm). Upon application to the skin, the yellow polyimide substrate used to print the anodic electrode can be observed (**Figure 2.3.2.1B, b**), the device remains damage free and well-attached to the skin throughout the on-body tests after IP sweat stimulation (**Figure 2.3.2.1B, c**).

The sweat generated at the anode is efficiently transported in the channels due to the strong adhesion between the inlet and the epidermis. After removal from the skin, the reservoir remains filled with sweat (colored with blue dye) demonstrating the ability of using the device for sweat collection (**Figure 2.3.2.1B, d**). These tests visually exhibited the successful resiliency of mechanical strain of the design, showing its suitability for on-body sweat analysis without any hindrance to the wearer.

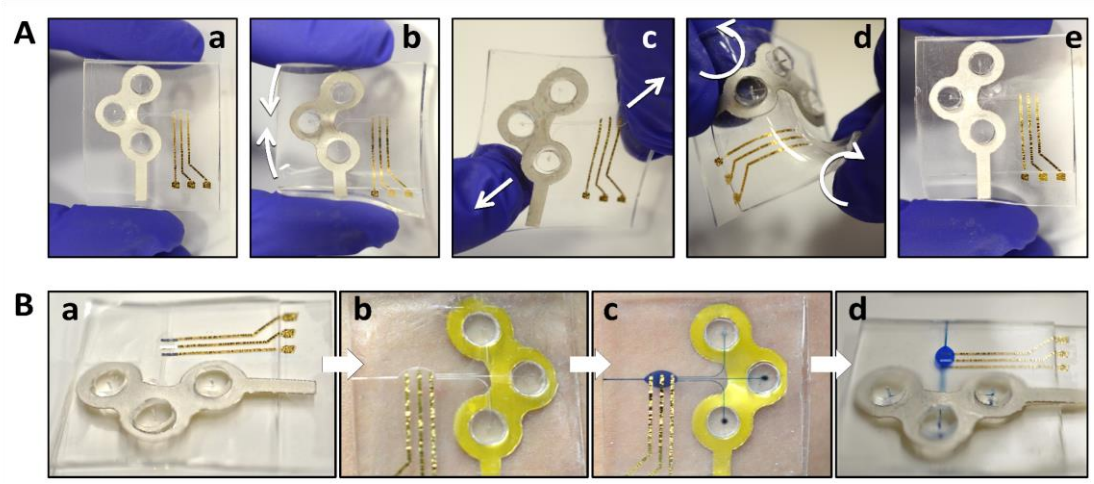

Figure 2.3.2.1. Deformation of the microfluidic platform.
A) Mechanical resilience study of the IP fluidic device. **(a)** before the deformations. Images taken during **(b)** bending. **(c)** stretching. **(d)** twisting and **(e)** after deformations. **B)** Depiction showing the device **(a)** before transferring to the skin with the inlets upwards. **(b)** After transferring to the skin and **(c)** after sweat stimulation. **(d)** Device filled, removed from skin after operation.

2.3.3 Optimization of Parameters for Sweat Extraction

To obtain the best operational conditions, parameters such as IP current density, number of inlets and iontophoretic delivery duration time were examined. The amount of generated sweat was measured by adopting a single channel microfluidic model. First, the current density was optimized by fixing an IP duration time of 5 min. The volume of sweat generated was calculated after sampling for 20 minutes. The volumetric analysis was carried by measuring the length (starting from reservoir section to outlet) of the single channel device filled with the biofluid (**Figure 2.3.3.1A, a**). Current densities ranging from 0.1 to 0.5 mA/cm^2 were studied, sweat volume was plotted against the current densities used. An increasing trend can be observed for current density values from 0.1 to 0.4 mA/cm^2, with the highest volume of sweat collected under a current density of 0.4 mA/cm^2 without causing any skin irritation, further values did not provide a significant increase in volume (**Figure 2.3.3.1A, b**). After optimization of the current density, the IP duration time, to the complete filling of a 3- inlet device, was studied. IP duration times of 5, 10 and 20 min were used. The iontophoretic time of 5 minutes showed the longest time (30 min) to completely fill the system, while 10 and 20 min displayed close filling time (14 and 13 min, respectively), since there was no significant difference, 10 min was selected (**Figure 2.3.3.1B, a).** The filling profile was monitored by taking photographs upon 15 min of finishing the delivery process (**Figure 2.3.3.1B, b)**.

After setting the optimal current density as 0.4 mA/cm^2 and the IP duration time as 10 min, the number of inlets was further investigated. Microfluidic devices with 2, 3 and 4 inlets were prepared and tested under the same optimized conditions. Filling information was plotted describing the relationship between number of inlets and the time to complete filling the device. The highest numeric value corresponded to the 2-inlets devices (28 min), while 3 and 4-inlets showed similar filling time (13 and 11 min, respectively). **Figure 2.3.3.1B-d** shows the devices after 10 minutes of finishing the delivery process. Besides having slightly higher filling time, the 3 inlets model was preferred in terms of fabrication and reproducibility, in addition, the reservoir is filled in 10 min (**Figure 2.3.3.1B, d**). The filling time was comparable to our previously reported epidermal microfluidic platform designed for exercise activities[22,26], showing attractive performance relative to similar exercising-based microfluidic devices[13,18].

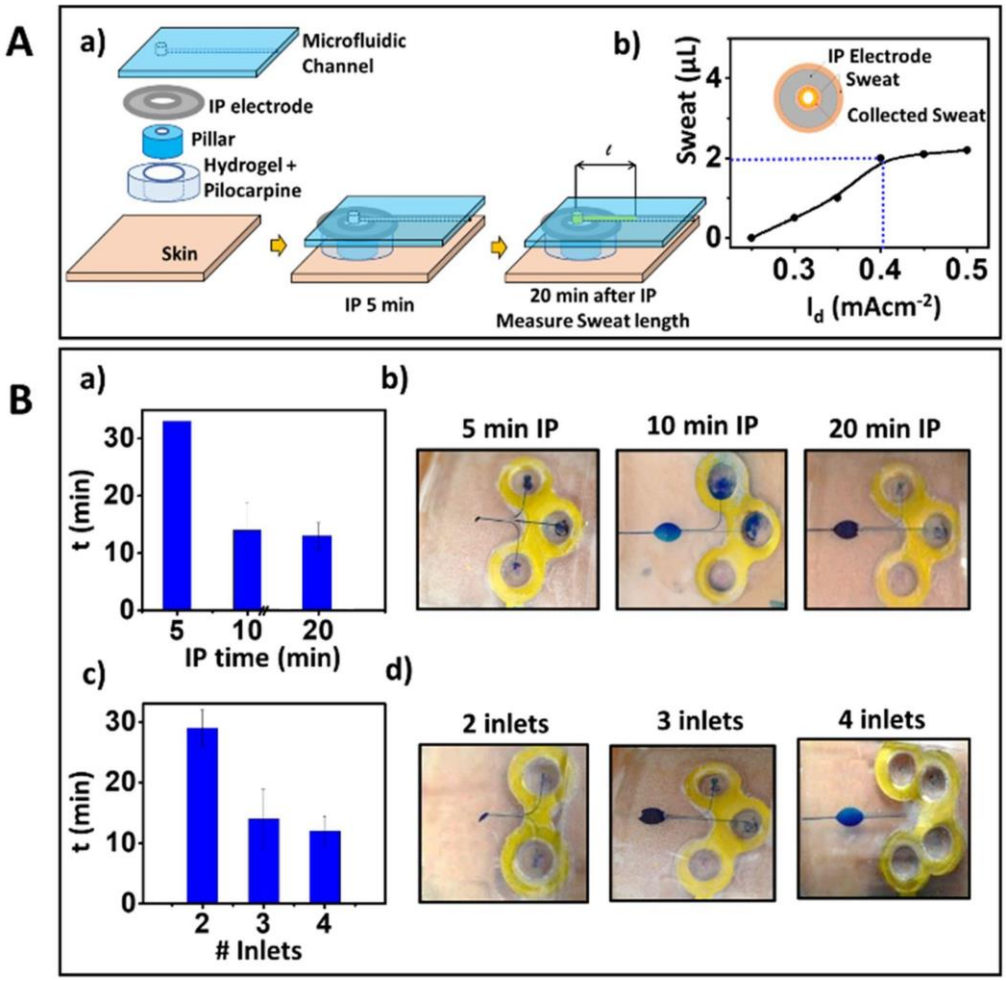

Figure 2.3.3.1 IP fluidic device optimization.
A) IP current density optimization using electrode with total area of 0.368 cm^2: (a) Schematics for a straight line – one inlet microfluidic device to measure the total volume of sweat generated after 5 minutes of iontophoresis (IP) with several current densities. (b) Plot corresponding to the volume of collected sweat with the microfluidic device after 5 minutes of IP with several current densities. (B) Optimization of IP time using the optimized current density of 0.4 mAcm^{-2}: (a) Plot showing IP time vs. filling time of 3 inlets of device. (b) On body tests of the 3 inlets device with the same subject after 5 min, 10 min, 20 min of IP. Pictures were taken 15 minutes after finishing every IP duration time, respectively. c) Optimization of number of inlets using the optimized current density of 0.4 mAcm^{-2} and 10 minutes of IP duration time for several number of inlets. Plot showing measured time to fill the device for several number of inlets. (d) On body tests of 2, 3 and 4 inlets with the same volunteer. Pictures were taken 10 minutes after the 10 min IP operation.

2.3.4 IP Microfluidics for on-body Glucose Analysis in Human Perspiration

On-body experimental trials for sweat glucose monitoring were performed with 9 different healthy volunteers in compliance with the UCSD approved IRB protocol. Volunteers were requested to arrive in a fasting stage (12 hours without any food consumption). After the cleaning and transferring procedures, sweat glucose monitoring was performed.

Sweat glucose levels were measured using an enzymatic (GOx) electrochemical biosensor located inside the microfluidic device reservoir. Specifically, amperometry was employed at -0.2 V (vs Ag/AgCl) and sweat glucose was monitored selectively by the reduction of the produced hydrogen peroxide, on the Prussian Blue mediator. Sweat was stimulated for 10 min, followed by continuous glucose quantification (**Figure 2.3.4.1A, a-b)**. Experiments were performed before (denoted as B.M.) and after meal (denoted as A.M.). Challenges such as poor pilocarpine delivery efficiency, were addressed by replacing the microfluidic device for a new one after meal consumption, and repeating the same cleaning and transfer protocol, this replacing process can be avoided by using long time sweat stimulation drugs such as carbachol[50]. Blood samples were taken before each on-body glucose analysis. Different filling times were observed for the volunteers, this variation is related to the pilocarpine delivery efficiency once different skin types may need different optimized IP parameters. In order to ensure a reliable signal for the glucose study, the signal was sampled at 20 min of data recording. This signal sampling time has shown to be enough to ensure stable signals for all volunteers (highlighted in a dotted green line in the amperogram). After finishing the on-body amperometric analysis, the current values (blue bar plot) at fasting and non-fasting stage were plotted against the blood glucose obtained from commercial glucometer (red bar plot) (**Figure 2.3.4.1B)**. The integrated device was able to measure glucose levels successfully, with the results displaying good correlation to the corresponding blood glucose levels (**Figure 2.3.4.2**) in agreement with early study[32]. In order to further investigate the sensor performance, control experiments were carried out at fasting state, when the blood glucose variations are minimal. In addition, control sweat glucose tests without any food consumption and with food consumption without the enzyme, showed no significant changes (**Figure 2.3.4.2**). The sensor was further evaluated by *in-vitro* experiments, where the selectivity of the electrochemical response to glucose in the presence of possible sweat interferents electroactive analytes (ascorbic acid, lactic acid, acetaminophen, and uric acid) was demonstrated (**Figure 2.3.4.3**).

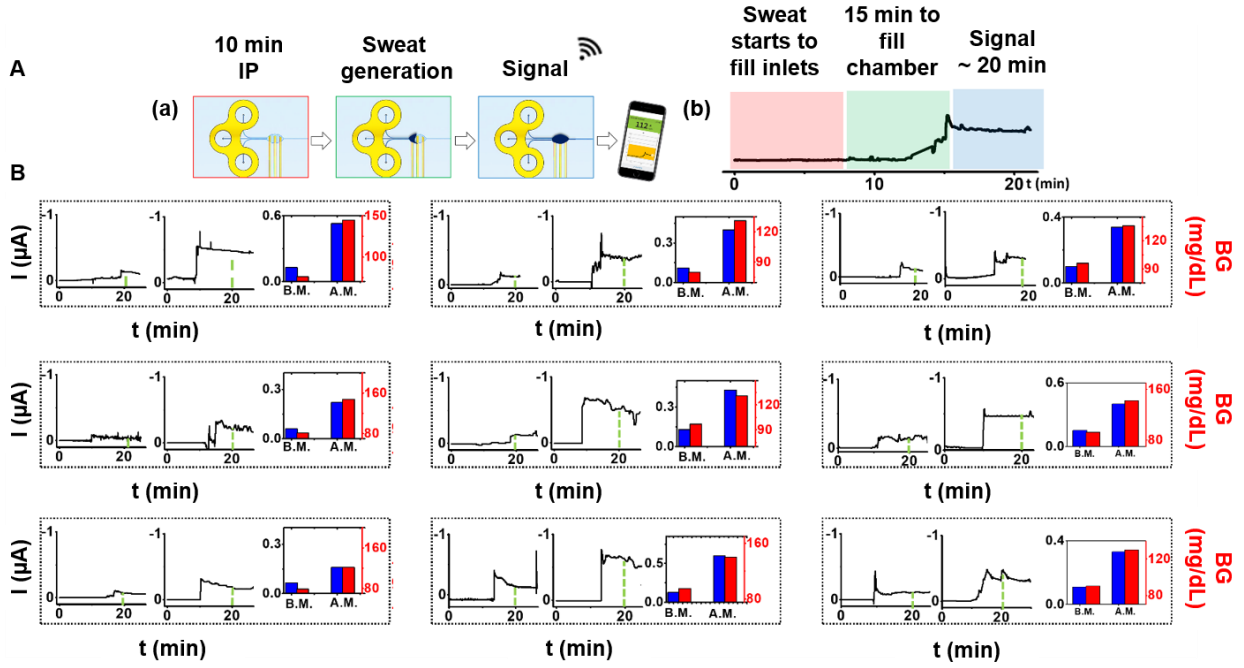

Figure 2.3.4.1. On body experiments for sweat glucose detection in stimulated sweat using the IP fluidic device, using a detection potential of -0.2 V vs Ag/AgCl.

A) (a) Timeline for the experiment with schematic representation of the microfluidic device. Sweat was colored with blue dye for better visualization. First, sweat enters the device through the inlets. After 10 to 15 min sweat starts filling the reservoir. Next, the current increases and stabilizes at 20 min. **b)** The electrochemical signal for glucose is taken at 20 min of data recording. **B)** Chronoamperograms for nine volunteers before (left) and after (right) taking a meal. On the right-side a bar plot shows the correlation between the current obtained for the glucose sweat and the blood glucose values.

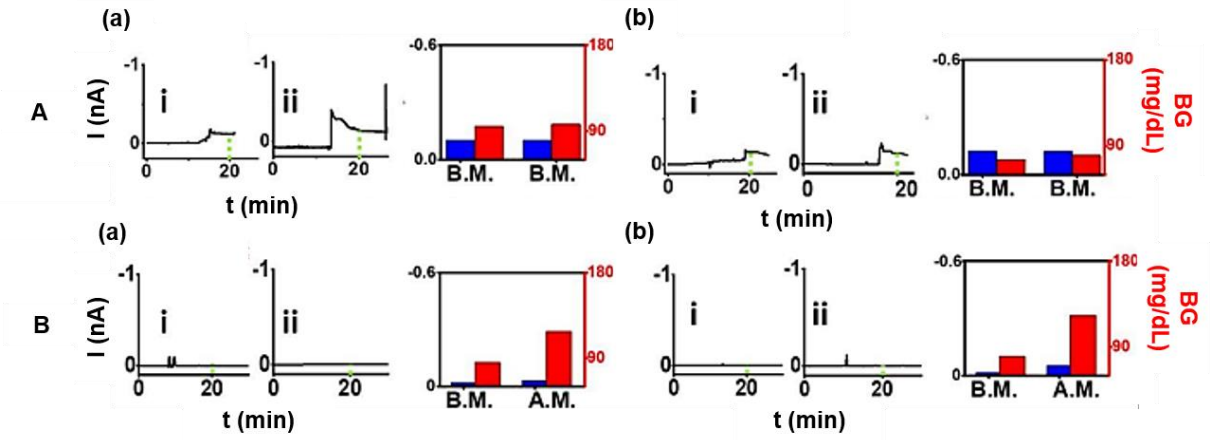

Figure 2.3.4.2. Control on body experiments for sweat glucose detection in stimulated sweat using the IP fluidic device.
A) Amperometric response at the same blood glucose value. Two different microfluidics devices (i, ii) were used for every subject (a, b). Subject sweat glucose was collected at a fasting state. Bar column graphics represent the current value (blue) obtained for every sensor and their respective blood glucose value (red). B) Chronoamperograms obtained using screen printed sensors without any enzymatic modification. Two different microfluidics devices (i, ii) were used for every subject (a, b). Subjects sweat glucose was collected at a fasting state and after food ingestion. Bar column graphics represent the current value (blue) obtained for every sensor and their respective blood glucose value (red).

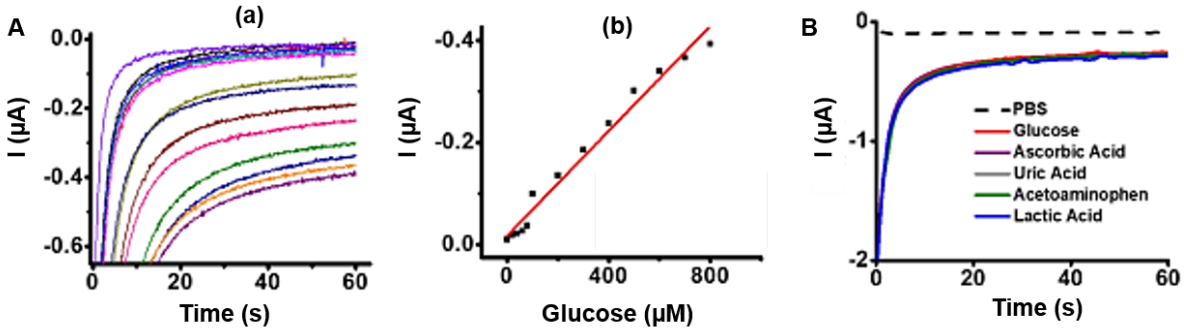

Figure 2.3.4.3. Glucose sensor in-vitro characterization.
A) Glucose calibration. (a,b) Glucose in-vitro calibration of the GOx/PB biosensor in PBS. Calibration was taken at fixed potential at -0.2V. Low calibration range was performed from 20 – to 100 µM and high calibration range from 200 -800 µM. B) Interferent analytes. Addition of 0.1 mM glucose, 0.1 mM ascorbic acid, 10 mM lactic acid, 0.1 mM acetaminophen and 0.1 mM uric acid.

2.4 Conclusions

We demonstrated, for the first time, the integration of an iontophoretic sweat stimulation and sensing system in a soft epidermal microfluidic device. The device was able to collect stimulated sweat without dilution or cross-contamination with the iontophoretic gels. The optimized iontophoretic and detection parameters are suitable for different volunteers. The sensing performance of the device was demonstrated by monitoring sweat glucose, presenting good correlation with blood glucose measurements. In addition, the mechanical stability and resilience of the microfluidic device was successfully tested under various mechanical strains that may occur during on-body operation. Such epidermal iontophoretic microfluidic devices can be further optimized by using improved adhesion of the inlets to the skin, which could avoid the leakage of sweat from the inlet collection area, decreasing the filling time, and consequently the time lag. Pilocarpine can be replaced by long term sweat stimulation drugs, such as carbachol, in order to increase the operational lifetime of the device.

This new concept of skin-mounted soft epidermal wireless microfluidic device offers an attractive route towards sweat monitoring which addresses limitations of existing epidermal fluidic devices. Such microfluidic devices offer great possibilities toward personalized healthcare. With this improved sweat stimulation/detection fluidic system, new sweat analytes can be investigated towards early detection and monitoring of diseases. This fully integrated epidermal microfluidic detector for performing continuous real-time on-body monitoring of sweat biomarkers can be readily extended to the monitoring of a plethora of different analytes, including extension to on-body bio affinity assays in connection to integrating microchannel actuators, such as valves and mixture chambers.

2.5 Adknowledgements

Chapter 2, in full, is a reprint of the material as it appears in G. Bolat, E. De la Paz, N. F. Azeredo, M. Kartolo, J. Kim, A. N. de Loyola e Silva, R. Rueda, C. Brown, L. Angnes, J. Wang, J. R. Sempionatto, Wearable soft electrochemical microfluidic device integrated with iontophoresis for sweat biosensing. *Analytical and Bioanalytical Chemistry*. **414**, 5411–5421 (2022).

2.6 References

1. Y. Yang, W. Gao, Wearable and flexible electronics for continuous molecular monitoring. *Chemical Society Reviews*. **48**, 1465–1491 (2019).

2. J. Kim, I. Jeerapan, J. R. Sempionatto, A. Barfidokht, R. K. Mishra, A. S. Campbell, L. J. Hubble, J. Wang, Wearable Bioelectronics: Enzyme-Based Body-Worn Electronic Devices. *Accounts of Chemical Research*. **51**, 2820–2828 (2018).

3. G. Matzeu, L. Florea, D. Diamond, Advances in wearable chemical sensor design for monitoring biological fluids. *Sensors and Actuators B: Chemical*. **211**, 403–418 (2015).

4. Y. Yang, Y. Song, X. Bo, J. Min, O. S. Pak, L. Zhu, M. Wang, J. Tu, A. Kogan, H. Zhang, T. K. Hsiai, Z. Li, W. Gao, A laser-engraved wearable sensor for sensitive detection of uric acid and tyrosine in sweat. *Nature Biotechnology*. **38**, 217–224 (2019).

5. J. R. Sempionatto, A. A. Khorshed, A. Ahmed, A. N. De Loyola e Silva, A. Barfidokht, L. Yin, K. Y. Goud, M. A. Mohamed, E. Bailey, J. May, C. Aebischer, C. Chatelle, J. Wang, Epidermal Enzymatic Biosensors for Sweat Vitamin C: Toward Personalized Nutrition. *ACS Sensors*. **5**, 1804–1813 (2020).

6. Y. Cheng, K. Wang, H. Xu, T. Li, Q. Jin, D. Cui, Recent developments in sensors for wearable device applications. *Analytical and Bioanalytical Chemistry*. **413**, 6037–6057 (2021).

7. M. Bauer, L. Wunderlich, F. Weinzierl, Y. Lei, A. Duerkop, H. N. Alshareef, A. J. Baeumner, Electrochemical multi-analyte point-of-care perspiration sensors using on-chip three-dimensional graphene electrodes. *Analytical and Bioanalytical Chemistry*. **413**, 763–777 (2020).

8. G. Chen, J. Zheng, L. Liu, L. Xu, Application of Microfluidics in Wearable Devices. *Small Methods*. **3**, 1900688 (2019).

9. J. R. Sempionatto, I. Jeerapan, S. Krishnan, J. Wang, Wearable Chemical Sensors: Emerging Systems for On-Body Analytical Chemistry. *Analytical Chemistry*. **92**, 378–396 (2019).

10. A. J. Bandodkar, W. J. Jeang, R. Ghaffari, J. A. Rogers, Wearable Sensors for Biochemical Sweat Analysis. *Annual Review of Analytical Chemistry*. **12**, 1–22 (2019).

11. J. Min, J. R. Sempionatto, H. Teymourian, J. Wang, W. Gao, Wearable electrochemical biosensors in North America. *Biosensors and Bioelectronics*. **172**, 112750 (2021).

12. J. R. Sempionatto, M. Lin, L. Yin, E. De la paz, K. Pei, T. Sonsa-ard, A. N. de Loyola Silva, A. A. Khorshed, F. Zhang, N. Tostado, S. Xu, J. Wang, An epidermal patch for the simultaneous monitoring of haemodynamic and metabolic biomarkers. *Nature Biomedical Engineering*. **5**, 737–748 (2021).

13. A. Koh, D. Kang, Y. Xue, S. Lee, R. M. Pielak, J. Kim, T. Hwang, S. Min, A. Banks, P. Bastien, M. C. Manco, L. Wang, K. R. Ammann, K.-I. Jang, P. Won, S. Han, R. Ghaffari, U. Paik, M. J. Slepian, G. Balooch, A Soft, Wearable Microfluidic Device for the Capture, Storage, and Colorimetric Sensing of Sweat. *Science translational medicine*. **8**, 366ra165 (2016).

14. S. B. Kim, K. Lee, M. S. Raj, B. Lee, J. T. Reeder, J. Koo, A. Hourlier-Fargette, A. J. Bandodkar, S. M. Won, Y. Sekine, J. Choi, Y. Zhang, J. Yoon, B. H. Kim, Y. Yun, S. Lee, J. Shin, J. Kim, R. Ghaffari, J. A. Rogers, Soft, Skin-Interfaced Microfluidic Systems with Wireless, Battery-Free Electronics for Digital, Real-Time Tracking of Sweat Loss and Electrolyte Composition. *Small*. **14**, 1802876 (2018).

15. A. J. Bandodkar, J. Choi, S. P. Lee, W. J. Jeang, P. Agyare, P. Gutruf, S. Wang, R. A. Sponenburg, J. T. Reeder, S. Schon, T. R. Ray, S. Chen, S. Mehta, S. Ruiz, J. A. Rogers, Soft, Skin-Interfaced Microfluidic Systems with Passive Galvanic Stopwatches for Precise Chronometric Sampling of Sweat. *Advanced Materials*. **31**, 1902109 (2019).

16. H. Y. Y. Nyein, L.-C. Tai, Q. P. Ngo, M. Chao, G. B. Zhang, W. Gao, M. Bariya, J. Bullock, H. Kim, H. M. Fahad, A. Javey, A Wearable Microfluidic Sensing Patch for Dynamic Sweat Secretion Analysis. *ACS Sensors*. **3**, 944–952 (2018).

17. J. C. Yeo, K. Kenry, C. T. Lim, Emergence of microfluidic wearable technologies. *Lab on a Chip*. **16**, 4082–4090 (2016).

18. J. Choi, D. Kang, S. Han, S. B. Kim, J. A. Rogers, Thin, Soft, Skin-Mounted Microfluidic Networks with Capillary Bursting Valves for Chrono-Sampling of Sweat. *Advanced Healthcare Materials*. **6**, 1601355 (2017).

19. S. Wang, T. Chinnasamy, M. A. Lifson, F. Inci, U. Demirci, Flexible Substrate-Based Devices for Point-of-Care Diagnostics. *Trends in Biotechnology*. **34**, 909–921 (2016).

20. A. J. Bandodkar, P. Gutruf, J. Choi, K. Lee, Y. Sekine, J. T. Reeder, W. J. Jeang, A. J. Aranyosi, S. P. Lee, J. B. Model, R. Ghaffari, C.-J. Su, J. P. Leshock, T. Ray, A. Verrillo, K. Thomas, V. Krishnamurthi, S. Han, J. Kim, S. Krishnan, Battery-free, skin-interfaced microfluidic/electronic systems for simultaneous electrochemical, colorimetric, and volumetric analysis of sweat. *Science Advances*. **5**, eaav3294 (2019).

21. J. Heikenfeld, A. Jajack, B. Feldman, S. W. Granger, S. Gaitonde, G. Begtrup, B. A. Katchman, Accessing analytes in biofluids for peripheral biochemical monitoring. *Nature Biotechnology*. **37**, 407–419 (2019).

22. A. Martín, J. Kim, J. F. Kurniawan, J. R. Sempionatto, J. R. Moreto, G. Tang, A. S. Campbell, A. Shin, M. Y. Lee, X. Liu, J. Wang, Epidermal Microfluidic Electrochemical Detection System: Enhanced Sweat Sampling and Metabolite Detection. *ACS Sensors*. **2**, 1860–1868 (2017).

23. A. Hauke, P. Simmers, Y. R. Ojha, B. D. Cameron, R. Ballweg, T. Zhang, N. Twine, M. Brothers, E. Gomez, J. Heikenfeld, Complete validation of a continuous and blood-correlated sweat biosensing device with integrated sweat stimulation. *Lab on a Chip*. **18**, 3750–3759 (2018).

24. A. Alizadeh, A. Burns, R. Lenigk, R. Gettings, J. Ashe, A. Porter, M. McCaul, R. Barrett, D. Diamond, P. White, P. Skeath, M. Tomczak, A wearable patch for continuous monitoring of sweat electrolytes during exertion. *Lab on a Chip*. **18**, 2632–2641 (2018).

25. R. Vinoth, T. Nakagawa, J. Mathiyarasu, A. M. V. Mohan, Fully Printed Wearable Microfluidic Devices for High-Throughput Sweat Sampling and Multiplexed Electrochemical Analysis. *ACS Sensors*. **6**, 1174–1186 (2021).

26. J. R. Sempionatto, A. Martin, L. García-Carmona, A. Barfidokht, J. F. Kurniawan, J. R. Moreto, G. Tang, A. Shin, X. Liu, A. Escarpa, J. Wang, Skin-worn Soft Microfluidic Potentiometric Detection System. *Electroanalysis*. **31**, 239–245 (2018).

27. B. Ma, J. Chi, C. Xu, Y. Ni, C. Zhao, H. Liu, Wearable capillary microfluidics for continuous perspiration sensing. *Talanta*. **212**, 120786 (2020).

28. Y. Ichimura, T. Kuritsubo, K. Nagamine, A. Nomura, I. Shitanda, S. Tokito, A fully screen-printed potentiometric chloride ion sensor employing a hydrogel-based touchpad for simple and non-invasive daily electrolyte analysis. *Analytical and Bioanalytical Chemistry*. **413**, 1883–1891 (2021).

29. H. Y. Y. Nyein, M. Bariya, B. Tran, C. H. Ahn, B. J. Brown, W. Ji, N. Davis, A. Javey, A wearable patch for continuous analysis of thermoregulatory sweat at rest. *Nature Communications*. **12**, 1823 (2021).

30. M. Bariya, L. Li, R. Ghattamaneni, C. H. Ahn, H. Y. Y. Nyein, L.-C. Tai, A. Javey, Glove-based sensors for multimodal monitoring of natural sweat. *Science Advances*. **6** (2020), doi:10.1126/sciadv.abb8308.

31. W. Tang, L. Yin, J. R. Sempionatto, J. Moon, H. Teymourian, J. Wang, Touch-Based Stressless Cortisol Sensing. *Advanced Materials*. **33**, 2008465 (2021).

32. J. R. Sempionatto, J.-M. Moon, J. Wang, Touch-Based Fingertip Blood-Free Reliable Glucose Monitoring: Personalized Data Processing for Predicting Blood Glucose Concentrations. *ACS Sensors*. **6**, 1875–1883 (2021).

33. J. Moon, H. Teymourian, E. De la Paz, J. R. Sempionatto, K. Mahato, T. Sonsa-ard, N. Huang, K. Longardner, I. Litvan, J. Wang, Non-Invasive Sweat-Based Tracking of L-Dopa Pharmacokinetic Profiles Following an Oral Tablet Administration. *Angewandte Chemie*. **133**, 19222–19226 (2021).

34. L. Yin, J.-M. Moon, J. R. Sempionatto, M. Lin, M. Cao, A. Trifonov, F. Zhang, Z. Lou, J.-M. Jeong, S.-J. Lee, S. Xu, J. Wang, A passive perspiration biofuel cell: High energy return on investment. *Joule*. **5**, 1888–1904 (2021).

35. B. Su, Recent progress on fingerprint visualization and analysis by imaging ridge residue components. *Analytical and Bioanalytical Chemistry*. **408**, 2781–2791 (2016).

36. K. Kuwayama, K. Tsujikawa, H. Miyaguchi, T. Kanamori, Y. T. Iwata, H. Inoue, Time-course measurements of caffeine and its metabolites extracted from fingertips after coffee intake: a preliminary study for the detection of drugs from fingerprints. *Analytical and Bioanalytical*

Chemistry. **405**, 3945–3952 (2012).

37. J. Kim, I. Jeerapan, S. Imani, T. N. Cho, A. Bandodkar, S. Cinti, P. P. Mercier, J. Wang, Noninvasive Alcohol Monitoring Using a Wearable Tattoo-Based Iontophoretic-Biosensing System. *ACS Sensors*. **1**, 1011–1019 (2016).

38. J. Kim, J. R. Sempionatto, S. Imani, M. C. Hartel, A. Barfidokht, G. Tang, A. S. Campbell, P. P. Mercier, J. Wang, Simultaneous Monitoring of Sweat and Interstitial Fluid Using a Single Wearable Biosensor Platform. *Advanced Science*. **5**, 1800880 (2018).

39. A. J. Bandodkar, W. Jia, C. Yardımcı, X. Wang, J. Ramirez, J. Wang, Tattoo-Based Noninvasive Glucose Monitoring: A Proof-of-Concept Study. *Analytical Chemistry*. **87**, 394–398 (2014).

40. S. Emaminejad, W. Gao, E. Wu, Z. A. Davies, H. Yin Yin Nyein, S. Challa, S. P. Ryan, H. M. Fahad, K. Chen, Z. Shahpar, S. Talebi, C. Milla, A. Javey, R. W. Davis, Autonomous sweat extraction and analysis applied to cystic fibrosis and glucose monitoring using a fully integrated wearable platform. *Proceedings of the National Academy of Sciences*. **114**, 4625–4630 (2017).

41. H. Y. Y. Nyein, M. Bariya, L. Kivimäki, S. Uusitalo, T. S. Liaw, E. Jansson, C. H. Ahn, J. A. Hangasky, J. Zhao, Y. Lin, T. Happonen, M. Chao, C. Liedert, Y. Zhao, L.-C. Tai, J. Hiltunen, A. Javey, Regional and correlative sweat analysis using high-throughput microfluidic sensing patches toward decoding sweat. *Science Advances*. **5**, eaaw9906 (2019).

42. H. Lin, Y. Zhao, S. Lin, B. Wang, C. Yeung, X. Cheng, Z. Wang, T. Cai, W. Yu, K. King, J. Tan, K. Salahi, H. Hojaiji, S. Emaminejad, A rapid and low-cost fabrication and integration scheme to render 3D microfluidic architectures for wearable biofluid sampling, manipulation, and sensing. *Lab on a Chip*. **19**, 2844–2853 (2019).

43. R. Peng, Z. Sonner, A. Hauke, E. Wilder, J. Kasting, T. Gaillard, D. Swaille, F. Sherman, X. Mao, J. Hagen, R. Murdock, J. Heikenfeld, A new oil/membrane approach for integrated sweat sampling and sensing: sample volumes reduced from μL's to nL's and reduction of analyte contamination from skin. *Lab on a Chip*. **16**, 4415–4423 (2016).

44. J. Kim, A. S. Campbell, B. E.-F. de Ávila, J. Wang, Wearable biosensors for healthcare monitoring. *Nature Biotechnology*. **37**, 389–406 (2019).

45. J. Kim, A. S. Campbell, J. Wang, Wearable non-invasive epidermal glucose sensors: A review. *Talanta*. **177**, 163–170 (2018).

46. M. Vettoretti, G. Cappon, G. Acciaroli, A. Facchinetti, G. Sparacino, Continuous Glucose Monitoring: Current Use in Diabetes Management and Possible Future Applications. *Journal of Diabetes Science and Technology*. **12**, 1064–1071 (2018).

47. E. V. Karpova, E. V. Shcherbacheva, A. A. Galushin, D. V. Vokhmyanina, E. E. Karyakina, A. A. Karyakin, Noninvasive Diabetes Monitoring through Continuous Analysis of Sweat Using Flow-Through Glucose Biosensor. *Analytical Chemistry*. **91**, 3778–3783 (2019).

48. J. Choi, Y. Xue, W. Xia, T. R. Ray, J. T. Reeder, A. J. Bandodkar, D. Kang, S. Xu, Y. Huang, J. A. Rogers, Soft, skin-mounted microfluidic systems for measuring secretory fluidic pressures generated at the surface of the skin by eccrine sweat glands. *Lab on a Chip*. **17**, 2572–2580 (2017).

49. Z. Sonner, E. Wilder, J. Heikenfeld, G. Kasting, F. Beyette, D. Swaile, F. Sherman, J. Joyce, J. Hagen, N. Kelley-Loughnane, R. Naik, The microfluidics of the eccrine sweat gland, including biomarker partitioning, transport, and biosensing implications. *Biomicrofluidics*. **9**, 031301 (2015).

50. Z. Sonner, E. Wilder, T. Gaillard, G. Kasting, J. Heikenfeld, Integrated sudomotor axon reflex sweat stimulation for continuous sweat analyte analysis with individuals at rest. *Lab on a Chip*. **17**, 2550–2560 (2017).

Chapter 3. Extended Non-Invasive Glucose Monitoring in Interstitial Fluid using an Epidermal Biosensing Patch

3.1 Introduction

Enhancing the convenience and reliability of glucose testing have been crucial goals of the management of diabetes mellitus (DM). Despite major advances and significant improvements[1], current devices remain invasive or minimally invasive, consisting of needles[2,3] or monofilaments[4] that can cause discomfort, as well as inconvenience. A sensor that is both non-invasive and wearable can significantly shift patient's receptivity and adherence. Along with medications and lifestyle changes, such reliable, non-invasive sensors could greatly contribute to improved glycemic control, by bolstering patients' engagement and adherence, and in turn leading to decreased risk of complications, as well as enhanced quality of life. Self-monitoring of blood glucose (SMBG) using glucometers has been the standard of care for patient-driven glucose testing since the mid-1980s. [5] However, over the past two decades we have witnessed the introduction of continuous glucose monitoring (CGM) devices that offer real-time measurements. [6] These efforts support the ongoing progress toward the ultimate goal of closed-loop insulin delivery systems.

Launched in 2002, the first wearable, non-invasive commercial device was the Glucowatch Biographer®.[7] This relied on IP for performing repetitive ISF glucose measurements at 20 minutes intervals up to 12 hours. Notable drawbacks included a 2–3-hour warm-up time, skin irritation and automatic shutdown of the device in case of sweating, which led to its retraction from the market[8]. Growing research efforts over the past decade have led to several innovative wearable platforms for non-invasive glucose monitoring. [9] These include contact lenses tears sensors, [10-12] skin-worn microfluidics, [13-16] epidermal biosensing devices[17-21] or mouthguard-based salivary sensors. [22, 23] A recent advance, reported by Bandodkar et. al, involved a single-use tattoo-based epidermal platform that combined IP extraction with amperometric biosensing for replacing fingerstick blood glucose measurements.[24] Another study focused on the fabrication of a 2-piece system, an amperometric biosensor and a paper-based battery for IP extraction. [19] While capable of operating for 5 days, it only provided 1 measurement per day and required removal of the sensor to place the battery for performing 20 minutes IP.

Here, we demonstrate a non-invasive tattoo-based ISF extraction-detection platform for an extended sensing operation time of 8 hours and demonstrates its attractive analytical performance in a clinical investigation involving individuals with diabetes mellitus (DM).

Our goal has been to extend the early disposable skin-worn tattoo IP-biosensor[24] from single-use to prolonged operation while circumventing the problems inherent to the GlucoWatch system[7]. The new platform, shown in **Figure 3.1.1**, couples the iontophoretic and sensing electrodes for the ISF extraction and glucose detection steps, respectively (**Figure 3.1.1A**). The sensing platform adheres to the skin, similar to a temporary tattoo, and is integrated with an electronic board that controls the IP-sensing operation, along with real-time wireless transmission towards extended daily glucose monitoring (**Figure 3.1.1B-C**). The epidermal glucose patch was fabricated by first placing the electrode compartments on a medical adhesive layer, and then covering the sensing and IP electrodes with two hydrogel membranes (**Figure 3.1.1D**). The 3-minutes short iontophoresis step allowed the collection of glucose in the negative terminal of the patch, using a small current of 0.7 mA, corresponding to a current density of 0.27 mA/cm^2 (**Figure 3.1.1F**). This was followed by highly selective amperometric biosensing of the extracted glucose at the GOx-modified Prussian-blue electrode operated at -0.20V. Such IP-extraction/detection operation was repeated every 90 minutes over 8 hours.

Contrary to the GlucoWatch, skin irritation was not observed after such prolonged operation (**Figure 3.1.1G**), reflecting the lower IP current density and lower testing frequency. We also addressed the potential memory effect, originating from the presence of previously extracted glucose[25], by compensating for the corresponding baseline change. This was accomplished by measuring the difference of the currents sampled (Δi) before and after IP (i.e., without and with the glucose extraction, respectively) for each measurement cycle. This current difference represents the actual current signal, associated with the changing glucose concentration (freshly extracted ISF glucose). Compared with the GlucoWatch, the present epidermal sensor provides a shorter warm-up time of 5 minutes and relies on lower IP current density (0.27mA/cm^2 during a shorter IP extraction time of 3 minutes, along with a lower testing frequency at 90 minutes intervals). Clinical trials, carried out in individuals with DM, demonstrated the reliable operation of the new patch over an extended operation, with a close correlation of the ISF and blood glucose levels (**Figure 3.1.1E**). Based on its attractive performance and operational characteristics, this skin-conformal low-cost wireless device holds considerable promise as a personalized non-invasive glucose sensing tool, towards improving the health of diabetes patients by providing better control and prevention of hypoglycemia or hyperglycemia events.

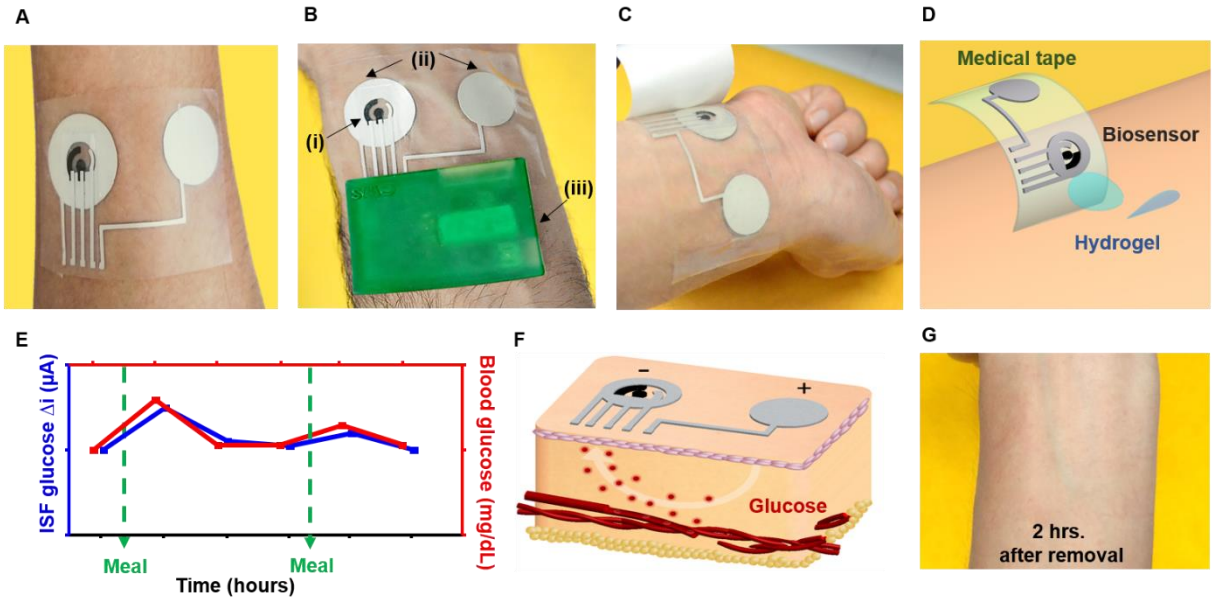

Figure 3.1.1 Concept of continuous glucose monitoring in ISF using a single sensing platform.
A) Illustration of wearable patch on the skin. **B)** Depiction of the complete assembly of the epidermal sensor: (i) Sensor is composed of a 3 electrode system including a Ag/AgCl reference electrode and Prussian blue counter and working electrode for quantification of glucose in the ISF, (ii) Ag/AgCl cathode (Left) and anode (Right) screen printed electrodes transport the glucose to the skin surface in the cathodic compartment by an iontophoresis mechanism. (iii) the integrated electronic board send the data (current) obtained from the electrochemical measurements to a computer for further processing. **C)** Transfer of the epidermal patch on to the skin. **D)** Wearable patch characteristics. The assemble of the device consists on depositing screen printed electrodes on top a medical tape layer followed by the addition of two agarose hydrogel disks on top of each electrode (Anode and Cathode). **E)** Performance of the glucose sensor during a 8 hours study. The line graphic shows the overall change and offset in glucose in blood and ISF during the extended test. **F)** Iontophoresis glucose extraction mechanism. Glucose is difused through the Cathodic section of the wearable patch to further be quantified by the electrochemical biosensor. **G**) Wrist pictures 2 hours after removing the device.

3.2 Experimental section

3.2.1. Chemicals and instruments

Glucose oxidase (GOx) from *Apergillus niger*, Type X-S, Nafion® perfluorinated resin solution, Glutaraldehyde solution, bovine serum albumin (BSA), sodium phosphate monobasic (NaH_2PO_4), sodium phosphate dibasic (Na_2HPO_4), D (+)- glucose, L(+)-ascorbic acid, uric acid, acetaminophen and agarose type IV were obtained from Sigma-Aldrich (St. Louis, MO). All reagents were used without further purification. Silver/silver chloride (Ag/AgCl) ink (E2141 Ercon Inc., Wareham, MA) and Prussian blue (PB) conductive carbon (C2070424P2, Gwent Group, UK) were used in the screen-printing process.

Polydimethylsiloxane (PDMS) silicone from Dow Corning, Sylgard 184, and 3M Medical Tape (#1521) (3M, Maplewood, MN) were used for the fabrication and assembly process of the wearable electrochemical platform.

3.2.2. Electrode fabrication

The integrated system consisted of two isolated parts: an iontophoretic current source and an amperometric sensor. The printed electrode patterns were designed in an AutoCAD 2018 software (Autodesk, San Rafael, CA) and were transferred to stainless steel plates (12×12 inch^2) etched to fabricate a metallic stencil (Metal Etch Services, San Marcos, CA). The electrochemical system, composed of a counter, working and reference electrodes, was screen printed using an MPM-SPM semi-automatic screen printer (Speedline Technologies, Franklin, MA). The iontophoretic electrode design was made using a Cricut Explore Air 2 machine. The screen-printing process consisted of printing first the Ag/AgCl patterns on a Polyethylene Terephthalate (PET) substrate followed by a 10-minutes curing step at 85 °C. Subsequently, the Prussian blue working, and counter electrodes were printed; the curing step was repeated under the same conditions as the Ag/AgCl patterns (**Figure 3.2.2.1**). The iontophoretic electrodes, used for the ISF extraction, consisted of three screen-printed Ag/AgCl layers (cured at 85 °C for 10 minutes separately) on PET substrates. The resulting substrate was then transferred to a Cricut Explorer machine to cut and obtained the anode and cathode electrode areas of 2.57 cm^2 and 3.22 cm^2, respectively.

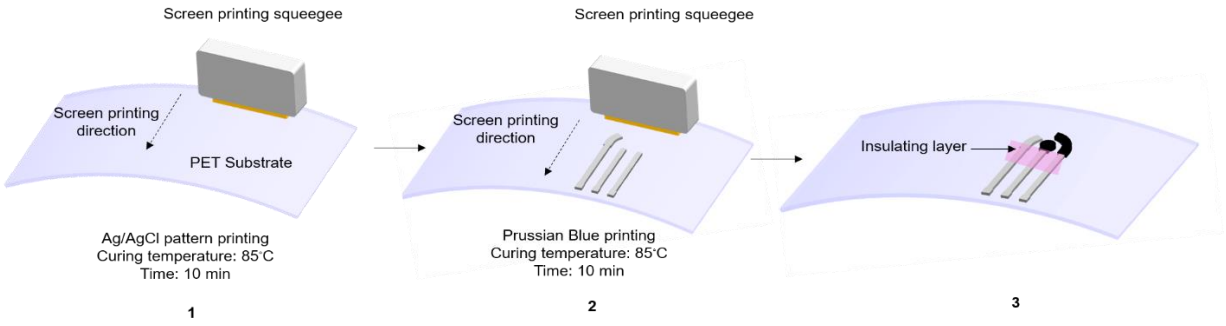

Figure 3.2.2.1. Screen printing process of the electrochemical biosensor.
Step 1: a PET substrate is cut and transfer to the screen-printing machine to print the first layer that corresponds to the Ag/AgCl interconnections and reference electrode. After the printing step was completed, the silver traces were cured at 85°C for 10 minutes. **Step 2:** After the successful printing of the first layer, the second layer which consist of Prussian blue carbon was printed on top of the silver connections. Afterward, the sensor was cured under the same parameters used in Step 1. **Step 3**: Lastly, the sensors were insulated using nail polish by covering the interconnections traces between the Ag/AgCl and Carbon Prussian Blue, this step was crucial to determine the area used for sensing and to avoid overflow of current during the measurements. After the connections were insulated, the sensor was left for drying.

3.2.3. Chemical modification

The Prussian blue working electrode (3 mm diameter disk) was functionalized using a mixture of the enzyme, crosslinker, and negatively charged membrane solutions. This mixture consisted of glucose oxidase (40 mg/mL) solution, Nafion 0.1% w/v and glutaraldehyde 50%, prepared using ratio of 1:1:0.33, respectively. After mixing, a 4 µL aliquot was drop casted on the surface of the working electrode, and the modified sensor was left inside the refrigerator overnight (4°C) for drying and storage until it was used.

3.2.4. Wearable tattoo glucose patch assembly and transfer

After electrode modification, and before transferring the tattoo patch to the body, electrodes were covered with hydrogel layers necessary for the iontophoretic extraction. Fabricating gels with the desired dimensions relied on previously prepared PDMS molds. The molds were fabricated by a mixture of 10:1 ratio of PDMS base and curing agent, respectively. The mixture was then mixed using a SpeedMixer™ (FlackTek Inc, Landrum, SC) at 3000 rpm for 5 minutes. The viscous blend was poured into glass slides (7.5x5 cm) until it reached a thickness of 1 mm. Subsequently, glass slides were placed inside an oven at 120 °C for 5 minutes. PDMS layers were removed from glass slides and circular shapes cuts were made on each layer (Area= 3.22 cm^2) using Cricut Explore air 2 machine. Layers with the final design were placed again in the glass slides for further use as molds.

Hydrogel layers were developed from a solution containing Agarose 3% w/v in 0.1 M potassium phosphate buffer (pH 7.4). The solution was heated at 150°C in constant stir until agarose was completely dissolved and a transparent color was observed. Aliquots of 300 µL were drop casted on the PDMS molds (Area= 3.2 cm^2; thickness=1 mm) and left for cooling. A few minutes later, a solid agarose circular-shaped gel was formed. The solid agarose gels were removed from the mold and kept in a sealed petri dish overnight inside a refrigerator. To improve current permeability through the epidermis, a physical skin treatment was performed before transferring the assembled patch to the skin. For this, a piece of 3M Medical Tape was used to strip the area continuously for 1 minute. According to the literature, such treatment removes the stratum corneum outer layer, which has less water content compared with the inner layers and therefore decreases the skin electric resistance properties. [26] The treated section was then cleaned with soap and sterile alcohol prep pads (MEDca™).

To transfer the sensor to the medical tape, an enzymatically-modified screen-printed electrode was placed on top of a cut piece of 3M Medical Tape (**Figure 3.2.4.1A, i**), followed by placing the iontophoretic cathodic electrode above the screen-printed electrode (**Figure 3.2.4.1A, ii**), with the anodic electrode located 1.5 cm away from the cathodic one (**Figure 3.2.4.1A, iii**). Followed this step, a single piece of agarose hydrogel was placed on top of each electrode and pressed gently for 1 minute to ensure good contact between electrode and hydrogel. Finally, the adhesive surface with the sensor was mounted on the wrist of the individual by removing the protective layer on top of the sensor (**Figure 3.2.4.1A**).

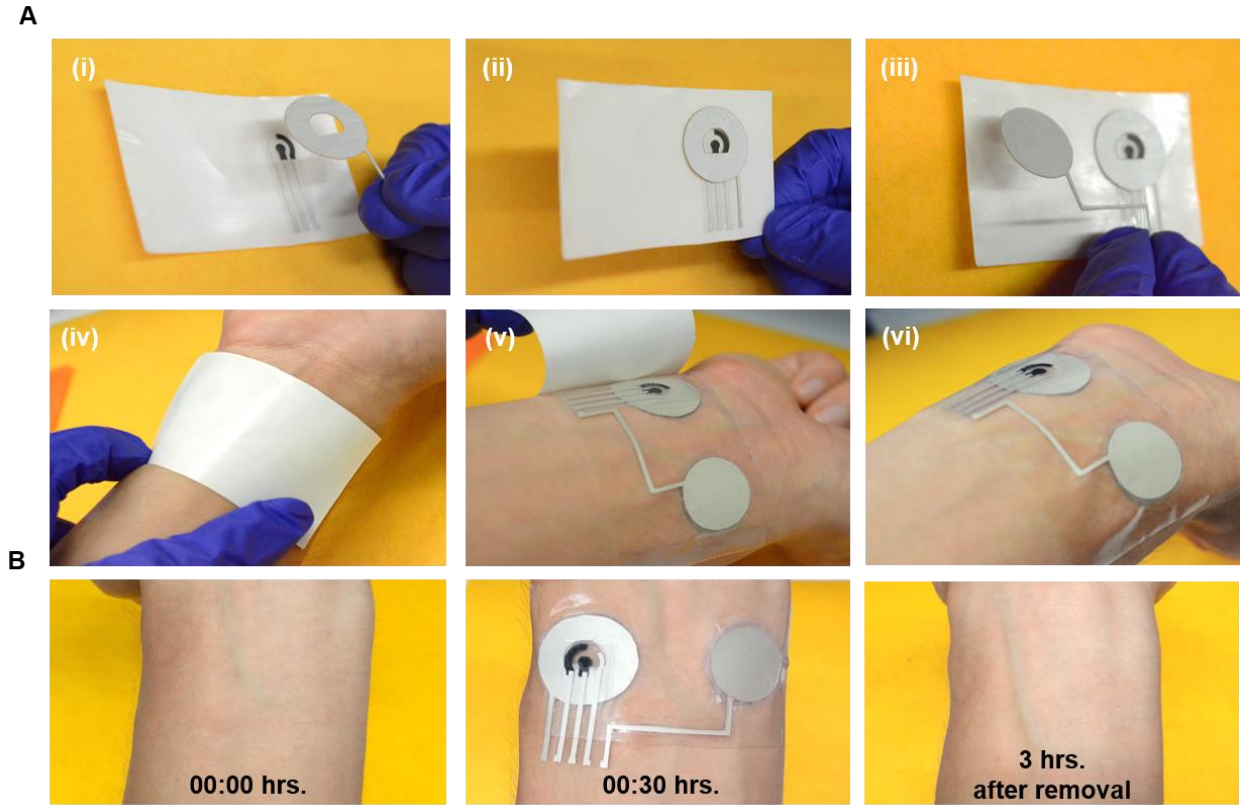

Figure 3.2.4.1 Assemble and transfer process of the ISF glucose wearable patch.
A) The screen-printed electrode system is transferred to a layer of adhesive tape (i). Afterward, the iontophoretic electrodes are placed on top of the adhesive layer, cathode is placed on top of the screen-printed array and anode electrode is set 1.5 cm away from the cathode (ii-iii). Next, a piece of agarose gel is placed on top of each electrode. The transfer process consists of placing the adhesive layer on the skin and removing the top layer of paper from the adhesive surface (iv-vi). **B)** Wrist pictures before (00:00hr), and after (00:30hr) transferring the sensing device onto the skin and 3 hours after removing the device.

3.2.5. Wireless instrumentation electronics

Both the iontophoretic and electrochemical subsystems were powered from a 350mAh lithium polymer battery (Adafruit 2750) and shared a common connection to the sensor. The battery-powered the electronics for multiple hours and contained a circuit to protect the battery from over-discharge. The electronics interface was connected to the sensor with a 17 pin ZIF connector (Molex 200529-0170). Of the 17 pins in the connector, four were used for positive iontophoretic current, 3 for the negative iontophoretic current, and two for each of the working, counter, and reference electrode connections. The remaining pins provided physical isolation between the other pins (**Figure 3.2.5.1**).

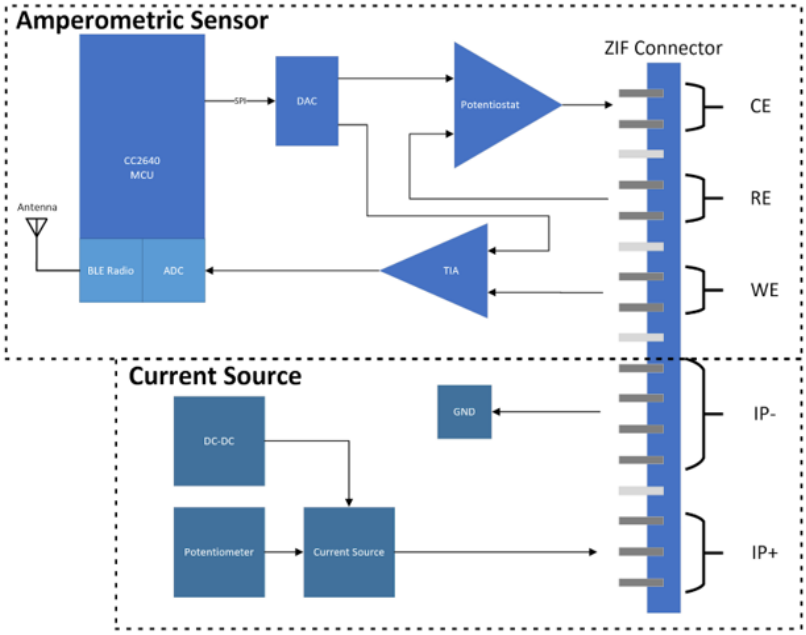

Figure 3.2.5.1. Zip connectors distribution inside the electronic board.
In total, the electronic board consisted of 17 pins to connect the multiple components of the wearable sensor. In the current source section, 4 pins were used for the positive iontophoretic current (IP+, Anode) and 3 for the negative iontophoretic current (IP-, Cathode). In the amperometric sensor section, 2 pins were used for the working electrode (WE), reference electrode (RE) and counter electrode (CE). The remaining pins provided physical isolation between the other pins.

The iontophoretic section of the electronics consists of 3 main components - a DC-DC boost converter (Texas Instruments TPS61040), a constant current source (Texas Instruments LM334MX), and a potentiostat. Together, these components make an adjustable constant current source, which is used for iontophoresis. The current source was set to 700 µA for this experiment.

The amperometric sensing section of the electronics contained DC-DC converters, an MCU with integrated 2.4 GHz radio, a digital-to-analog converter, a potentiostat, and a trans-impedance amplifier. The DC-DC converters are used to regulate the battery voltage. The MCU (Texas Instruments CC2640) is the heart of the sensing section; it is programmed with a firmware that allows amperometric measurements to be taken and sends the results over Bluetooth Low Energy to a companion MATLAB application running on a nearby computer. The MCU also contains an integrated analog-to-digital converter which is used to convert the output of the potentiostat. The digital-to-analog converter (Texas Instruments DAC8563) is used to bias the potentiostat. The potentiostat is implemented using operational amplifiers and is responsible for controlling the potential of the electrochemical cell. The trans-impedance amplifier is also implemented using operational amplifiers. This amplifier converts the current from the electrochemical cell into a voltage that can be measured by the analog-to-digital converter in the MCU.

3.2.6. Electrochemical characterization

The performance of the ISF glucose continuous monitoring patch was first evaluated in vitro using a CH Instruments electrochemical analyzer (model 621A, Austin, TX) in a buffer medium (pH 7.4) under concentration ranges corresponding to glucose ISF. Typically, glucose concentration in blood ranges from 2-40 mM, possessing a wider range compared to the levels in ISF, which can be found from 0.1-6 mM[27]. Therefore, the electrochemical response of the glucose patch was evaluated under this concentration range. Additions of 2 mM from a stock solution of 10 mM glucose were added to an initial volume of 100 µL of 0.1 M PBS buffer (0 mM). After every addition made, the aliquot was mixed 10 times and the solution was kept 1 minute under incubation. Glucose increments were made until reaching a final concentration of 22 mM (**Figure 3.2.6.1A**). After analytical measurements, current responses were used to construct a calibration curve (**Figure 3.2.6.1A, inset**). The electrochemical response of glucose in the presence of relevant potential interfering ISF constituents was also evaluated by comparing the amperometric current obtained by adding successive additions of 10 µM Acetaminophen (AC), Ascorbic acid (AA), Lactate (LA), and Uric acid (UA) (**Figure 3.2.6.1B**). Since the electrochemical sensor performed extended glucose measurements, the sensor stability overtime was also analyzed by running 10 repetitive scans at a fixed concentration of 2 mM glucose (**Figure 3.2.6.1C**).

The relative response (i/i_0*100) of each run was determined by dividing the current of each amperogram (i) by the initial amperometric run (i_0). The resulting number was then multiplied by 100 to acquire the percentage difference. (**Figure 3.2.6.1C, inset**). Before moving to on-body trials on human volunteers, the response of the glucose patch was optimized. For this, the glucose wearable patch was transferred onto the individual's wrist. The iontophoresis procedure was performed using the Autolab type III PGSTAT302N (Metrohm) with NOVA software version 1.11. During this test, 3 parameters were studied to obtain the appropriate conditions for long-time operation. Glucose current difference (calculated by the difference between the amperometric current acquired after and before IP) (Z-axis) was compared by increasing both current intensity (Y-axis) and iontophoresis duration time (X-axis) (**Figure 3.2.6.1D**).

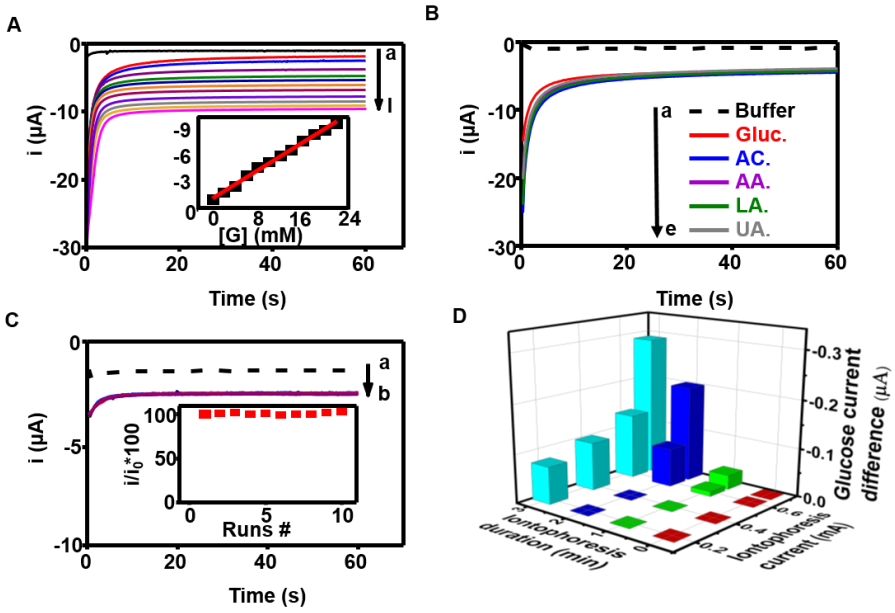

Figure 3.2.6.1. Electrochemical characterization of the ISF glucose sensors: in-vitro testing.
A) Glucose calibration curve. Amperometric response to increasing glucose concentrations from 0 mM (a) to 22 mM (l) in pH 7.4 buffer solution with 2 mM increments. The inset shows the corresponding calibration plot. **B)** Interference study in the presence of 2 mM glucose (a) followed by the additions of 10 μM (b) acetaminophen, (c) Ascorbic acid, (d) Lactate and (e) Uric acid. **C)** Reproducibility of the electrochemical response of 2 mM glucose during 10 repetitive measurements: amperometric response and corresponding plot. The inset shows the relative response (i/i_0*100) in the presence of 2 mM glucose addition after running the repetitive runs. Amperometric measurements were carried out for 60 seconds using a potential step to-0.2 V (vs Ag/AgCl). **D)** Optimization of iontophoresis current (mA) and time based on the glucose current difference collected from the sensor.

3.2.7 Extended on-body monitoring of ISF glucose in human volunteers without DM (8-hour study)

For the first part of the study, four individuals without DM were enrolled. Volunteers fasted 8 hours before the test. Measurements were carried out every 90 minutes, over 8 hours (6 measurements in total) (**Figure 3.2.7.1**). During the entire study, two meals were provided, before the 2^{nd} and 5^{th} measurements. IP was used to extract glucose from ISF in the cathodic compartment (where the electrochemical transducer is located). Continuous monitoring of ISF glucose starts with a "warm-up" step (00:00 hours). This step consists of inducing an iontophoretic current of $0.27 mA/cm^2$ for 5 minutes without any chronoamperometric quantification. It is assumed that the warm-up procedure enhances the current flow through the skin in which facilitates glucose extraction during the following. As mentioned in the introduction, to compensate for the memory effect (due to the previous glucose measurements), a current difference (Δi) before (no glucose extraction) and after IP (with glucose extraction) for every single sampling is determined. After the warm-up step, glucose sensing began without any food consumption by performing chronoamperometry at -0.2 V (vs Ag/AgCl) without IP. To stabilize the sensor, 6 consecutive chronoamperometric runs (1 minute each) were performed until a stable signal was observed during the last scan (6^{th} run). To be consistent throughout the study, 6 chronoamperometric 'conditioning' runs were performed for all measurements, and the 6^{th} scan was used for recording the ISF glucose reading. At the same time and while performing the amperometric measurements before IP, a commercial glucose meter (Accu-Chek Aviva meter) was also used to measure the blood glucose (BG) value 13 minutes before IP, these BG readings were correlated to the sensor response. Such time offset will provide an approximate 13-minute delay between blood glucose and ISF measurements, which accounts for the time lag between ISF and blood glucose concentrations. After the amperometric measurements were concluded, 3 minutes IP was applied to extract glucose from the ISF, followed by the second amperometric reading. At this stage, the two amperometric signals (before and after IP) are used to calculate the current difference (Δi) that reflects the glucose value in the ISF during the first measurement at 00:30 hours. After the recording of the glucose levels in the fasting state, volunteer subjects were provided with a high-calorie meal to ensure a high glucose concentration in the body (2^{nd} measurement). After the food intake, subjects waited 5 minutes to collect the second blood glucose sample. Subsequently, the amperometric measurement was performed.

Next, ISF glucose was extracted by applying IP for 3 minutes (around 12 minutes after food consumption). This was followed by chronoamperometric scans (6 consecutive runs), obtaining the second measurement at 02:00 hours. To examinate the capability of the sensor for continuous measurements, the study continued by two more amperometric readings without any food intake, for the next three hours (one measurement every hour and a half for both ISF glucose and blood glucose). This accounts for the 3rd measurement at 03:30 hours and 4th measurement at 05:00 hours. Next, a second meal was provided 30 minutes upon completing the 4th measurement, followed by blood and amperometric ISF monitoring (5th measurement at 06:30 hours). Continuous monitoring concluded at 08:00 hours by performing a glucose measurement without food intake and 90 minutes after the previous food intake (6th measurement). Once the in-vivo test was concluded, the device was retrieved from the volunteer's wrist followed by a gentle cleaning using alcohol pads in the area where the device was located.

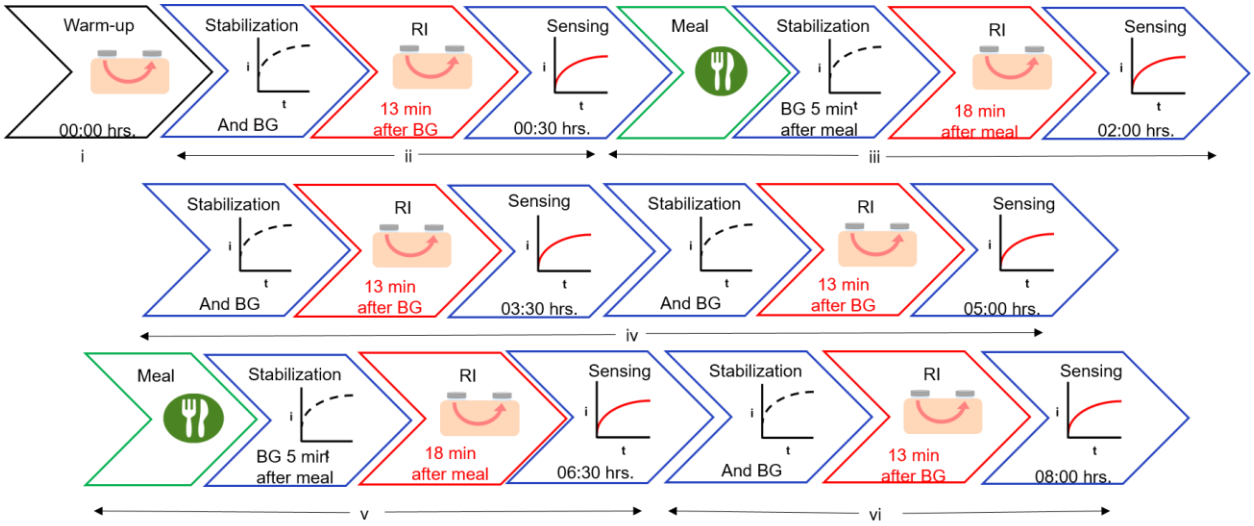

Figure 3.2.7.1. Extended monitoring timeline for an 8-hour performance.
(i) Extended monitoring starts with applying IP for 5 minutes as a warm-up conditioning step. During this step there is no sensing process performed. (ii) After the warm-up step, the sensor was stabilized by running 6 repetitiveve amperometric scans, during this step a blood sample (BG) was taken the record the glucose level in the blood. Next, IP was applied for 3 minutes followed by the sensing step. Here, 6 repetitive amperometric scans were recorded. This step was performed having the individual in a fasting stage. (iii) The third step consist of providing a meal to the individual followed by the same process of stabilization, IP and sensing carried out in (ii). (iv) After the sensor recorded the increase in glucose, 2 recordings without any food consumptions were taken, repeating the same procedure as in (ii). (v) This stage includes a meal and the same procedure applied in stage (iii). Being this, the last recording of ISF and blood glucose with food provided. (vi) In the last measurement, the ISF and blood glucose were monitored repeating the same step as (ii).

3.2.8 Data analysis to correlate blood and ISF glucose measurements

After the in-vivo evaluation of the sensor, the current values obtained during each measurement (before and after IP) were analyzed to calculate the current difference (Δi). This step allowed us to rule out the history effect, by considering the accumulated glucose concentrations during the previous measurements or even generated by sweat perspiration during study. To correlate a set of data obtained from a single individual, the first ISF glucose (first Δi) and blood glucose values recorded at 00:30 and 00:17 hours respectively were normalized. After completing this step, the following blood glucose values were normalized using the same normalization factor. Regarding the clinical studies as described below, for each step, three blood glucose measurements were performed, and the average value was used to normalize the data using the first ISF and average blood glucose from 00:20 and 00:07 hours, respectively.

3.2.9 ISF glucose continuous monitoring on-body evaluation in diabetic human subjects (4-hour study)

The second part of this study included a clinical trial (National Clinical Trial #04088201) conducted at the University of California, San Diego Altman Clinical and Translational Research Institute (UCSD ACTRI). Three individuals with DM (Type 1 or Type 2) were recruited to perform 4-hour glucose monitoring. This study was previously approved by the Human Research Protections Program at UCSD. Volunteers were asked to arrive fasting over the previous night. All participants provided written informed consent to perform the study. Glucose readings were recorded every 1 hour, giving in total 5 measurements. (**Figure 3.2.9.1**).

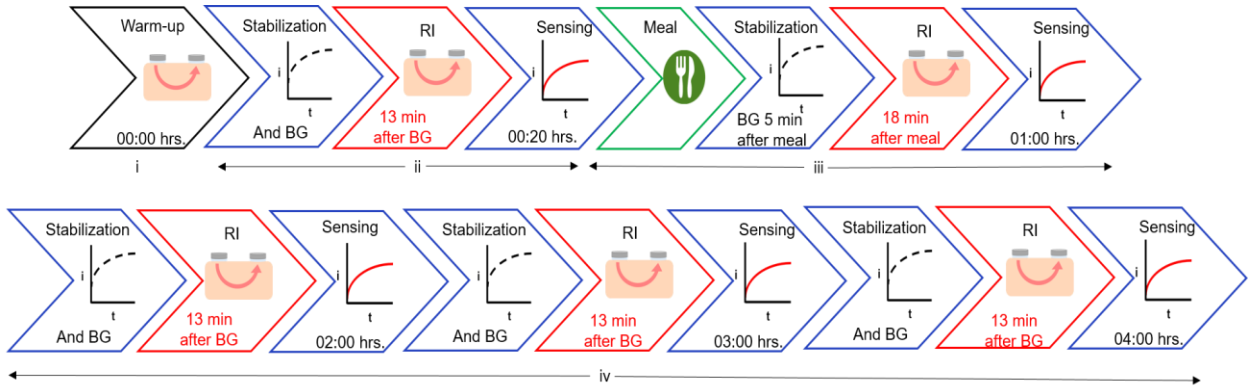

Figure 3.2.9.1. Extended monitoring timeline for a 4-hour performance.
(i) Extended monitoring starts with applying IP for 5 minutes as a warm-up conditioning step. During this step there is no sensing process performed. (ii) After the warm-up step, the sensor was stabilized by running 6 repetitive amperometric scans. Afterward, 3 blood samples (BG) were taken the record the glucose level in the blood. Next, IP was applied for 3 minutes followed by the sensing step, in this step, 6 repetitive amperometric scans were recorded. This step was performed having the individual in a fasting stage. (iii) The third step consist of providing a meal to the individual followed by the same process of stabilization, IP and sensing carried out in (ii). (iv) After the sensor recorded the increase in glucose, three recordings without any food consumptions were taken, repeating the same procedure as in (ii).

Similar measurement procedures as the healthy subjects were conducted. To do so, after the transfer step of the adhesive patch to the individual's wrist, a warm-up step was carried out at 00:00 hours, this step consisted of applying a low current density IP for 5 min without any glucose signal recording. After the warm-up stage was completed, three BG samples were collected by a licensed vocational nurse (LVN) at the clinical institution using a standard hospital grade glucometer. At the same time, the sensor was also stabilized under the same parameters used in the 8-hour studies, and the current value was recorded; glucose was then extracted from the ISF by applying IP for 3 min. Upon completing the IP process, chronoamperometric steps were performed (in a similar way as in the 8-hour trials) and the glucose current response, corresponding to the fasting state (00:20 hours) was obtained (1st measurement). Next, a rich carbohydrate meal (75 grams and 500 cal.) was provided to the volunteers using an approximate time of 30 minutes for the food consumption. After food intake, signal recording took place following the same procedure used in the 1st measurement along with the three BG samples by the LVN. Subsequently, the glucose containing ISF was extracted by IP for 3 min and amperometric measurement was then performed (2nd measurement, 01:00 hours). The next three glucose readings (3rd, 4^{th,} and 5th measurements) were performed without any food consumption at 02:00, 03:00, and 04:00 hours. After concluding the experiment, the device was removed from the patient's wrist, and the skin surface area used for patch attachment was cleaned with alcohol pads.

3.3 Results and discussion

3.3.1 In vitro evaluation and optimization

The analytical performance of the developed tattoo sensor was evaluated first in vitro. To obtain the dynamic range of the sensor towards glucose detection, the corresponding calibration curve was constructed by successive 2 mM glucose additions. As illustrated in the inset of **Figure 3.2.6.1A**, the graphic displays a linear response over the entire 0-22 mM glucose range with a sensitivity (slope) of 0.4 µA/mM. Such wide range covers the physiological range of glucose concentration in the interstitial fluid. [27] Subsequently, the sensor selectivity was evaluated in the presence of potential interferences. As illustrated in **Figure 3.2.6.1B**, such selectivity test involved measurement of the response to 2 mM glucose followed by additions of Acetaminophen, Ascorbic acid, Lactate, and Uric acid. These potential interfering compounds exhibited a negligible effect upon the glucose current signal. Such high specificity reflects the combination of the Prussian-blue-based transducer operated at a low potential of -0.20V, along with the Nafion coating that excludes potential interferences. The glucose sensor showed a reproducible and stable response. The repetitive chronoamperometric runs shown in **Figure 3.2.6.1C,** displayed the current response for 10 successive measurements of 2 mM glucose, indicating negligible current changes (less than 2%) between such repetitive measurements. Monitoring glucose current difference response during on-body experiments, by systematically varying iontophoresis parameters, revealed the optimized iontophoresis current and time of 0.7 mA for 3 minutes, respectively (**Figure 3.2.6.1D**).

In addition, these data illustrated that applying current intensities ranging from 0.2-0.6 mA using a maximum time of 3 minutes, generated small current differences between -0.08 and -0.12 µA. On the other hand, applying a 2-minute iontophoresis time while applying a 0.7 mA current provided signals up to -0.2 µA. Considering the high electrical skin resistance of some individuals and the need for longer iontophoresis time, 3 minutes was then selected as the optimized iontophoresis time.

3.3.2 Extended 8 hours on-body glucose monitoring

After optimizing and evaluating the in-vitro performance of the wearable glucose detection patch, the device was further assessed for on-body experiments on human subjects. Four healthy volunteers (without DM) were recruited to perform 8-hour monitoring tests using a single patch without removing it throughout the complete study (**Figure 3.3.2.1, A-D**). Non-invasive ISF measurements were carried every 90 minutes. During each experiment, the measured ISF glucose concentration was correlated to blood glucose measurements. These data indicated a very good correlation between the ISF and blood glucose measurements. For instance, the glucose levels changed in response to the food consumption, with potential lag times between the blood and ISF concentrations, reflecting the glucose transport from the plasma to the ISF. Typically, blood glucose levels peak approximately 30 minutes within food intake. Therefore, food consumption took place 30 minutes before starting the tests (after meal tests at 02:00 and 6:30 hours). Subsequently, blood samples were obtained 5 minutes after eating and ISF glucose monitoring 18 minutes after eating (accounting for the 3 minutes of glucose extraction). As a result, a time lag of approximately 13 minutes was established between blood and ISF. Such a time gap is similar to the one reported for a CGM device [28].

One point taken into consideration in this part of the study was the time gap (4:30 hours) between both "after meal" tests; this time was selected as the mean time where insulin activity tends to finish. Natural delivered insulin (bolus) can rapidly increase, reaching its peak between 45 minutes to 1 hour, followed by its gradual decrease to the initial state within 2-6 hours. Taking this into account, the second test involving food consumption (6:30 hours) ensured a higher probability to start the measurement with a low insulin activity. [29] A similar trend observed in all four subjects was the higher glucose levels in blood and ISF after meal consumption, compared to the absence of food intake. We attributed this behavior to the regular glucose homeostasis present in healthy individuals. As previous reports demonstrated, blood glucose levels can return to a pre-prandial glucose stage within 2 hours of food consumption. [30] Considering the intermittent time of 90 minutes between glucose measurements, we expected blood and ISF values to be close to the ones acquired in the initial stage of each trial.

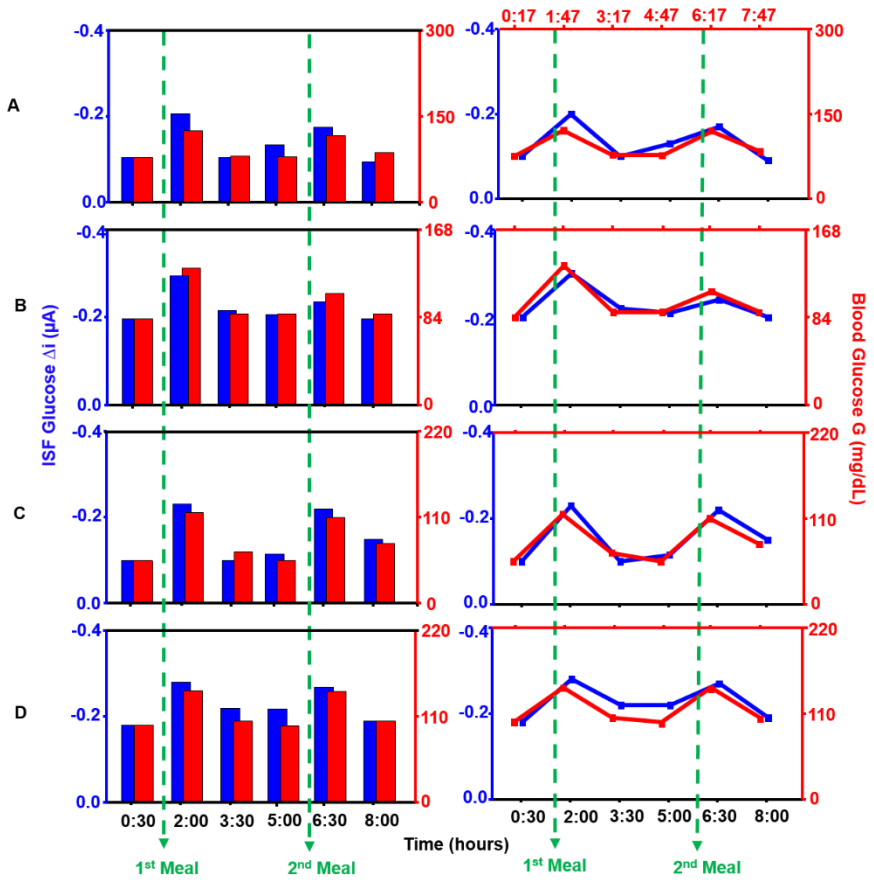

Figure 3.3.2.1 Electrochemical characterization of the ISF glucose sensor for a period time of 8 hours, along with parallel blood measurements.
(**A-D**) Column graphic representation shows the comparison of the normalized ISF glucose (blue bars) and blood glucose (red bars) profiles obtained every 90 minutes. On the right side, the line plot depicts the real offset between the normalized ISF glucose (blue line), and blood glucose (red line) obtained from the time differences each biofluid was monitored. The second horizontal axis included on the upper part of each graphic shows the time of blood glucose sampling, accounting for the 13 minutes delay. ISF glucose measurements were performed with a step potential of -0.2 V (vs Ag/AgCl) and sampling after 60 seconds. The green dotted lines correspond to the two food intakes carried out before the 2nd and 5th measurements.

To prove that glucose differences were due to the food ingestion, we performed control experiments without food ingestion for 4 hours. Such studies did not show any change in the current difference during the whole study (**Figure 3.3.2.2**). The study performed followed the procedure shown in **Figure 3.2.9.1**. Similarly, negligible glucose ISF signals were observed in further control experiments, without the enzymatic recognition layer or without applying IP (**Figure 3.3.2.3** and **Figure 3.3.2.4**).

Overall, these tests demonstrated the reliable performance of the ISF glucose patch. It should be pointed out that the human subjects did not experience any discomfort, while the skin showed no apparent irritation or damage following such prolonged operation of the patch. The latter is clearly indicated from **Figure 3.2.4.1B** which shows images of the skin before such operation and 3 hours after the sensor removal (following the completion of an 8-hour test).

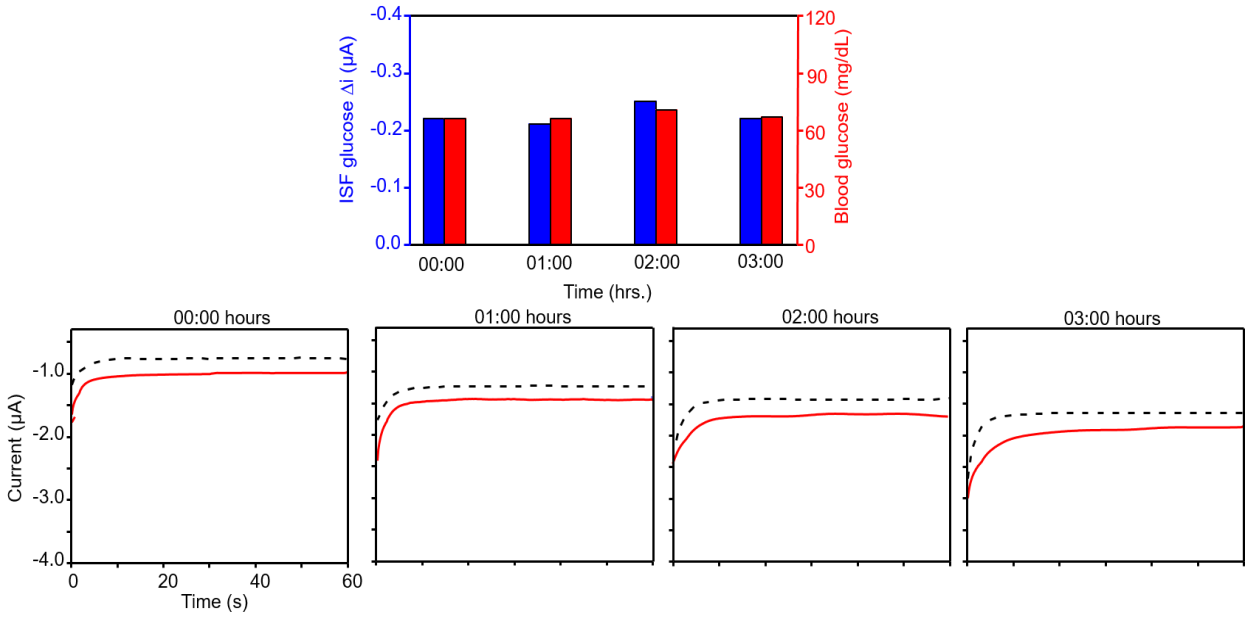

Figure 3.3.2.2. Control experiment without any food consumption.
Bar code graphic. (Top, left) Current different obtained (ISF Glucose Δi) in 4 measurements performed for 03:00 hours. (Top, right) Blood glucose readings taken in 4 measurements performed for 03:00 hours. (bottom) Amperometric scans performed in 1 individual for 3 hours. Amperometric currents obtained in the 6th scan during the stabilization step (black dotted line) and the 6th scan obtained after reccording the ISF glucose (red solid line) obtained by IP were used to calculate the current difference ((ISF Glucose Δi) obtained every hour.

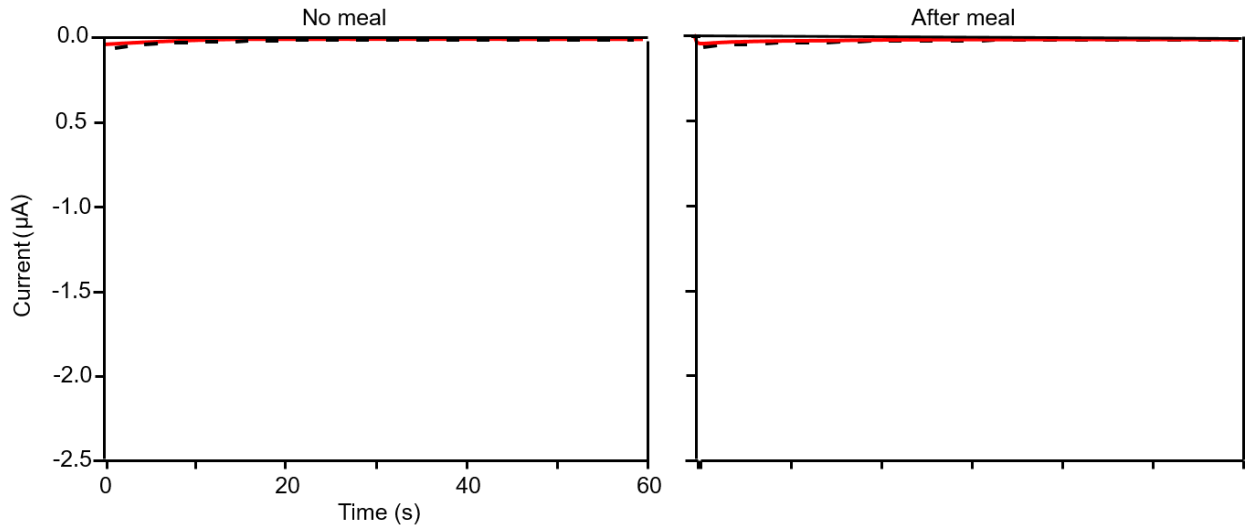

Figure 3.3.2.3. Control experiment without any enzyme layer modification.
Amperometric currents obtained in the 6th scan during the stabilization step (black dotted line) and the 6th scan obtained after recording the ISF glucose (red solid line) obtained by IP. On the left side the currents were obtained before any food consumption (No meal). On the right side, currents were recorded after the individual consumed a high-carbohydrate meal (After meal).

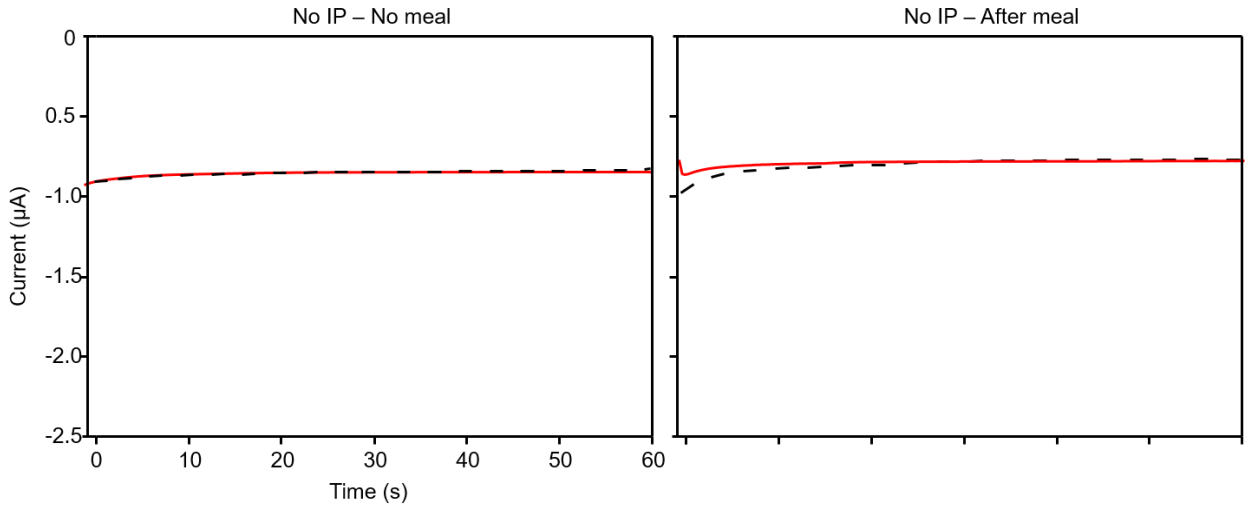

Figure 3.3.2.4. Control experiment without any IP applied for glucose extraction.
Amperometric currents obtained in the 6th scan during the stabilization step (black dotted line) and the 6th scan obtained after waiting 3 minutes without any IP applied (red solid line). On the left side the currents were obtained before any food consumption. On the right side, currents were recorded after having individual consumed a high-carbohydrate meal.

3.3.3. Extended 4 hours on-body glucose monitoring in diabetes patients

After the initial on-body studies performed with healthy subjects demonstrated the ability to closely follow the blood glucose concentrations over an 8-hour long operation without issues of skin irritation or discomfort, the wearable glucose patch was tested in patients with DM wearing the device for 4 hours (**Figure 3.3.3.1**). The recruited individuals from the ACTRI at UC San Diego, underwent identical blood and ISF glucose sample recording protocols as used in the early 8-hour tests, along with similar preparation steps. During these clinical trials we noticed that all blood glucose measurements in the fasting stage were above 100 mg/dL (**Figure 3.3.3.1A-C**), reflecting the higher glucose ISF levels compared with the healthy volunteers without DM (**Figure 3.3.2.1A-D**). In these experiments, the first two measurements (0:20 and 1:00 hours) showed small changes in the glucose levels in both biofluids, with a sharp concentration rise observed 1 hour after the food ingestion (2:00 hours). Good correlations between blood and ISF glucose concentrations are observed also in the DM subjects. Unlike the healthy subjects that display a rise behavior in blood glucose within 30 minutes, type 1 and 2 patients typically show their maximum glucose increase peak between 60-90 minutes after the food consumption.

The slow decrease of glucose after eating (3:00-4:00 hours) was expected, as previous reports suggest that glucose level falls back at a lower rate compared to the increase stage. [31] By comparing bar and line graphics obtained for every subject, a low increase and decrease trend was observed. Overall, the close agreement between the ISF and the corresponding blood readings observed in **Figure 3.3.3.1**, confirmed the reliability of such non-invasive glucose measurements and their potential for extended glucose measurements.

Figure 3.3.3.1. Electrochemical characterization of the ISF Glucose continuous monitoring patch for a period time of 4 hours on 3 Diabetic individuals recruited.
(**A-C, i**) 60 seconds amperometric scans obtained before (black dotted line) and after (red line) IP every hour. In every measurement, the 6th amperometric scan (red line and black dotes line) at 60 seconds is used to calculate the current difference (Δi) that correspond to the glucose concentration in ISF. The green dotted line corresponds to the food intake performed before the 2nd measurement. (**A-C, ii**) The column graphic shows the comparison of the normalized ISF glucose (blue bars), and blood glucose (red bars) profiles obtained every hour. On the right side, the line plot depicts the real offset between the ISF glucose (blue line) and blood glucose (red line) obtained from the time differences each biofluid was monitored. The second horizontal axis included on the upper part of each graph shows the time of blood glucose sampling, accounting for the 13 minutes delay. ISF glucose measurements were performed with a step potential of -0.2 V (vs Ag/AgCl) and sampling after 60 seconds. Green dotted lines correspond to the food intake carried out before the 2nd measurement.

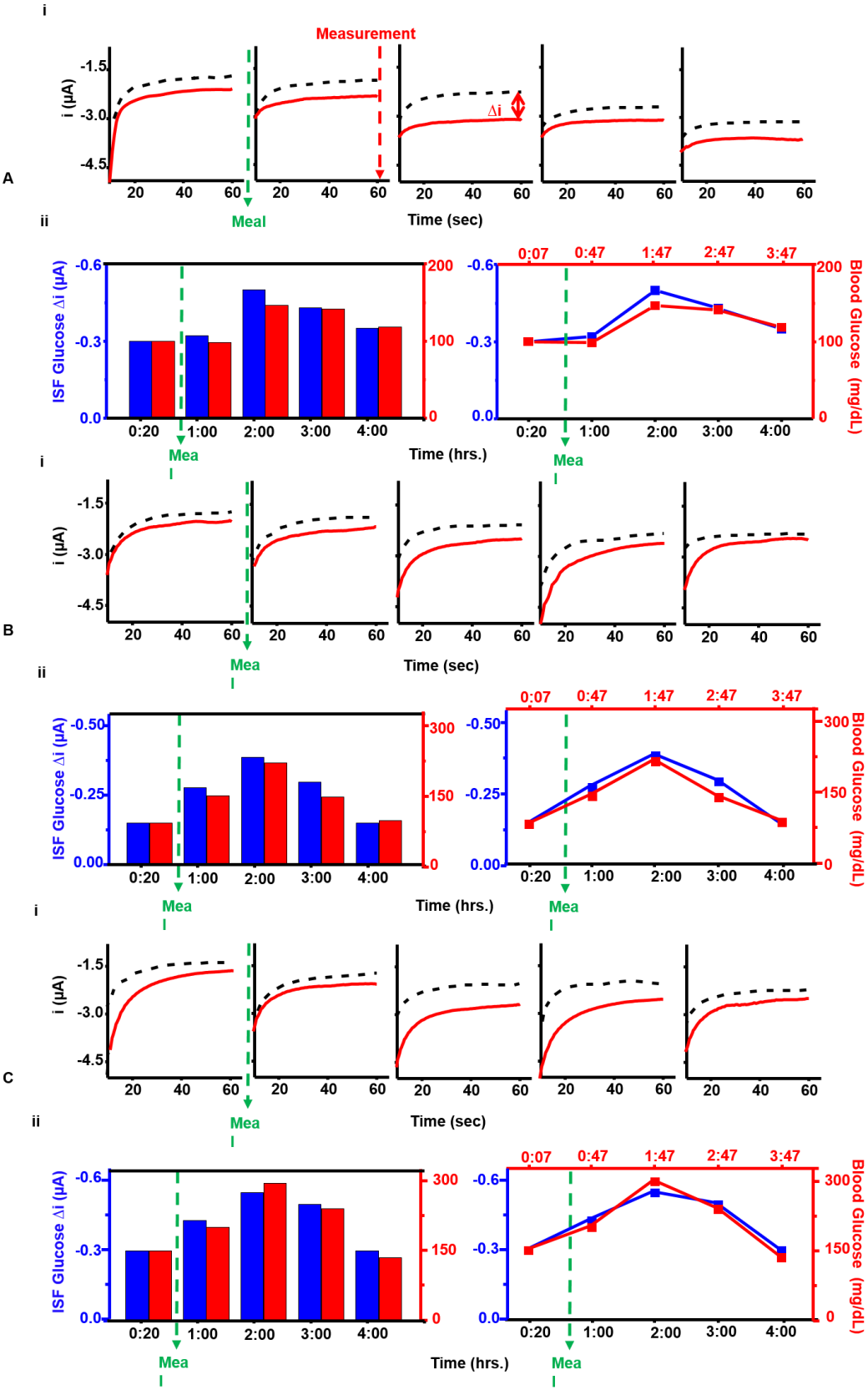
A
i
Measurement
i (μA)
-1.5
-3.0
-4.5
Δi
20
40
60
Meal
Time (sec)
ii
ISF Glucose Δi (μA)
-0.6
-0.3
0.0
200
100
0
0:20
1:00
2:00
3:00
4:00
Mea
Time (hrs.)
0:07
0:47
1:47
2:47
3:47
Blood Glucose (mg/dL)
B
i
i (μA)
-1.5
-3.0
-4.5
Mea
Time (sec)
ii
ISF Glucose Δi (μA)
-0.50
-0.25
0.00
300
150
0
Time (hrs.)
C
i
i (μA)
-1.5
-3.0
-4.5
Mea
Time (sec)
ii
ISF Glucose Δi (μA)
-0.6
-0.3
0.0
300
150
0
Time (hrs.)

3.4. Conclusions

The wearable non-invasive epidermal sensing platform, described in this study, couples iontophoretic ISF extraction with amperometric detection of ISF glucose. We have extended the operation of such RI-sensing tattoos from a single-measurement operation[24] to prolonged on-body operation of up to 8 hours. This was realized by using a lower current density of 0.27mA/cm^2, RI time of 3 minutes, testing frequency every 90 minutes and a short 5 minutes warm up time. Clinical evaluations of the sensor in DM patients for 4 hours, revealed a close correlation between blood and ISF glucose concentrations. Trials carried out in individuals without diabetes illustrated the capability of the sensor of performing reliable measurements of ISF glucose over long time periods, up to 8 hours, while monitoring dynamically changing levels upon food consumption, with no evidence of skin irritation after such long operation. Such flexible disposable system is mass-produced by low-cost screen-printing technology. Future improvements include extending the operation time, increase the testing frequency, and miniaturization of the device. The conformal system could thus pave the way for the development of next-generation non-invasive glucose monitoring devices, combining further technological refinements with enhanced patient convenience and comfort, to facilitate improved glycemic control and compliance. These design and function factors can help engage patients and assist health care professionals to personalize DM management recommendations, which could reduce the risk of complications of DM, and improve clinical outcomes as well as quality of life.

3.5 Acknowledgments

Chapter 3, in full, is a reprint of the material as it appears in E. De la Paz, A. Barfidokht, S. Rios, C. Brown, E. Chao, J. Wang, Extended Noninvasive Glucose Monitoring in the Interstitial Fluid Using an Epidermal Biosensing Patch. *Analytical Chemistry*. **93**, 12767–12775 (2021). The dissertation author was the primary author of this paper.

3.6 References

1. J. Wang, Electrochemical Glucose Biosensors. *Chemical Reviews*. **108**, 814–825 (2008).

2. K. B. Kim, W.-C. Lee, C.-H. Cho, D.-S. Park, S. J. Cho, Y.-B. Shim, Continuous glucose monitoring using a microneedle array sensor coupled with a wireless signal transmitter. *Sensors and Actuators B: Chemical*. **281**, 14–21 (2019).

3. W. C. Lee, K. B. Kim, N. G. Gurudatt, K. K. Hussain, C. S. Choi, D. S. Park, Y.-B. . Shim, Comparison of enzymatic and non-enzymatic glucose sensors based on hierarchical Au-Ni alloy with conductive polymer. *Biosensors and Bioelectronics*. **130**, 48–54 (2019).

4. E. Oppel, S. Kamann, F. Reichl, C. Högg, The Dexcom glucose monitoring system—An isobornyl acrylate-free alternative for diabetic patients. *Contact Dermatitis*. **81**, 32–36 (2019).

5. J. D. Newman, A. P. F. Turner, Home blood glucose biosensors: a commercial perspective. *Biosensors and Bioelectronics*. **20**, 2435–2453 (2005).

6. W. Villena Gonzales, A. Mobashsher, A. Abbosh, The Progress of Glucose Monitoring—A Review of Invasive to Minimally and Non-Invasive Techniques, Devices and Sensors. *Sensors*. **19**, 800 (2019).

7. M. J. Tierney, J. A. Tamada, R. O. Potts, L. Jovanovic, S. Garg, Clinical evaluation of the GlucoWatch® biographer: a continual, non-invasive glucose monitor for patients with diabetes. *Biosensors and Bioelectronics*. **16**, 621–629 (2001).

8. S. K. Vashist, Non-invasive glucose monitoring technology in diabetes management: A review. *Analytica Chimica Acta*. **750**, 16–27 (2012).

9. J. Kim, A. S. Campbell, J. Wang, Wearable non-invasive epidermal glucose sensors: A review. *Talanta*. **177**, 163–170 (2018).

10. J. Kim, M. Kim, M.-S. Lee, K. Kim, S. Ji, Y.-T. Kim, J. Park, K. Na, K.-H. Bae, H. Kyun Kim, F. Bien, C. Young Lee, J.-U. Park, Wearable smart sensor systems integrated on soft contact lenses for wireless ocular diagnostics. *Nature Communications*. **8**, 1–8 (2017).

11. J. Park, J. Kim, S.-Y. Kim, W. H. Cheong, J. Jang, Y.-G. Park, K. Na, Y.-T. Kim, J. H. Heo,

C. Y. Lee, J. H. Lee, F. Bien, J.-U. Park, Soft, smart contact lenses with integrations of wireless circuits, glucose sensors, and displays. *Science Advances*. **4**, eaap9841 (2018).

12. F. J. Ascaso, V. Huerva, Noninvasive Continuous Monitoring of Tear Glucose Using Glucose-Sensing Contact Lenses. *Optometry and Vision Science*. **93**, 426–434 (2016).

13. A. Martín, J. Kim, J. F. Kurniawan, J. R. Sempionatto, J. R. Moreto, G. Tang, A. S. Campbell, A. Shin, M. Y. Lee, X. Liu, J. Wang, Epidermal Microfluidic Electrochemical Detection System: Enhanced Sweat Sampling and Metabolite Detection. *ACS Sensors*. **2**, 1860–1868 (2017).

14. J. Sheng, L. Zhang, J. Lei, H. Ju, Fabrication of tunable microreactor with enzyme modified magnetic nanoparticles for microfluidic electrochemical detection of glucose. *Analytica Chimica Acta*. **709**, 41–46 (2012).

15. S. Gu, Y. Lu, Y. Ding, L. Li, H. Song, J. Wang, Q. Wu, A droplet-based microfluidic electrochemical sensor using platinum-black microelectrode and its application in high sensitive glucose sensing. *Biosensors and Bioelectronics*. **55**, 106–112 (2014).

16. L. Cao, G.-C. Han, H. Xiao, Z. Chen, C. Fang, A novel 3D paper-based microfluidic electrochemical glucose biosensor based on rGO-TEPA/PB sensitive film. *Analytica Chimica Acta*. **1096**, 34–43 (2020).

17. L. Lipani, B. G. R. Dupont, F. Doungmene, F. Marken, R. M. Tyrrell, R. H. Guy, A. Ilie, Non-invasive, transdermal, path-selective and specific glucose monitoring via a graphene-based platform. *Nature Nanotechnology*. **13**, 504–511 (2018).

18. X. Xuan, H. S. Yoon, J. Y. Park, A wearable electrochemical glucose sensor based on simple and low-cost fabrication supported micro-patterned reduced graphene oxide nanocomposite electrode on flexible substrate. *Biosensors and Bioelectronics*. **109**, 75–82 (2018).

19. Y. Chen, S. Lu, S. Zhang, Y. Li, Z. Qu, Y. Chen, B. Lu, X. Wang, X. Feng, Skin-like biosensor system via electrochemical channels for noninvasive blood glucose monitoring. *Science Advances*. **3**, e1701629 (2017).

20. Q. Xue, Z. Li, Q. Wang, W. Pan, Y. Chang, X. Duan, Nanostrip flexible microwave enzymatic biosensor for noninvasive epidermal glucose sensing. *Nanoscale Horizons*. **5**, 934–943 (2020).

21. A. Wiorek, M. Parrilla, M. Cuartero, G. A. Crespo, Epidermal Patch with Glucose Biosensor: pH and Temperature Correction toward More Accurate Sweat Analysis during Sport Practice. *Analytical Chemistry*. **92**, 10153–10161 (2020).

22. T. Arakawa, Y. Kuroki, H. Nitta, P. Chouhan, K. Toma, S. Sawada, S. Takeuchi, T. Sekita, K. Akiyoshi, S. Minakuchi, K. Mitsubayashi, Mouthguard biosensor with telemetry system for monitoring of saliva glucose: A novel cavitas sensor. *Biosensors and Bioelectronics*. **84**, 106–111 (2016).

23. L. F. de Castro, S. V. de Freitas, L. C. Duarte, J. A. C. de Souza, T. R. L. C. Paixão, W. K. T. Coltro, Salivary diagnostics on paper microfluidic devices and their use as wearable sensors for glucose monitoring. *Analytical and Bioanalytical Chemistry*. **411**, 4919–4928 (2019).

24. A. J. Bandodkar, W. Jia, C. Yardımcı, X. Wang, J. Ramirez, J. Wang, Tattoo-Based Noninvasive Glucose Monitoring: A Proof-of-Concept Study. *Analytical Chemistry*. **87**, 394–398 (2014).

25. J. Kim, J. R. Sempionatto, S. Imani, M. C. Hartel, A. Barfidokht, G. Tang, A. S. Campbell, P. P. Mercier, J. Wang, Simultaneous Monitoring of Sweat and Interstitial Fluid Using a Single Wearable Biosensor Platform. *Advanced Science*. **5**, 1800880 (2018).

26. H. S. Gill, S. N. Andrews, S. K. Sakthivel, A. Fedanov, I. R. Williams, D. A. Garber, F. H. Priddy, S. Yellin, M. B. Feinberg, S. I. Staprans, M. R. Prausnitz, Selective removal of stratum corneum by microdermabrasion to increase skin permeability. *European journal of pharmaceutical sciences : official journal of the European Federation for Pharmaceutical Sciences*. **38**, 95–103 (2009).

27. G. M. Steil, K. Rebrin, F. Hariri, S. Jinagonda, S. Tadros, C. Darwin, M. F. Saad, Interstitial fluid glucose dynamics during insulin-induced hypoglycaemia. *Diabetologia*. **48**, 1833–1840 (2005).

28. W. K. Ward, J. M. Engle, D. Branigan, J. E. Youssef, R. G. Massoud, J. R. Castle, The effect of rising vs. falling glucose level on amperometric glucose sensor lag and accuracy in Type 1 diabetes. *Diabetic medicine : a journal of the British Diabetic Association*. **29**, 1067–1073 (2012).

29. A. D. Sanlioglu, H. A. Altunbas, M. K. Balci, T. S. Griffith, S. Sanlioglu, Clinical utility of insulin and insulin analogs. *Islets*. **5**, 67–78 (2013).

30. R. A. Rizza, Pathogenesis of Fasting and Postprandial Hyperglycemia in Type 2 Diabetes: Implications for Therapy. *Diabetes*. **59**, 2697–2707 (2010).

31. S. Daenen, A. Sola-Gazagnes, J. M'Bemba, C. Dorange-Breillard, F. Defer, F. Elgrably, E. Larger, G. Slama, Peak-time determination of post-meal glucose excursions in insulin-treated diabetic patients. *Diabetes & Metabolism*. **36**, 165–169 (2010).

Chapter 4. An epidermal patch for the simultaneous monitoring of haemodynamic and metabolic biomarkers

4.1 Introduction

Intertwined with concepts of telehealth, internet of medical things, and precision medicine, wearable sensors offer attractive features to actively and remotely monitor physiological parameters. Wearable sensors can generate data continuously without causing any discomfort[1,2] or interruptions to daily activity, thus enhancing wearer's self-monitoring compliance and improving patient care quality.[2–4] The monitoring of physical parameters, such as electrocardiogram (ECG)[5–7] and blood pressure (BP),[8–10] and of biochemical parameters, such as glucose,[11–15] using non-invasive wearable sensors has been reported. Recent efforts have led to the integration of physical and chemical sensors into a single wearable device, such as sensors for ECG with lactate[16] or glucose[17] for monitoring athlete's performance, and temperature with metabolites and electrolytes for signal calibration.[12,18] Yet, to the best of our knowledge, the in-depth study of the correlation of cardiovascular parameters, particularly BP and heart rate (HR), with biomarker levels using an integrated hybrid wearable sensor, remains unexplored.

BP and HR, two of the most important vital signs, can dynamically and directly reflect the physiological status of the body. These cardiovascular parameters can be affected by fluctuations of various biomarker concentrations originated from activities, such as movement, stress, or intake of food, drinks, and drugs. Multimodal BP-chemical sensing could thus have a tremendous clinical value, especially for people with underlying health conditions, such as the elderlies, obese individuals, diabetic and cardiovascular patients, as their physiological response to normal day-to-day activities might differ from healthy people. Further, the prevention, diagnosis, and treatment of many diseases can greatly benefit from the simultaneous monitoring of cardiovascular parameters and biomarker levels. These include acute and deadly septic shock, which commonly involves sudden drops in BP accompanied by rapidly increasing blood lactate levels[19] and hypo/hyperglycemia-induced hypo/hypertension which increases the risks of stroke, cardiac diseases, retinopathy, and nephropathy in diabetic patients.[20–23] The recent global pandemic has also highlighted the urgent needs for remote self-monitoring devices, with particular attention to the management of high BP and diabetes, which are the major factors in the deaths of COVID-19 patients.[24]

A comprehensive cardiovascular/biomarker self-monitoring platform would enhance users' self-awareness to their health conditions, and alert them and their caregivers to the occurrence of abnormal physiological changes.

Herein, we present for the first time, a conformal, stretchable, and integrated wearable sensor that can simultaneously monitor BP, HR, and levels of glucose, lactate, caffeine, and alcohol, toward dynamic and comprehensive health self-monitoring. We use ultrasonic transducers for monitoring the BP and HR, and electrochemical sensors for measuring the levels of biomarkers. Through strategic material selection, layout design, and fabrication innovation, we integrated rigid and soft sensor components, namely customized piezoelectric lead zirconate titanate (PZT) ultrasound transducers and printed polymer composites via innovative solvent-soldering process, into a single wearable conformal platform with high mechanical resiliency and free of sensor crosstalk. Such rational design overcomes engineering challenges related to the integration of the different sensing modalities and materials to allow real-time monitoring of cardiovascular parameters and biomarker levels, in connection to parallel sampling of the interstitial fluid (ISF) and sweat biofluids. The resulting epidermal hybrid device can emit ultrasonic pulses and sense echoes from arteries, while stimulating sweat and extracting ISF through iontophoresis (IP), allowing simultaneous measurements of BP and HR, along with multiple biomarkers in these biofluids. We carried out on-body trials with multiple human subjects experiencing diverse activities and stimuli (exercising, having alcohol, food, and caffeine) (**Figure 4.1.1d**). The correlations between metabolic variations and hemodynamic activities, under these stimuli, were monitored and evaluated. The improved sensor assembly process, leveraging the SEBS-based stretchable materials, allows the fast and reliable fabrication of a stretchable and conformal epidermal sensor for simultaneous acoustic and electrochemical sensing. Such device offers (i) comprehensive tracking of the effect of daily activities and stimuli upon the users' physiological status, and (ii) enables the collection of previously unavailable data towards understanding of the body response to such stimuli, while addressing the critical post-pandemic needs for remote telemetric patient monitoring.

The multimodal sensing platform is depicted in **Figure 4.1.1.1a**. Styrene-ethylene-butylene-styrene block copolymer (SEBS) was used as the stretchable and conformal substrate to support the electrodes and connections printed with customized inks (**Figure 4.1.1e**). The stretchable substrate and inks allow the high conformity, flexibility (Figure 4.1.**1f-i**) and stretchability (**Figure 4.1.1f-ii**) required for wearable devices. The BP sensor consists of an array of eight piezoelectric transducers, which are aligned with the carotid artery upon applying on the neck to obtain optimal ultrasonic signals. During sensing, the piezoelectric transducers were activated with electrical pulses, transmitting ultrasound beams to the artery, and the time of flight of the echoes from the anterior and the posterior walls of the artery was analyzed to gauge the dilation and contraction of arteries (Figure 4.1.**1c**, **h**). The chemical sensing has been realized through non-invasive sweat stimulation (via transdermal pilocarpine delivery) at the IP anode, alongside with ISF extraction at the IP cathode. (Figure 4.1.**1b**). Chronoamperometry (CA) was used for electrochemical detection of the hydrogen peroxide product of the glucose oxidase (GOx), lactate oxidase (LOx), and alcohol oxidase (AOx) enzymatic reactions, while differential pulse voltammetry (DPV) was used for the detection of caffeine.

Figure 4.1.1 Design and Mechanism of the stretchable integrated blood pressure-chemical sensing patch.
a, A photo image of the sensor on body. **b**, Illustration of the sensor's acoustic and electrochemical sensing components along with hydrogel for sweat stimulation and ISF extraction. **c**, Acoustic sensing and iontophoresis mechanism of the integrated sensor. The transducer applies ultrasound pulses which generate echoes from the anterior and posterior walls of the artery. Chemical sensing starts with applying an iontophoretic current from a positive terminal (anode +) to a negative terminal (cathode -) that allows the electro-repulsive delivery of a sweat stimulating molecule P+ (Pilocarpine nitrate). After pilocarpine delivery, stimulated sweat containing biomarkers (such as lactate, caffeine, and alcohol) is collected and quantified in the left side of the device. The iontophoretic current leads to osmotic flow of biomarkers (such as glucose) from the interstitial fluid to the skin surface, allowing its collection and analysis on the right side of the sensor. **d**, Schematic showing the different daily activities inputs performed by an individual and the corresponding biomarkers (alcohol, caffeine, lactate, and glucose) followed by the effect on the individual´s system (body response). The inputs are transduced and outputted as BP, HR and electrochemical signals by the device reflecting the body's physiological status. **e,** Layer-by-layer layout of the integrated sensor. **f,** Photos of the sensor under **i**, bending and **ii**, stretching. **g**, Mechanisms of the electrochemical sensors. **i**, amperometric measurements using enzyme-based sensors. The Prussian blue (PB) working electrode was modified either with the LOx, GOx or AOx redox enzymes, allowing the biocatalytic oxidation of lactate, glucose or alcohol molecules to pyruvate, gluconic acid or acetaldehyde (product) respectively, along with the production of hydrogen peroxide. The typical electrochemical reduction of the liberated hydrogen peroxide (H_2O_2) to hydroxyl ions (OH^-) (Left scheme) was performed in PBS pH 7.4 by applying a potential of -0.2 V. An increase of negative current is observed by the increase in concentration of chemical analyte (Right scheme). **ii**, caffeine non-enzymatic measurements. During the sensing process, caffeine was oxidized which resulted in the production of uric acid analog molecules and electrons (Left scheme). A carbon electrode modified with multiwall carbon nanotubes (MWCNT) allowed the pulse-voltammetric detection of caffeine following 30 s accumulation at -1.2 V and scanning between +0.5 V and +1.5 V; E_{step}: 0.004 V; E_{pulse}: 0.05 V; t_{pulse}: 0.05 s; scan rate: 0.02 V/s. By increasing the concentration of caffeine, an increasing oxidation signal is observed (Right scheme). **h,** Signal generation mechanism of the ultrasound transducer. The pulsed ultrasound signal from the transducer is reflected from the anterior and the posterior walls of the artery and collected by the transducer. Signal processing of the ultrasound signal. The time of flight (TOF) of the reflected echo can be converted into BP via established transfer functions.

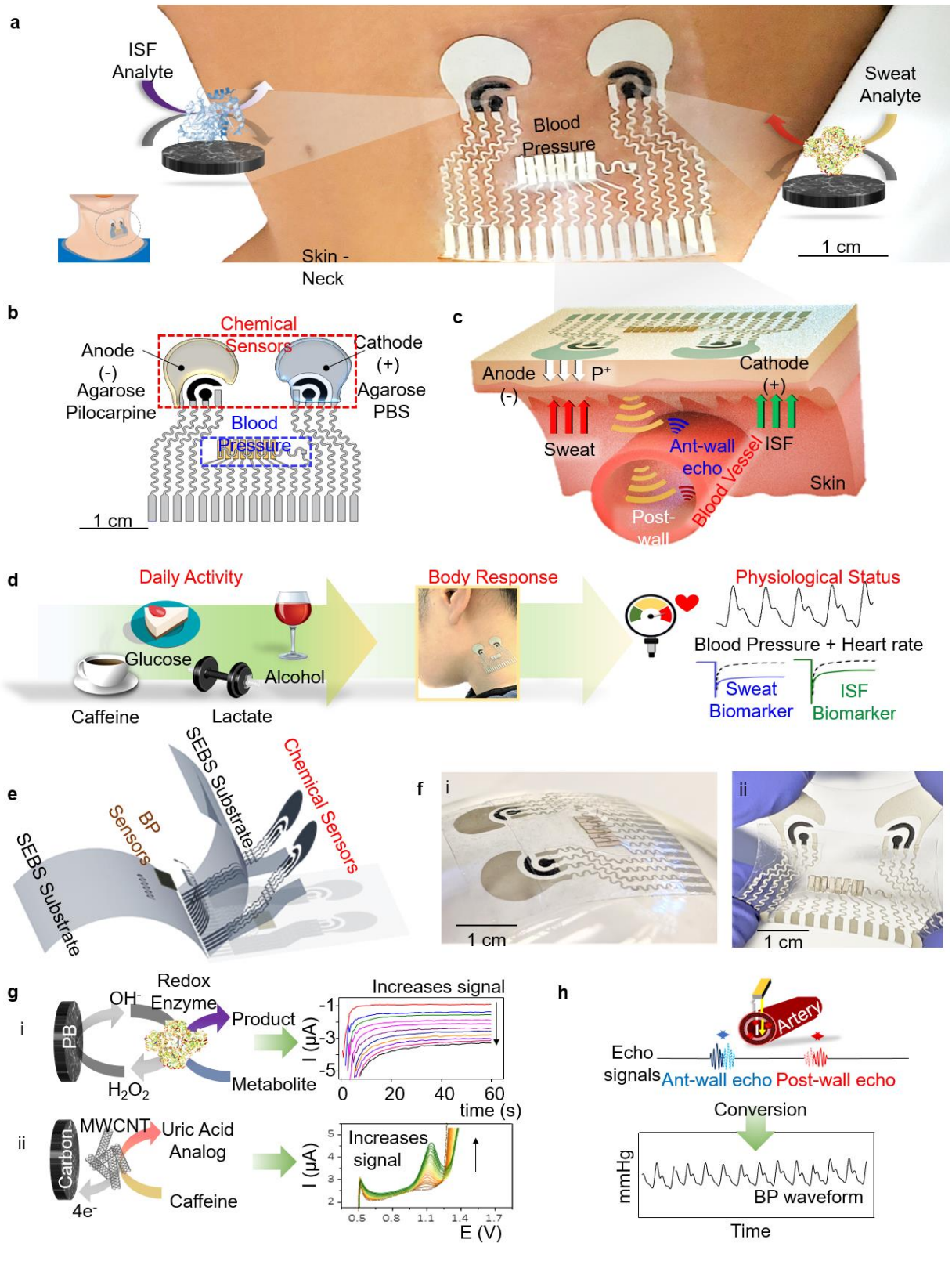
a
ISF
Analyte
Sweat
Analyte
Blood
Pressure
Skin -
Neck
1 cm
b
Chemical
Sensors
Anode
(-)
Agarose
Pilocarpine
Cathode
(+)
Agarose
PBS
Blood
Pressure
1 cm
c
Anode
(-)
P+
Cathode
(+)
Sweat
Ant-wall
echo
ISF
Blood Vessel
Skin
Post-
wall
d
Daily Activity
Body Response
Physiological Status
Glucose
Alcohol
Caffeine
Lactate
Blood Pressure + Heart rate
Sweat
Biomarker
ISF
Biomarker
e
SEBS Substrate
BP
Sensors
SEBS Substrate
Chemical Sensors
f
i
1 cm
ii
1 cm
g
i
Redox
Enzyme
OH-
PB
Product
Metabolite
H2O2
Increases signal
I (μA)
-1
-3
-5
0
20
40
60
time (s)
ii
MWCNT
Uric Acid
Analog
Carbon
4e-
Caffeine
Increases
signal
I (μA)
5
4
3
2
0.5
0.8
1.1
1.4
1.7
E (V)
h
Artery
Echo
signals
Ant-wall echo
Post-wall echo
Conversion
mmHg
BP waveform
Time

4.2 Experimental section

4.2.1 Materials and reagents

Chitosan, acetic acid, bovine serum albumin (BSA), L-lactic acid, sodium phosphate monobasic (NaH_2PO_4), sodium phosphate dibasic (Na_2HPO_4), D(+)-glucose, glucose oxidase (GOx) from Aspergillus niger type X-S (EC 1.1.3.4), Nafion®, agarose, pilocarpine nitrate, Prussian blue (soluble), toluene, ethanol, and silver flakes were obtained from Sigma-Aldrich (St. Louis, MO). Graphite powder was purchased from Acros Organics (USA). Lactate oxidase (LOx) (activity 101 U mg^{1}) was purchased from Toyobo Corp. (Osaka, Japan). SEBS (G1645) was received from Kraton Corporation (Houston TX, USA) while Ecoflex® 00-30 was purchased from Smooth-on Inc. (Easton PA, USA). Super-P carbon black was obtained from MTI Corporation (Richmond, CA, USA). The ultrasound gel pad (AQUAFLEX®) was purchased from Parker Laboratories Inc. (Fairfield, NJ, USA). All reagents were used without further purification.

4.2.2. Sensor Fabrication, Assembly and Electrode Modification

The screen-printing was carried out using a semi-automatic MPM-SPM printer (Speedline Technologies, Franklin, MA) and custom stainless-steel stencils developed using AutoCAD software (Autodesk, San Rafael, CA) and produced by Metal Etch Services (San Marcos, CA), with dimensions of 12 in × 12 in and 125 µm thickness. The viscus SEBS resin was prepared by dispersing SEBS beads in toluene with a weight ratio of 1: 2. The mixture was left on a linear shaker (Scilogex, SK-L180-E) overnight or until the mixture became transparent and homogeneous. A PET film with non-stick coating was used as the temporary casting substrate, and a doctor blade set at 1 mm height was used to cast the SEBS resin into a sheet on the PET substrate. The cast resin was firstly dried in ambient environment for 1 h, followed by curing in a conventional oven at 80 °C for additional 1 h to remove the excess solvent. The transparent, uniform SEBS film was peeled off from the PET substrate for subsequent sensor fabrication. The formulation of the stretchable silver ink is based on early reports.[1] The ink was synthesized by mixing silver flakes, toluene, and SEBS, in a weight ratio of 4: 2.37: 0.63, in a dual asymmetric centrifugal mixer (Flacktek Speedmixer, DAC 150.1 KV-K) with a speed of 1800 RPM for 10 min or until obtaining a homogeneous ink. The stretchable PB ink was synthesized by mixing super-P carbon black, graphite powder, PB, SEBS and toluene, in a weight ratio of 0.5: 3: 1: 1.26: 4.74, in the mixer at 2150 RPM for 10 min or until the ink was homogeneous.

Before printing the stretchable inks, the ink viscosity was analyzed visually and, if necessary, (~200 µL) toluene was added and the ink was centrifuged before use. The electrodes were printed layer-by-layer as illustrated in (**Figure 4.2.2.1**). Bulk PZT was used for ultrasound transducers, which were diced (Disco Automatic Dicing Saw DAD3220) into 0.8 mm by 3 mm rectangular-shaped pixels and sandwiched by two layers of stretchable silver inks as electrodes.

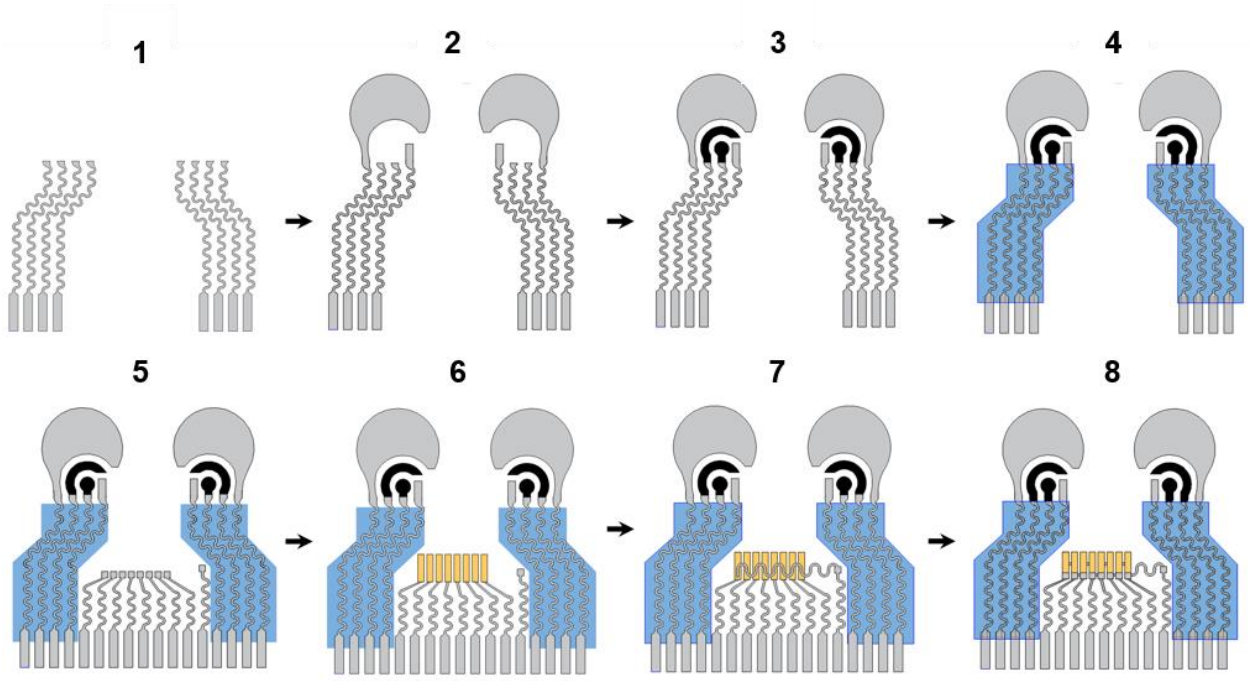

Figure 4.2.2.1. Layer-by-layer printing and assembling steps of the integrated sensor.
Stretchable silver and PB ink were used to print the pattern over the SEBS substrate. Step 1: Printing the stretchable serpentine interconnection using the silver ink. Step 2: Printing of the IP electrodes and the reference electrodes using the silver ink. Step 3: Printing the the counter (curved) and working electrodes (round) using the PB ink. Step 4: Printing an insulating layer to define the working electrode area and insulate the interconnections using the SEBS resin. Step 5: Flip the SEBS substrate backside up. Print the serpentine interconnects for the transducers and ground using the silver ink. Step 6: Solvent solder the transducer chips onto the silver interconnects. Step 7: Solvent solder the ground to the other side of the transducers and connect it to the reserved ground interconnect. Step 8: Finished. Ready for sensor modifications.

The connection between the transducers and the silver traces was realized by adding a toluene droplet to the printed silver traces and placing the transducers on the softened ink. After attaching the PZT transducers, the screen-printed ground connection was placed on the sensor by dissolving the printed traces in a similar fashion (**Figure 4.2.2.2**)

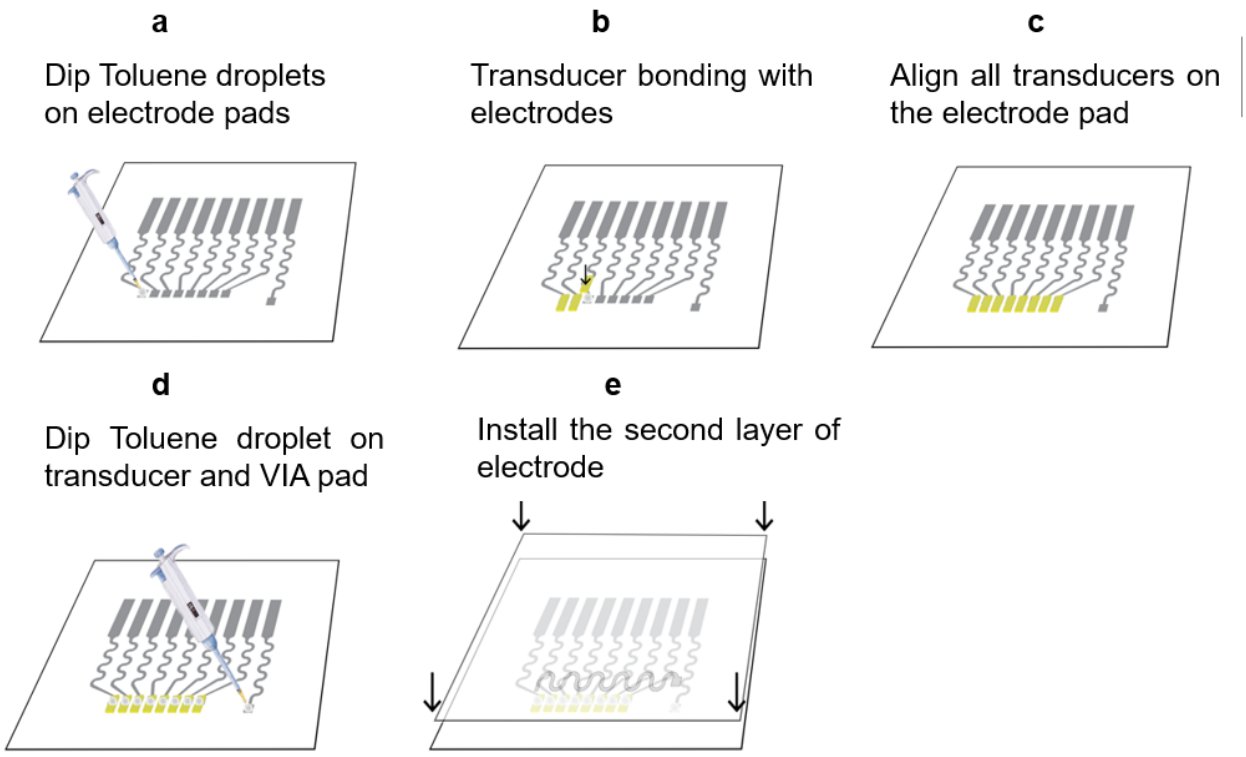

Figure 4.2.2.2. Assembly process of ultrasound transducers.
a, Dip toluene droplets on the connection pad of the interconnects using a pipette to partially dissolve the silver traces. **b**, Place the transducer on the softened pad for bonding. **c**, Repeat steps in **a**-**b** and align all the transducers along the pattern. **d**, Dip toluene droplets on transducers and the ground interconnect pad using a pipette. **e**, Apply the ground wire to the transducers and connect to the ground interconnect pad.

The biosensor electrodes were subsequently modified by drop casting the respective enzymes and polymer layers. All PBS used in the electrode modification was prepared in 0.1 M with a pH of 7.4. All BSA solution was prepared with a concentration of 10 mg/mL in PBS. The chitosan solution was prepared by dissolving chitosan in 0.1 M acetic acid with a concentration of 0.5 wt%. For preparing the lactate biosensor, the chitosan solution was mixed with LOx (40 mg/mL) in BSA solution, in a ratio of 1: 1 (v/v), followed by drop casting a 2 µL aliquot of the mixture onto the working electrode surface. For preparing the glucose biosensor, GOx (40 mg/mL) in BSA solution, glutaraldehyde in water (5 wt%) and Nafion in water (0.5 wt%) were mixed in a ratio of 1: 1: 0.33 (v/v/v) , and a 1.5 µL aliquot was drop cast onto the working electrode surface. For preparing the alcohol biosensor, AOx (10-40 units/mg), BSA solution and the chitosan solution were mixed in a ratio of 8:1:1 (v/v/v), and a 4 µL aliquot of the mixture was drop cast to the working electrode surface. After drying at room temperature for 1 hr, 2 µL of the chitosan solution was drop cast to all previously enzyme-modified surfaces. Upon completing the corresponding modification steps, the resulting biosensors were stored at 4°C overnight before using. For the caffeine sensor, a solution of 0.1 mg/mL of MWCNT was dispersed in 50% EtOH (v/v in DI water) in an ultrasound bath for 10 min, and a 2 µL aliquot of the dispersed solution was drop cast onto the working electrode surface. After drying at room temperature for 1 hr, 2 µL of 0.01% v/v of Nafion in water solution was drop cast onto the previously MWCNT-decorated working electrode and dried at room temperature overnight

4.2.3. Sensor In-vitro calibration

The fabricated sensors, including the lactate, glucose, alcohol and caffeine biosensors, and the PZT acoustic sensors, were calibrated separately in in-vitro settings. The biosensors were calibrated by using 0.1 M PBS (pH 7.4) or 0.01 M acetate buffer (pH 4.5) with successive spiking of corresponding analytes, and recording the corresponding CA (for lactate, glucose and alcohol) and DPV (for caffeine).

4.2.3.1 Lactate sensor

The calibration curve of the lactate sensor was obtained using an initial PBS droplet with 100 µL volume on the sensor surface. The solution was spiked with 1 µL of 0.5 M lactate solution to incrementally increase the concentration of the lactate from 0 to 30 mM with CA at -0.2 V for 60 s after each spiking. The selectivity of the lactate sensor was evaluated by performing CA while spiking the PBS successively with lactate (2 mM), glucose (0.2 mM), ascorbic acid (10 µM), uric acid (60 µM), and acetaminophen (10 µM).[2]

The stability of the lactate sensor was examined by performing 10 repetitive CA measurements of 2 mM lactate and calculating its relative response changes in %.

4.2.3.2 Glucose sensor

The calibration curve of the glucose sensor was obtained using an initial 100 µL PBS droplet on the sensor surface The solution was spiked with 1 µL of 0.1 M glucose solution to incrementally increase the concentration of glucose from 0 to 10 mM with CA at -0.2 V for 60 s after each spiking. The selectivity of the glucose sensor was evaluated by performing CA while spiking the PBS successively with glucose (2 mM), lactate (10 mM), ascorbic acid (10 µM), uric acid (10 µM), and acetaminophen (10 µM).[2] The stability of the glucose sensor was examined by performing 10 repetitive CA measurements of 2 mM glucose and calculating its relative response changes in %.

4.2.3.3 Alcohol sensor

The calibration curve of the alcohol sensor was obtained using an initial PBS droplet with 100 µL volume on the sensor surface. The solution was spiked with 1 µL of 0.8 M ethanol solution to incrementally increase the concentration of alcohol from 0 to 32 mM with CA at -0.2 V for 60 s after each spiking. The selectivity of the alcohol sensor was evaluated by performing CA while spiking the PBS measured successively with ethanol (20 mM), lactate (10 mM), glucose, (0.2 mM), ascorbic acid (10 µM), uric acid (60 µM), and acetaminophen (10 µM).[2] The stability of the alcohol sensor was evaluated by performing 10 repetitive CA measurements of 2 mM ethanol and calculating its relative response changes in %.

4.2.3.4 Caffeine sensor

DPV was utilized for evaluating the caffeine sensor with the following parameters: accumulation at -1.2 V for 30s; $E_{initial}$: +0.5 V; E_{final}: +1.5 V; E_{step}: 0.004 V; E_{pulse}: 0.05 V; t_{pulse}: 0.05 s; scan rate: 0.02 V/s. For calibration curve tests, 100 µL of 0.01 M acetate buffer (pH 4.5) were used to cover the sensing area of the device. The background response was recorded repeatedly until the signal was stable. The caffeine DPV response was then recorded after each consecutive addition of 1 µL of 1 mM caffeine in DI water for obtaining 10 µM increments of the caffeine concentration, up to 210 µM. The selectivity of the caffeine sensor was evaluated by performing DPV while spiking the acetate buffer successively with caffeine (20 µM), lactate (10 mM), ascorbic acid (10 µM), uric acid (60 µM), and acetaminophen (10 µM).[2]

The stability of the caffeine sensor was examined by performing 10 repetitive DPV measurements of 20 μM caffeine and calculating its relative peak current changes in %. For the on-body tests an agarose gel loaded with acetate buffer pH 4.5 was used, covering only the caffeine sensor. A standard additions voltammetric method, involving spiking caffeine to a collected sweat sample, is used to validate the amount of caffeine in sweat. This method was used once to construct the calibration plot for correlating directly the wearable patch signal to sweat caffeine concentrations.

4.2.4. Sensor Mechanical Tests

The mechanical testing was conducted via controlled stretching tests. A programmable motorized linear stage (X-LRQ, Zaber Technologies Inc.) was used for stretching the device with controlled strain and speed. One of the edges of the printed device was taped at the fixed end of the stage and the other to the moving end of the stage. The device was firstly stretched at 3 mm/s speed to 120% of its original length in the horizontal direction and release back to its original size at the same speed. This process was programmed to be repeated 200 times, so that the device could be taken from the stage for measurements before remounting back for subsequent stretching. The process was repeated until 1,000 cycles of stretching were completed. This process was repeated for deformations on the vertical directions using the same device. Electrochemical tests under constant deformation of 120% stretching (horizontal and vertical directions) were conducted after every 200 stretching cycles, up to 1000 stretching deformations.

4.2.5. Sensor Crosstalk Tests

The crosstalk between the acoustic and electrochemical signals was analyzed on-body by monitoring the changes in one signal while the other signal was generated intermittently. For analyzing the co-sensor interference from the CA electrochemical measurement to the BP waveform, the BP signals were recorded continuously for at least 4 s in two stages. Initially when the CA was already being performed by applying a potential of -0.2 V to the electrochemical sensors , and when the detection potential was turned on after the BP recording had already started. The interference tests from the BP sensor on the CA measurements were performed in the same fashion for the anodic and cathodic sensors as follows. For analyzing the crosstalk effect of the acoustic signal generation upon the electrochemical signal acquisition, the CA signal was recorded continuously for 180 s while the electric pulses for the BP measurements were delivered to the PZT transducer in an off-on-off-on-off-on pattern with a period of 30 s for each phase.

The crosstalk from the differential pulse voltammetry (DPV) to the acoustic signal was evaluated in the same fashion as in the CA tests as follows. The effect of the acoustic signal upon the caffeine sensor was evaluated in two stages, first by recording the DPV signal while the BP recording was being applied, following by terminating the BP signal when the DPV reached the peak potential and by recording the DPV signal prior to initiating the BP acquisition at peak potential. All signal generation and data acquisition were performed using μAutolab III electrochemical analyzer (Metrohm) for the chemical sensors and the 5077PR pulser-receiver (Olympus) for the acoustic sensors. The potentiostat was configurated with +/- 5 V voltage and 1 mA current limit to avoid overcurrent/overvoltage. The device was inspected visually to ensure that the transducers were fully covered by the SEBS substrates for insulation. No capacitive coupling, short-circuiting nor breakdown conduction were observed during the experiment.

4.2.6. Sensor On-body Test Protocols

Epidermal evaluation of the device was performed on healthy consenting subjects with no prior history of heart conditions, diabetes, or chronic pain, and in strict compliance with the protocol approved by the Institutional review board (IRB) at the University of California, San Diego. The device was placed on the neck of the volunteers for all on-body evaluations. Prior to every set of measurements using the integrated sensor, the glucose, lactate, alcohol, and BP signals were validated with a commercial glucometer (ACCU-CHEK, USA), blood lactate (NOVA biomedical, USA), breathalyzer (BACtrack S80 Pro) and FDA approved blood pressure cuff (LOVIA, USA), respectively. Caffeine concentrations were estimated by standard addition methodology using the collected sweat. Sweat stimulation and ISF extraction were realized simultaneously by using a μAutolab III electrochemical analyzer to apply a current density of 0.3 mA cm^{-2} between the cathode and anode electrodes for 10 min. Prior to sweat generation, a pre-conditioning step was carried out on the skin by applying the same current density using agarose gels (preparation as shown in **Figure 4.2.6.1**) in the cathode and anode compartments for 10 min, following by immediate placement of the device with pilocarpine delivery gel on the conditioned area. Before placing the sensor, the skin was thoroughly cleaned with soap and alcohol wipes. The patch was transferred to the skin by using a double-sided clean laser tattoo transfer adhesive (Papilio, TM).

Openings were made in the adhesive film to expose the sensors and IP electrodes to the skin. For all measurements, a single device was used for each volunteer to perform the "before" and "after" tests. The device was kept in the volunteer's neck during the entire experiment, unless otherwise specified.

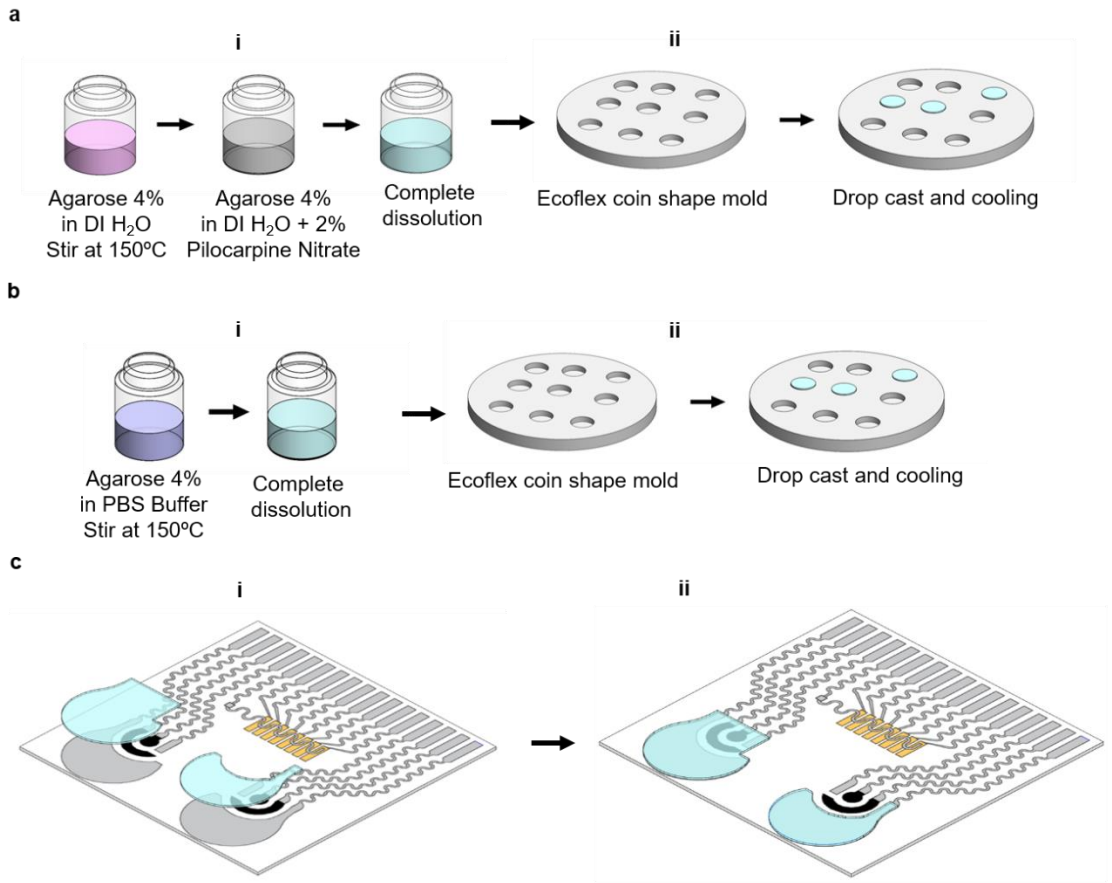

Figure 4.2.6.1. Preparation and assembling of the hydrogel layers.
a, Anode hydrogel preparation. (i) A mixture of 4% agarose and DI water kept under continuous stirring at 150ºC until complete dissolution. Next, the addition of 2% pilocarpine nitrate under stirring. (ii) 300 µL of the solution was then drop cast in the Ecoflex molds. After cooling, the viscous solution on the mold became a solid coin shape hydrogel. **b,** Cathode hydrogel preparation: (i) The mixture of 4% agarose and 0.1 M PBS (pH 7.4) buffer was kept at continuous stirring at 150ºC until observing complete agarose dissolution. (ii) 300 µL of the solution was then drop cast in Ecoflex molds. After cooling, the viscous solution on the mold became a solid coin shape hydrogel. **c,** Hydrogel assembly: (i) A coin shape anode and cathode hydrogel disks were cut with the shape of the screen-printed pattern of the anode and cathode respectively. (ii) After the shape was provided, the anode hydrogel was placed on the left side and the cathode hydrogel was placed on the right side.

The on-body results were acquired using a benchtop CHI 1230A electrochemical analyzer for the biosensors and 5077PR pulser-receiver (Olympus) for the acoustic sensors. Food intake refers to the intake of sugar-rich food (100 g cheesecake, 350 kcal, 22g sugar). Alcohol intake refers to the intake of alcohol (200 mL wine, alcohol 19% vol.). Caffeine intake refers to the intake of a sugar-free caffeinated drink (248 mL, 80 mg caffeine). Exercise refers to a 30-min exercise session on a stationary bike with constant intensity followed by a 5-min cooling period. For experiments involving exercising step, BP and lactate signals were acquired before and after exercising for three healthy volunteers. The device was removed from their skin during the 30 min stationary bike exercise and kept in a wet chamber at room temperature. After exercising, and following a 5 min cooling period, the volunteer's neck was cleaned with soap and alcohol pads for replacing the same sensor in the same area. For experiments involving alcohol intake, BP and alcohol levels were measured before and 20 minutes after the alcohol consumption. The device was kept on the volunteer's neck during the entire experiment. For experiments involving food consumption, BP and ISF glucose signals were acquired in the fasting state (16 hours) for three healthy volunteers and 15 min after consuming the sugar-rich food. The device was kept on the volunteer's neck during the whole experiment. For experiments involving caffeine intake, subject's volunteer's caffeine levels in sweat were monitored before and 30 min after consuming the sugar-free caffeine drink. The device was kept on the volunteer's neck during the entire experiment. For the on-body tests an agarose gel loaded with acetate buffer pH 4.5 was used, covering only the caffeine sensor. Prior to the caffeine ingestion, stimulated sweat was collected for the standard addition caffeine determination. During experiments with simultaneous alcohol and food intake, the dual modality of the sensor was tested by combining alcohol and food intakes. BP, ISF glucose, and sweat alcohol levels were measured before and after 20 min of the simultaneous consumption of an alcoholic beverage and the sugar-rich food. The device was kept on the volunteer's neck during the whole experiment. During experiments with simultaneous exercise and food intake, the dual modality of the sensor was tested toward the monitoring of blood pressure, glucose, and lactate levels. The subject was first asked to consume a sugar-rich food. Fifteen minutes after the food consumption, ISF glucose, sweat lactate and BP were measured. Next, the device was removed from the subject, kept in a wet chamber at room temperature, and the volunteer was asked to perform the physical exercise on a stationary bicycle for 30 min followed by cooldown for 5 min.

After the cooldown interval the subject's skin was cleaned and the same sensor was used for subsequent measurement of the SIF glucose, sweat lactate, and BP levels. For experiments that involved lactate and BP sensing during exercise, subjects with different fitness levels (physically active and non-active) were asked to perform 30 minutes of cycling activity at constant intensity while wearing the sensor. Iontophoresis and the iontophoretic gels were not used for this portion of the study, as sweat was generated spontaneously from the activity. The BP and blood lactate were measured right before the start of the exercise and the initial sweat lactate level was measured 5 min after starting the exercise when sweat was firstly generated. Within ~10 minutes, BP and blood lactate signal were recorded again. The BP and blood lactate were recorded also upon completion of exercising for validation.

4.3. Results and Discussions

4.3.1 Crosstalk Study

The performance of the integrated sensor for multiplexed simultaneous sensing requires reliable data generation from the individual sensors, with no crosstalk between the two sensing modalities. Here, the signal crosstalk between the acoustic and electrochemical transducers was prevented by spatially separating both components and using solid-state ultrasound and sensing hydrogel layers (**Figure 4.3.1.1**).

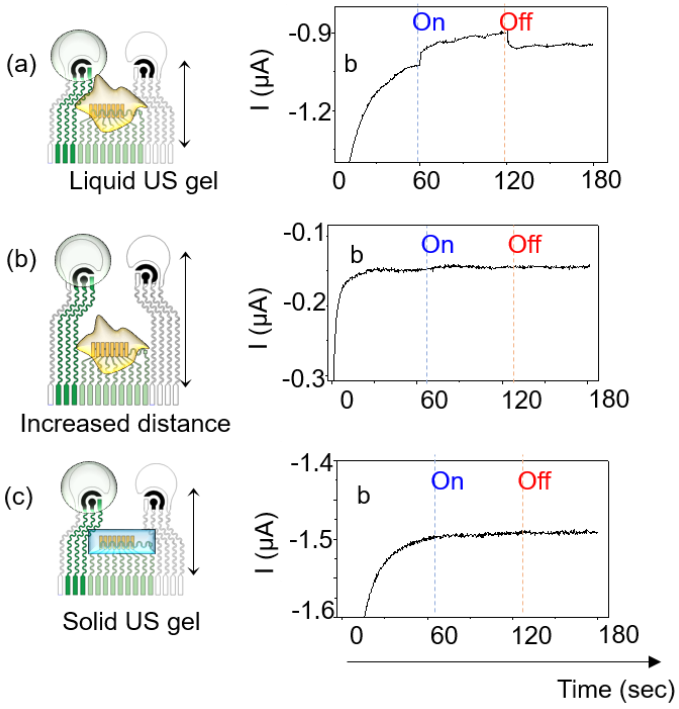

Figure 4.3.1.1. In-vitro cross-talking evaluation of multimodal wearable sensor.
In vitro measurements were performed using the agarose-PBS hydrogel and the ultrasound gel placed over the blood pressure transducers. **a,** The PBS hydrogel and ultrasound gel were in contact while the ultrasound pulse was turned on and off (right), respectively. A decreasing (more positive current) was observed when the gels were in contact. **b**, A different design with increased distance between the gels were used in vitro with the same amount of ultrasound gel, due to the physical distance, no cross-talking was observed (right). **c**, The same design (with a shorter distance between the blood pressure and chemical sensors) was used with a solid hydrogel and no apparent cross-talking was observed (right).

The device was designed with optimal distance between the individual detection compartments to ensure successful acoustic BP and HR sensing, IP extraction, and electrochemical monitoring. As shown in Error! Reference source not found.**a** and **Figure 4.3.1.2d**, the BP transducers were located 1 cm below the chemical sensors, a distance optimized by assessing the crosstalk between the neighboring sensors. The signal generation of the acoustic sensor relies on high-voltage high-frequency pulses that may induce signal drift in the chemical sensors, while the IP extraction, potentiostatic sensing, and potential-sweep sensing may also induce noises in the acoustic signals. Such crosstalk effect between the electrochemical and BP sensors were evaluated by recording the corresponding signals during on-body operations.

The BP signals were acquired while the potentiostatic electrochemical input was turned on and off repeatedly to assess the effect of the electrochemical sensing of the anodic (**Figure 4.3.1.2e**) and cathodic (**Figure 4.3.1.2b**) sensors on the BP signal. Similarly, the effect of the acoustic sensing on both sides of the electrochemical sensing was examined by recording the amperometric response while turning the acoustic pulses on and off repeatedly every 30 s (**Figure 4.3.1.2c, f**).

Figure 4.3.1.2 Characterization of the multimodal wearable sensor.
a-c, Signal interference crosstalk studies between the ISF electrochemical and the BP sensors (a), including BP signal recording while applying and removing the CA detection potential (b), and ISF sensor signal recording while start and pausing ultrasound signal generation with 30 s intervals within 3 min (c). **d-f**, Signal interference crosstalk studies between sweat electrochemical sensor and the BP transducer (d), including BP signal recording while applying and removing the CA detection potential (e), and sweat sensor signal recording while start and pausing ultrasound signal generation with 30 s intervals within 3 min (f). **g**, Photos of the sensor under 20% vertical strain. **h**, Envelopes of the raw echo signals before and after every 200 stretching cycles until 1000 cycles. **i**, Electrochemical response every 200 stretching cycles until 1000 cycles. **j**, Photos of the sensor under 20% horizontal strain. **k**, Envelopes of the raw echo signals before and after every 200 stretching cycles until 1000 cycles. **l**, Electrochemical response every 200 stretching cycles until 1000x. **m**, PZT transfer process. Toluene is drop cast on the electrode pad to dissolve the SEBS trace (i). Softened silver ink ready for bonding with the transducer (ii). Drop cast toluene on transducers for bonding with the ground wire (iii). Binding of the ground layer to the reserved electrode channel (iv). **n**, Adhesion of the PZT transducers to the substrate. The photo images of the pristine device under indentation (i), during horizontal stretching (ii) and after transferring the ground layer (iii). **o-q**, Skin conformability and mechanical integrity of the device while twisting (o), bending (p), and after these deformations (q).

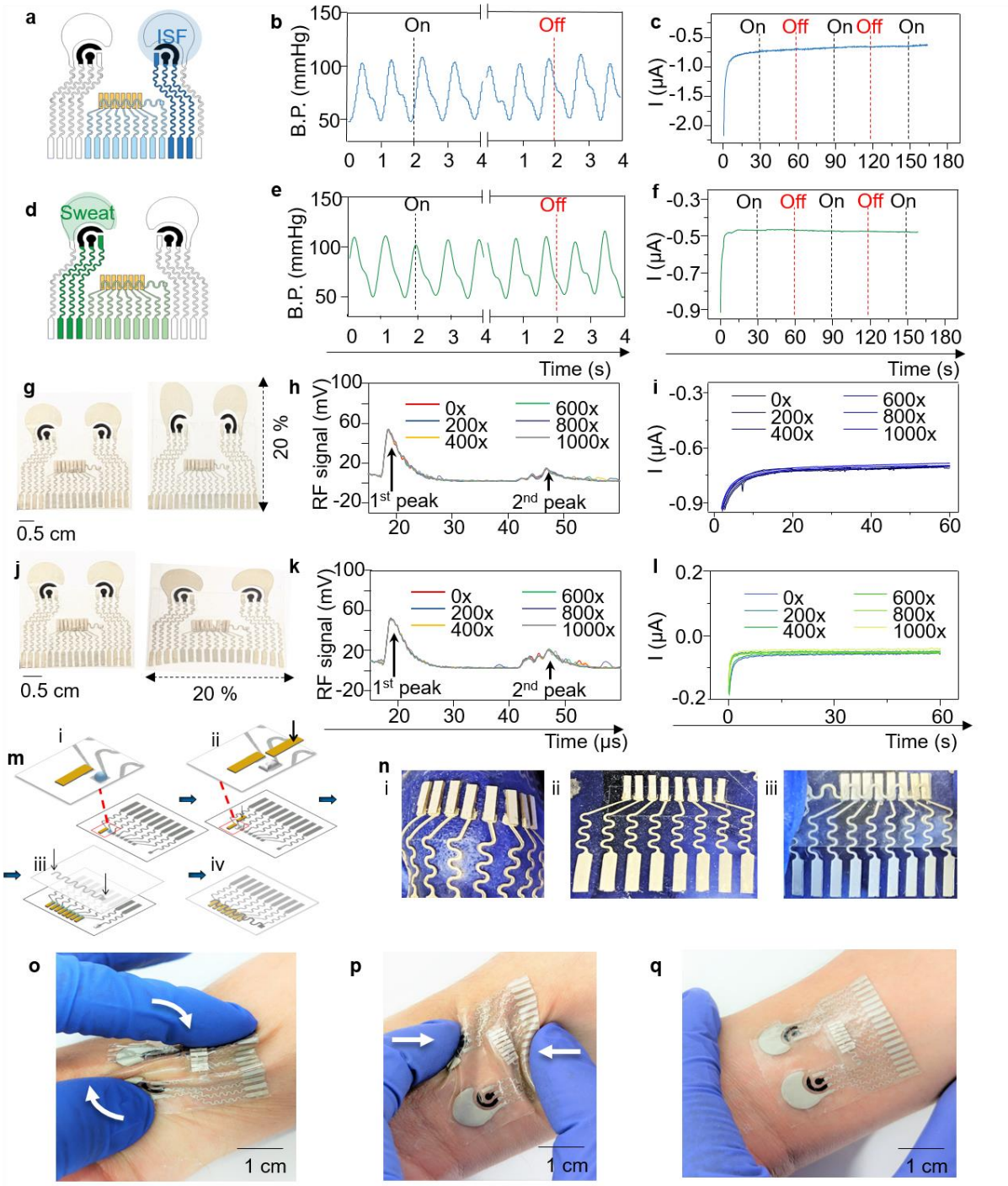
a
ISF
b
B.P. (mmHg)
On
Off
c
I (μA)
On Off On Off On
d
Sweat
e
Time (s)
f
g
20 %
0.5 cm
h
RF signal (mV)
0x
200x
400x
600x
800x
1000x
1st peak
2nd peak
i
j
k
Time (μs)
l
m
i
ii
iii
iv
n
o
p
q
1 cm

4.3.2 Mechanical Performance

Mechanical stability is another crucial factor that dictates the reliability of skin-worn sensors when tensile deformations are expected. The impedance of the chemical sensor and the contact resistance to the PZT transducers may vary with the strain applied to the soft conformal device leading to changes in the measured signals that affect the reliability of the device. The stability of the PZT contact upon mechanical stress was realized by developing a novel solvent-soldering process based on the fast dissolution and room-temperature curing of SEBS-based materials. During the assembly process, the PZT transducers can be quickly mounted and bonded onto the SEBS substrate and connected to the SEBS-based stretchable silver ink by wetting the electrode surface with toluene (**Figure 4.3.1.2m**). The solvent soldered PZT chips can thus be securely bonded to the printed electrodes without delamination during stretching deformations (**Figure 4.3.1.2n**), with their assembly efficiency largely improved compared to previous reports.[10] The effects of stretching on the sensing performance were assessed by stretching tests at 20% uniaxial strain. The device was stretched repeatedly along the vertical direction (**Figure 4.3.1.2g**) and horizontal direction (**Figure 4.3.1.2j**). The ultrasonic echo signals, against a two-layered Ecoflex, and the current CA signal, in buffer solution, were recorded after every 200 cycles of stretch at 20% strain.

As shown in **Figure 4.3.1.2h** and **Figure 4.3.1.2k**, although the intensity of the acoustic transducer signal decreased slightly with stretching, the temporal relationship between each peak that corresponded to two echoes did not change, and hence the deformations did not affect the recorded waveform. Similarly, the electrochemical sensors did not show any significant current change as the stretching cycle progressed (**Figure 4.3.1.2i, l**). The device has also shown good mechanical resilience after transferring it to the body. **Figure 4.3.1.2o-q** illustrate the twisting and bending of the sensor on the skin. The SEM images depicting the surfaces structural changes of the printed stretchable silver and carbon traces are displayed in **Figure 4.3.2.1**, demonstrating that the printed composites are not affected by the mechanical deformation.

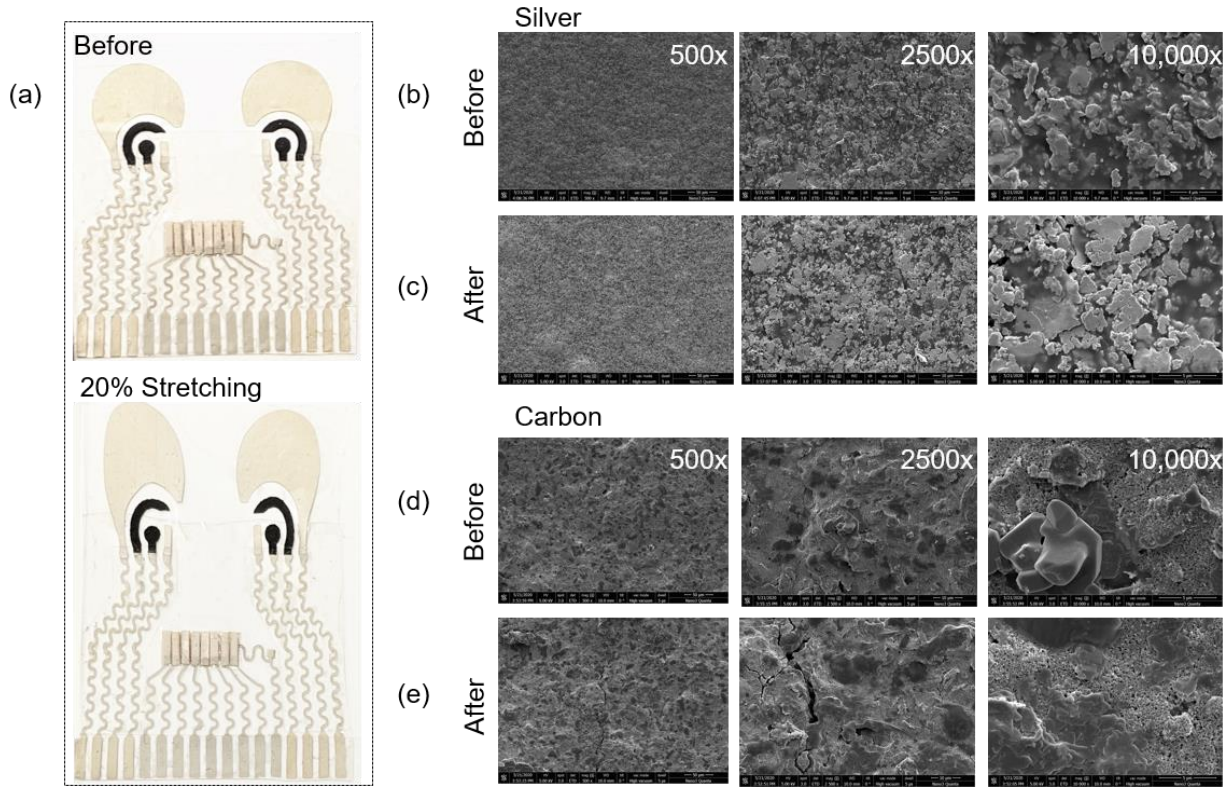

Figure 4.3.2.1. Structural integrity of the stretchable silver and PB/carbon ink composites.
a, Photo illustration of the device before and after stretched to 120%. **B-e**, SEM images in different magnifications of the silver trace before (**b**) and after (**c**) 1000 cycles of 20% stretching, and of the carbon trace before (**d**) and after I 1000 cycles of 20% stretching.

4.3.3 Tracking cardiovascular activities and biomarker levels

The ability of the device to simultaneously monitor dynamic cardiovascular parameters and biomarkers concentrations allows evaluating the effects of common daily activities on individual's physiological status and to continuously collect data about their response to such everyday activity. The levels of lactate, glucose, alcohol, and caffeine in our bodies can fluctuate due to common daily activities, whose impact on our BP also varies based on individual's physical conditions. The simultaneous measurement of biomarkers and BP allows the data collection of individual's responses to such daily activities. The device's ability to track multiple biomarkers while capturing cardiac parameters can further help deconvolute the additive effects of multiple stimuli on physiological parameters, which holds significant implication towards self-monitoring for personalized health management.

Exercise, comprising any action which demands physical efforts, has a major impact on the body physiological response, including changes in lactate levels, HR, and BP. During prolonged exercising, lactate level elevates due to metabolic stress, HR increases to meet the muscle demand for oxygen, while BP surges due to increased availability of vasodilatory mediators such as nitric oxide.[25] To study these effects, several volunteering subjects were asked to perform stationary cycling in a fixed level for 30 min, followed by 20 min resting. BP was recorded while the sweat was stimulated before and after the exercise for the lactate measurements, and the obtained BP and lactate level data were validated by a commercial cuff-style blood pressure monitor and a blood lactate meter. As expected, significant changes in BP and HR were thus observed in **Figure 4.3.3.1a** after the exercise, increasing up to 150 mmHg and 98 bpm, respectively (**Figure 4.3.3.1a i-ii**). Sweat lactate also increased, with low lactate levels recorded in the beginning and increased two-fold after the exercise (**Figure 4.3.3.1aiv-v**). The BP and sweat lactate data collected from the device agreed well with the validation methods, as shown on **Figure 4.3.3.1aiii-vi**. As another commonly seen unhealthy stimulus, excessive alcohol consumption, has shown to increase cardiovascular risks via alcohol-induced hypotension and hypertension.[26,27] Alcohol may have different effects on the BP, depending on the amount and frequency of its consumption and on genetic factors related to resistance or sensitivity to alcohol.[28,29] BP variations upon alcohol ingestion are related to the direct vasodilation, surge in cortisol secretion, and reduced insulin sensitivity.[30] For the sensor experiments focusing on alcohol as the stimulus, the BP and sweat alcohol level were measured before and 20 min after drinking 200 mL of an alcoholic beverage (19% vol.) (**Figure 4.3.3.1b**). A commercial alcohol breathalyzer was used for correlation with blood alcohol level. As shown in **Figure 4.3.3.1b**, the alcohol consumption resulted in an increased HR (from 69 to 85 bpm) and BP (120 to 136 mmHg) of the volunteer (**Figure 4.3.3.1b i-ii**). These results agree with studies showing that a single alcohol intake by non-heavy drinkers can lead to a temporary BP spike.[30] It is worth noting that for heavy drinkers, there might be a considerable BP morning surge that greatly increases the risk of stroke.[30] Simultaneously, the sensor allows reliable detection of sweat alcohol, as this small polar molecule can be found in sweat with a 1:1 correlation to blood (**Figure 4.3.3.1biv-v**).[31]

Metabolites, such as glucose, can also affect the BP waveform by changing the blood viscosity. Blood viscosity increases under conditions of insulin resistance, altering the flux of blood in the capillaries and hence the shape of the BP pulse.[32,33] Studies have shown that subjects with high blood pressure are prone to significantly higher blood glucose levels.[34] To test the effect of the rise in glucose upon the BP, healthy non-diabatic subjects were asked to consume a high sugary meal after fasting. The BP and ISF glucose levels were recorded using the device before and 15 min after consuming the food, with the glucose level validated using a commercial glucometer at both times. As shown in **Figure 4.3.3.1i-ii,** the sensor evaluation, during the food consumption experiment, resulted in negligible changes in the BP and HR. In contrast, the electrochemical biosensor readily detected changes in the ISF glucose levels after the meal consumption (**Figure 4.3.3.1c iv-v**). This data is within the expectation for the non-diabetic subject, as glucose-induced BP changes occur only when glucose levels increase significantly to alter the blood pumping through the arteries, which is not common for non-diabetic individuals whose glucose is readily regulated by the responsive release of insulin.

Lastly, caffeine was chosen as another chemical stimuli commonly used in our daily lives. Caffeine-intake is known to lead to an increased BP through the inhibition of adenosine receptor and release of stress hormones, such as norepinephrine or cortisol.[35] These biochemical changes can result in transient contractions of the arterial smooth muscle and influence the vascular tone by phosphodiesterase inhibition.[36] The effect of caffeine on the BP varies, and are shown to be more pronounced in hypertensive subjects.[35,36] The epidermal BP/caffeine sensor patch was evaluated on subjects with and without caffeine-intake habits, and their BP and sweat caffeine were measured before and 30 min after consuming a caffeine-rich (80 mg) sugar-free energy drink. The amount of caffeine in sweat was validated through a standard additions voltammetric method, spiking caffeine to a collected sweat sample (**Figure 4.3.3.2**). As illustrated in **Figure 4.3.3.3b**, the on-body tests on subject with habitual caffeine-intake showed no significant changes in the BP and HR after consumption of high caffeine doses, reflecting the caffeine tolerance and healthy blood pressure levels of the volunteer. In contrast, the BP variation was more pronounced for the subject with no habitual caffeine intake (**Figure 4.3.3.1d**). The caffeine sensor displayed a flat DPV baseline response prior to the caffeine intake, whereas the sweat DPV recorded 30 min after the caffeine intake showed a distinct anodic peak current at 1.2 V, corresponding to the caffeine oxidation (**Figure 4.3.3.1d-iv-v**)[37,38].

Current levels before and after the caffeine intake were compared against the results obtained through the standard additions method for caffeine, showing a good correlation between both parameters (**Figure 4.3.3.1d-vi**). Note that the in vitro electrochemical characterization of the caffeine sensor in pH 4.5 showed current peaks around 1.1 V (**Figure 4.3.3.2**). Such small potential shift is attributed to the difference in sweat pH, which typically fluctuates between 4.5-7.0.

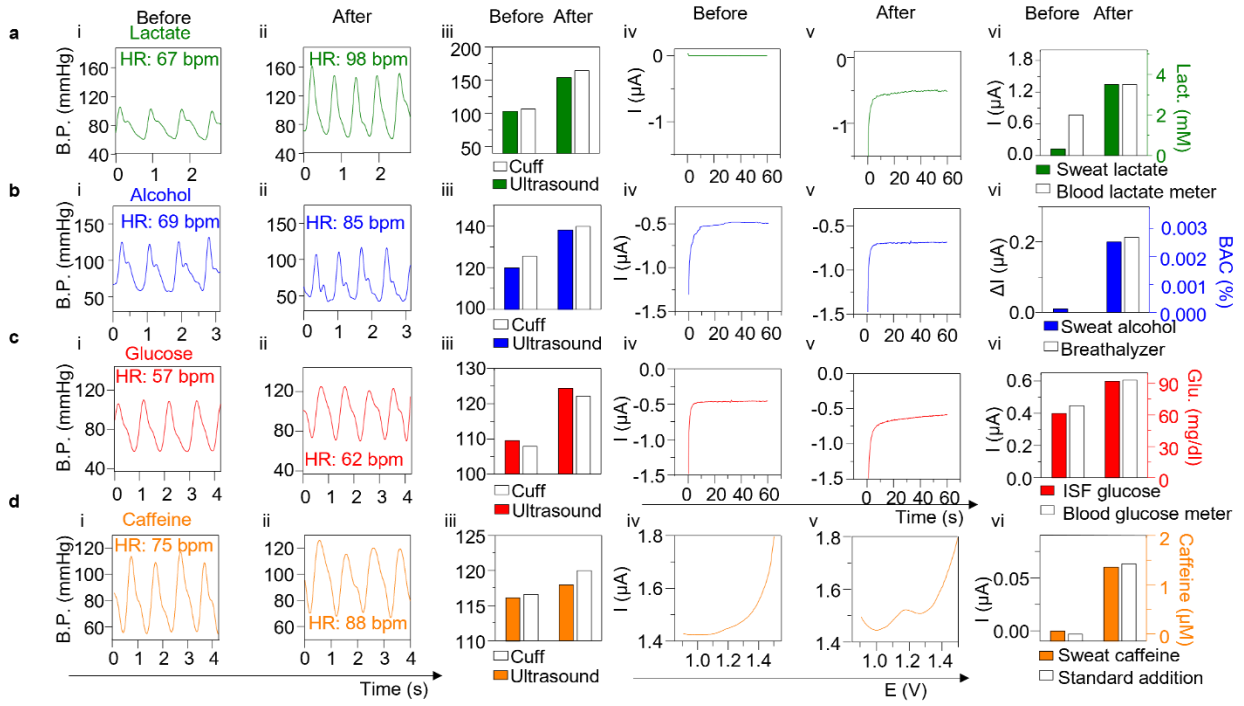

Figure 4.3.3.1. Individual chemical biomarker and BP/HR monitoring.
a, BP/HR and sweat lactate studies. Signal recording for BP/HR performance before (i) and after (ii) exercise. Bar graphics represent the sensor validation using a commercial cuff (white) and BP readings obtained with ultrasound transducer (green) (iii). Signal recording for sweat lactate before (iv) and after (v) exercise. Bar graphics represent the sensor validation using a commercial blood lactate meter (white) and readings obtained with the electrochemical sensor (green) (vi). **b**, BP/HR and sweat alcohol studies. Signal recording for BP/HR performance before (i) and after (ii) alcohol intake. Bar graphics represent the sensor validation using a commercial cuff (white) and BP readings obtained with ultrasound transducer (blue) (iii). Signal recording for sweat alcohol before (iv) and after (v) alcohol intake. Bar graphics represent the sensor validation using a commercial breathalyzer (white) and readings obtained with the electrochemical sensor (blue) (vi). **c**, BP/HR and ISF glucose studies. Signal recording for BP/HR performance before (i) and after (ii) food intake. Bar graphics represent the sensor validation using a commercial cuff (white) and BP readings obtained with ultrasound transducer (red) (iii). Signal recording for ISF glucose before (iv) and after (v) food intake. Bar graphics represent the sensor validation using a commercial blood glucometer (white) and readings obtained with the electrochemical sensor (red) (vi). **d**, BP/HR and sweat caffeine studies. Signal recording for BP/HR performance before (i) and after (ii) caffeine intake. Bar graphics represent the sensor validation using a commercial cuff (white) and BP readings obtained with ultrasound transducer (orange) (iii). Signal recording for sweat caffeine before (iv) and after (v) caffeine intake. Bar graphics represent the sensor validation through standard addition method (white) and readings obtained with the voltammetric sensor (orange) (vi).

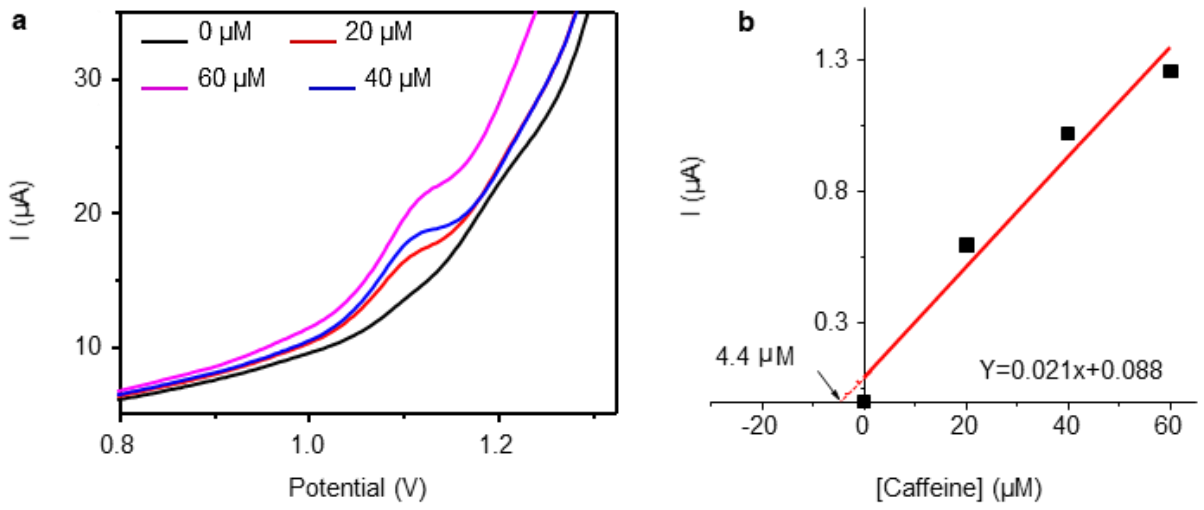

Figure 4.3.3.2. Standard additions to determine caffeine concentration in sweat.
a, DPV of caffeine in collected sweat (after drinking 114 mg caffeine). Increasing concentrations of caffeine were added to the collected sweat and the respective calibration curve was used to analyze the initial caffeine concentration in sweat **b,** Calibration curve. The horizontal axis shows the concentration range used in the test. The vertical axis shows the current change after each addition.

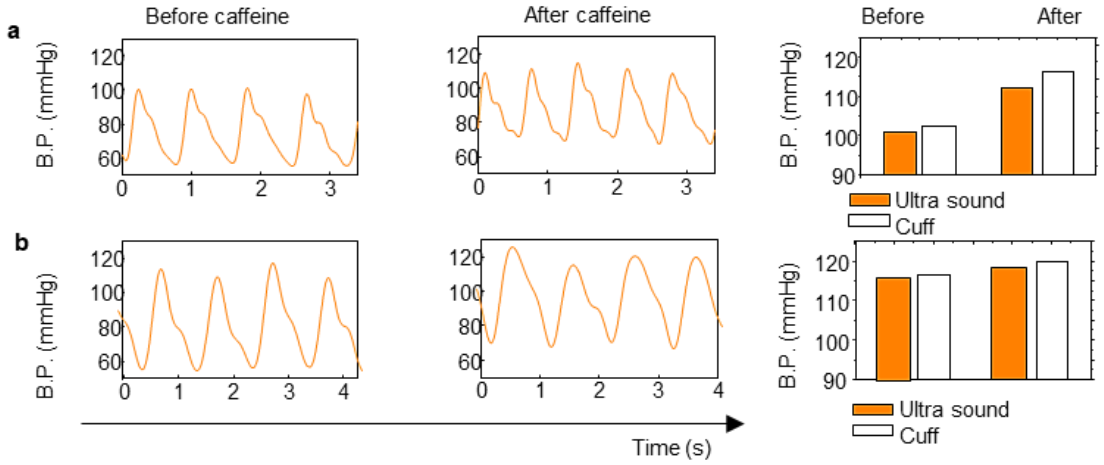

Figure 4.3.3.3. On body evaluation for caffeine intake.
a, On-body evaluation of BP changes for a volunteer with no habitual caffeine intake (caffeine intolerant)**.** Before and after caffeine sugar-free beverage consumption (Right). Bar graphics represent the sensor validation using a commercial cuff (white) and BP readings obtained with the ultrasound transducers (orange). **b,** On-body evaluation of BP changes for a volunteer with regular caffeine intake habits (caffeine tolerant)**.** Before and after caffeine sugar-free beverage consumption (Right). Bar graphics represent the sensor validation using a commercial cuff (white) and BP readings obtained with the ultrasound transducers (orange).

4.3.4 Device Monitoring Multiple Stimuli

Then we evaluated the device in real-life scenarios, where people usually experience multiple activities that may have synergistic or counteracting effects on the body's physiological response. The use of the device for monitoring cardiovascular parameters along with multiple biomarker levels was evaluated on subjects exposed to multiple stimuli. A common example of counteracting effect to the glucose levels is exercising along with food intake, as glucose can be quickly consumed during exercise to produce energy[39]. Exercise is also expected to increase the BP and lactate level in the subject, as was shown in previous single-stimuli tests. To study this scenario, the subject was asked to consume a sugar-rich meal, followed by exercising on a stationary bike for 30 min, with the ISF glucose, sweat lactate, and BP monitored before and after each step. As shown in **Figure 4.3.4.1a**, normal systolic BP level, high glucose levels (> 100 mg/dL) and low lactate level were observed before the biking activity. After the exercise, glucose levels decreased, accompanied by a considerable increase in the BP, HR, and lactate level, as predicted from previous tests. Control experiments – performed without any food or exercise - were used to corroborate that the change in signal resulted solely from the increase of lactate and glucose levels (**Figure 4.3.4.2**).

Overall, **Figure 4.3.4.1a** illustrates that the new sensor is able to capture the complex processes resulting from the simultaneous food and exercise stimuli, including the digestion of food to produce glucose as the energy reservoir, the glycolysis reaction consuming the glucose and oxygen to release energy, the increased BP and HR compensating for the oxygen depletion, and the lactate generation during the hypoxic condition in exercise.

The influence of the simultaneous intake of alcohol and glucose on the BP and HR, simulating a typical alcohol consumption during meals, was also studied on volunteering subjects. Based on previous observations, increasing glucose levels are not expected to cause significant changes in the BP of the subjects, whereas an increasing BP is expected after an alcohol intake. Therefore, an additive effect in the rise in BP and glucose is expected when combining the intake of alcohol and sugary food. Moreover, the digestion of alcoholic drinks, along with the reduced insulin sensitivity caused by alcohol consumption, can further aggravate the increase in the glucose level and the BP.[15] On the other hand, excessive alcohol intake can lead to severe hypoglycemia and hypotension, even when combined with glucose intake, particularly for insulin-dependent diabetes subjects.[40] Therefore, the simultaneous monitoring of glucose and BP is important for distinguishing the case of moderate or excessive drinking and preventing drinking-induced accidents, especially for subjects with underlying health conditions.[41,42] Sweat alcohol, ISF glucose, and BP signals were recorded in the fasting state, after the alcohol consumption, and after the food intake.

As shown on **Figure 4.3.4.1b iv-vi**, before any food or alcohol consumptions, blood glucose and alcohol showed a typical non-diabetic fasting state reading of 90 mg/dL glucose and a 0% BAC level, whereas increasing BP, glucose, and alcohol signals were observed for 20 min after the stimuli. The observed increase in BP following the alcohol intake alone was 16 mmHg (**Figure 4.3.3.1b-iii**), rising further to 20 mmHg after the concurrent intake of sugary food (**Figure 4.3.4.1b-iii**). Such BP variations demonstrate the synergetic effect of combining alcohol and glucose intakes on the BP. Smaller changes in HR were observed following the alcohol and food intakes as compared to the alcohol intake alone, indicating different mechanism for the increased BP. Control experiments carried out without intakes of food or drink were used to corroborate that the observed signal changes were solely due to the increase of alcohol and glucose (**Figure 4.3.4.3)**.

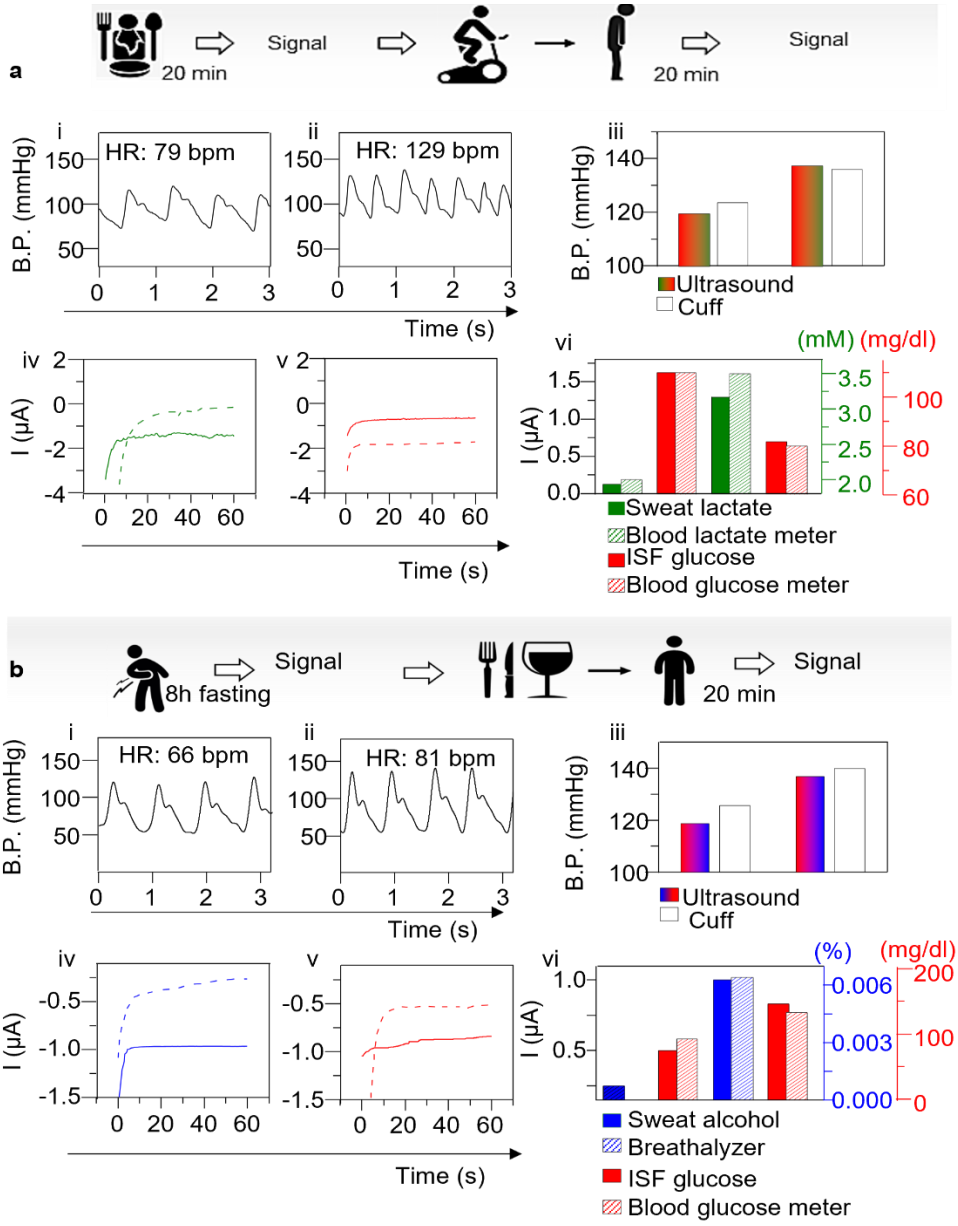

Figure 4.3.4.1. Blood pressure and dual chemical monitoring.
a, Lactate/glucose/BP performance. BP/HR signal recording before (i) and after (ii) exercise. Bar graphic comparison between BP signal using a commercial cuff (white) and the ultrasound transducer (green/red) (iii). Electrochemical sensor signal recording for sweat lactate before (dotted line) and after (solid line) exercising (iv). Electrochemical sensor signal recording for glucose after having a meal and before exercising (dotted line) and after exercise (solid line) (v). Bar graphic comparison between lactate levels in sweat using the electrochemical sensor (green solid) and a commercial blood lactate meter (green/white), glucose levels in ISF using the electrochemical sensor (red solid) and blood using a blood glucose meter (red/white) (vi). **b**. Alcohol/glucose/BP performance. BP/HR signal recording before (i) and after (ii) food and alcohol intake. Bar graphic comparison between BP signal using a commercial cuff (white) and the ultrasound transducer (blue/red) (iii). Electrochemical sensor signal recording for sweat alcohol before (dotted line) and after (solid line) alcohol intake (iv). Electrochemical sensor signal recording for ISF glucose before (dotted line) and after (solid line) food intake (v). Bar graphic comparison between alcohol levels in sweat using the electrochemical sensor (blue solid) and a commercial breathalyzer (blue/white), glucose levels in ISF using the electrochemical sensor (red solid) and blood using a blood glucose meter (red/white) (vi).

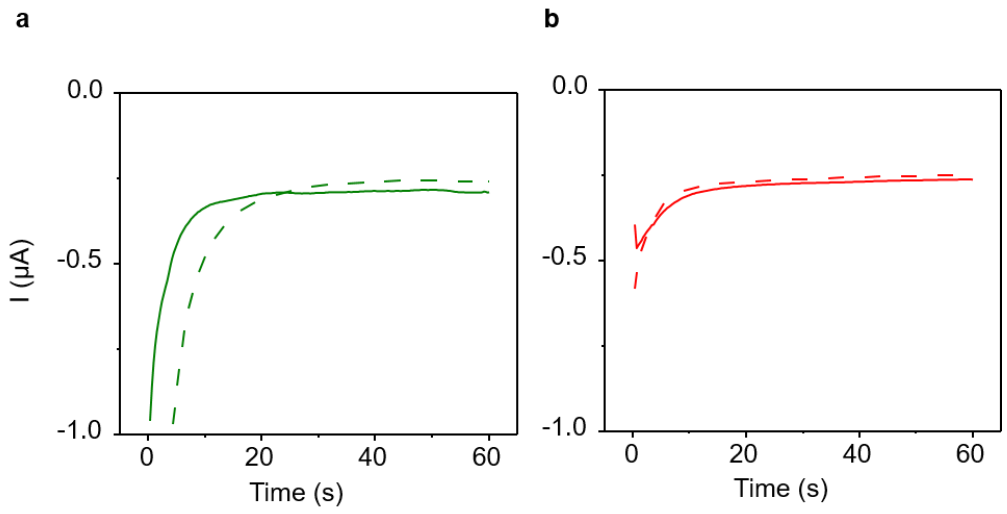

Figure 4.3.4.2. Control experiments: Response for lactate and glucose recording without exercise and food ingestion. **a**, The lactate sensor response after the first sweat stimulation (green dash line) and second sweat stimulation (green solid line). **b**, The glucose sensor response after the first ISF extraction (red dash line) and second ISF extraction (red solid line). Applied potential, -0.2 V.

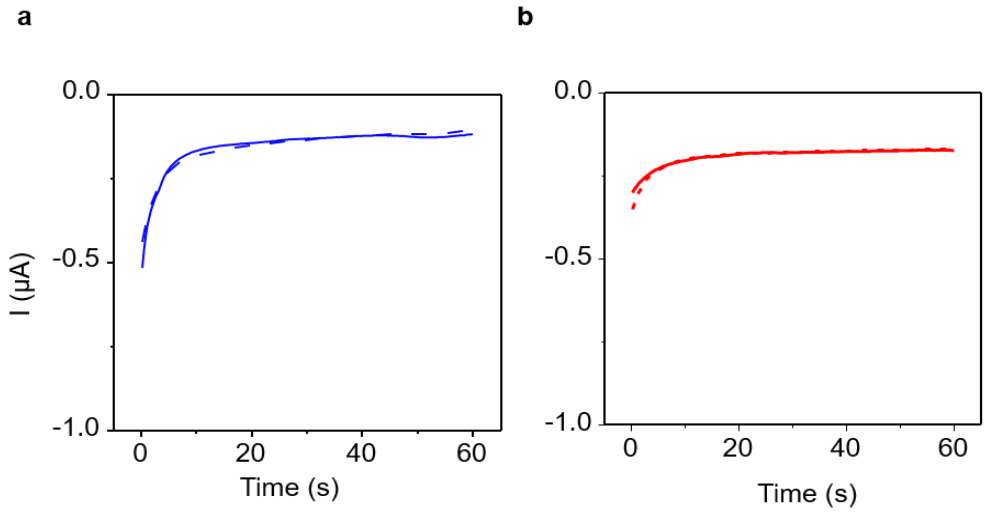

Figure 4.3.4.3. Control experiments: Response for alcohol and glucose recording without alcohol and food ingestion. **a**, The alcohol the first sweat stimulation (blue dash line) and second sweat stimulation (blue solid line). **b**, Response of the glucose sensor after the first ISF extraction (red dash line) and second ISF extraction (red solid line). Applied potential, -0.2 V.

4.3.5. Continuous BP and Biomarker Monitoring

The ability of the sensor to capture the dynamic biomarker and BP fluctuations while performing physical activity was also demonstrated. Physically active individuals are expected to have lower resting BP, reducing considerably the risk of heart failure events.[43,44] The lower resting BP can further be reflected in smaller increase in BP during exercising, as physically active individuals signal the body earlier to release nitric oxide (NO) to promote enhanced vasodilation.[43] Smaller increases in lactate levels are also expected for active individuals compared with non-active ones.[45] BP is expected to decrease following intense exercise activity, eventually retuning to its original value, regardless of the fitness level.[46] Further, studies demonstrated a close relation between the magnitude of the post exercise BP decrease and the lactate levels, showing that elevated blood lactate levels after high intensity exercise promotes larger differences between pre- and post-exercise BP values.[47] Such complex dynamic processes thus require the hybrid sensor to operate continuously for capturing these real-time fluctuations throughout the activity. Subjects with different fitness levels (physically active and non-active) were asked to perform a 30 min cycling activity at constant intensity while wearing the device, and their BP and sweat lactate levels were monitored continuously until the exercise was stopped. IP was not used for this portion of the study, as sweat was generated spontaneously from the activity.

Validation data were also recorded before, 10 min into, and after the exercise. As shown in **Figure 4.3.5.1a** (for physically active subject) and **Figure 4.3.5.1b** (for sedentary subject), a considerably higher sweat lactate level and increased BP values were observed during the exercise for the sedentary subject compared to the active subject. Higher HR, BP, and sweat lactate levels are expected during exercise for the non-active subjects due to the elevated catecholamine levels compared to physically active subjects, leading to differences in BP depending on the fitness levels and cardiovascular system.[48]

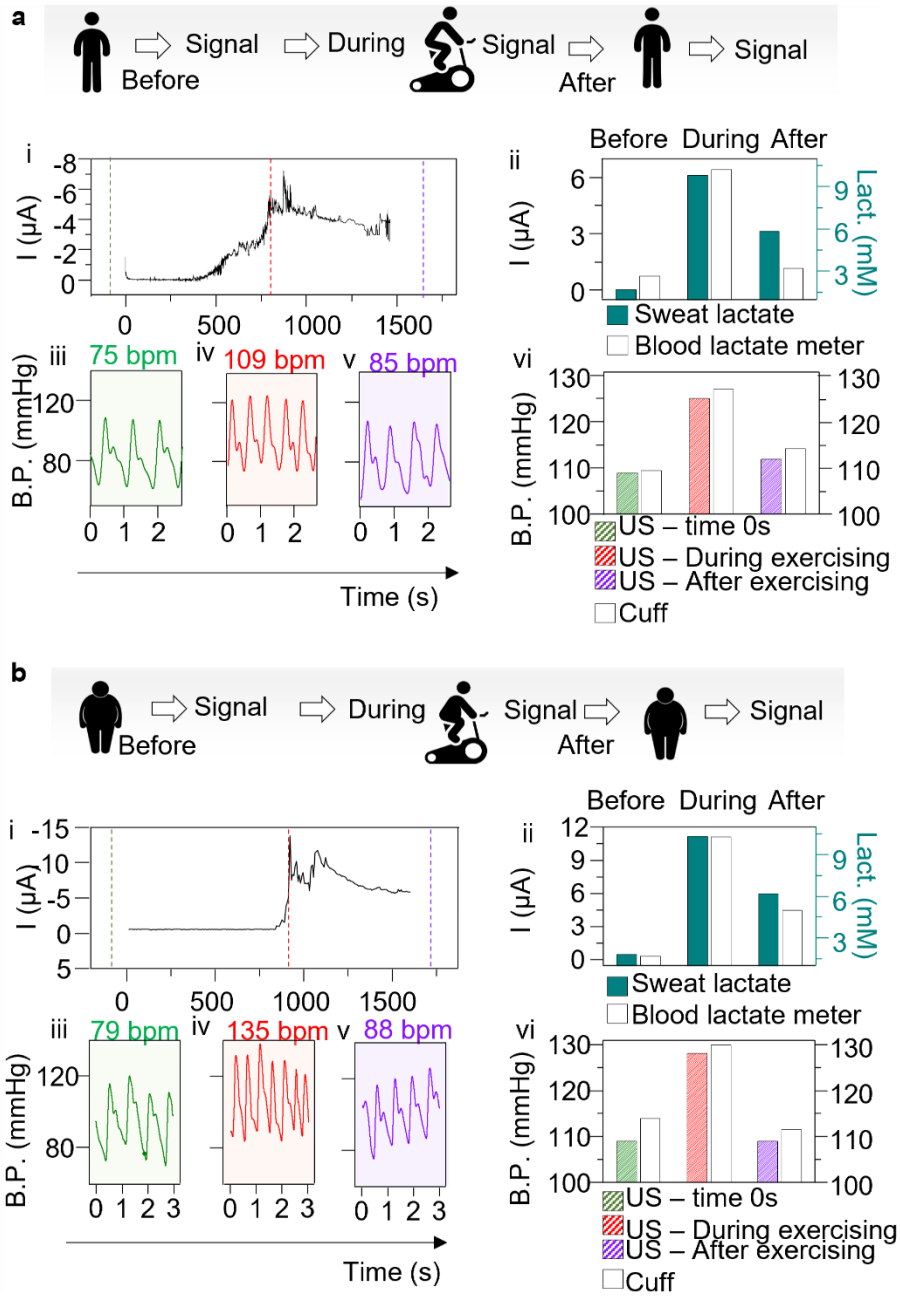

Figure 4.3.5.1.Blood pressure and lactate monitoring.
a, Continuous lactate/BP/HR performance for actively fit volunteer. Continuous signal recording showing sweat lactate profile during stationary biking (i). Bar graphics showing validation using a commercial blood lactate meter (white) and electrochemical sensor readings (green) (ii). BP/HR signal recording before (iii), during (iv), and after (v) stationary biking. Bar graphic comparison between BP signal using a commercial cuff (white) and the ultrasound before (green), during (red), and after (purple) of the exercise performance (vi). **b,** Continuous Lactate/BP/HR performance for sedentary volunteer. Continuous current recording showing sweat lactate profile during stationary biking (i). Bar graphics showing validation using a commercial blood lactate meter (white) and electrochemical sensor readings (green) (ii). BP/HR signal recording before (iii), during (iv), and after (v) stationary biking. Bar graphic comparison between the BP signal of a commercial cuff (white) and the ultrasound before (green), during (red), and after (purple) of the exercise activity (vi).

4.4 Conclusions

The present work reports the first example of a conformal skin-worn device capable of simultaneous monitoring of BP, HR, and multiple biomarkers. This advance has been realized by elegantly addressing major engineering challenges in integrating rigid ultrasound transducers and soft and stretchable electrochemical sensors into a single flexible and stretchable platform while ensuring mechanical performance and avoiding signal crosstalk. The novel SEBS-based solvent-soldering process has greatly simplified the assembly of a sensor with complex structure while ensuring reliable mechanical behavior and continuous epidermal BP and biomarker signal recordings under different chemical and physical stimuli and activities. Signal crosstalk between the acoustic and electrochemical transducers was prevented by spatially separating both components and using solid-state sensing hydrogel layers. Repeated mechanical deformation tests demonstrated outstanding durability and reliability of the electrochemical and acoustic sensors.

Such simultaneous acoustic and electrochemical sensing offers continuous monitoring of the users' physiological status and its response to multiple everyday activities and stimuli. This multimodal wearable platform has thus been shown useful for correlating common daily activities, such as exercise, drinking, and eating, with changes in BP, HR, and biomarker levels. The encouraging results support the possibility of developing more advanced hybrid wearable sensors that involve complex integration of chemical and physical sensors on a single conformal platform for simultaneously monitoring multiple relevant parameters. Such sophisticated integration of reliable and comprehensive epidermal sensors can only be realized with the judicious material selection, optimized structural engineering, and novel high-throughput fabrication process in mind. While displaying attractive features, there are still opportunities for improving the BP/HR/metabolites patch: (i) The integrated patch relies on the iontophoretic pilocarpine stimulation of sweat, which limits the operational use due to the depletion of pilocarpine. Long term sweat stimulating drugs (e.g., carbachol) can be used to extend the operation period. (ii) Full miniaturization of the device through the development of electronics with integrated ultrasound and potentiostatic capabilities, along with signal processing and wireless transmission functionalities. (iii) Conducting extensive validations involving a large number of subjects with various health conditions, including diabetes and cardiovascular patients.

By addressing these opportunities and adding more sensing parameters, we envision a fully integrated multiplexed wearable health monitoring device that offers significant new insights into the health and physiological status of individuals towards the prevention and management of chronic diseases. This device represents an important first step towards multimodal wearable sensors that fuse acoustic and electrochemical sensors towards more comprehensive monitoring of human physiology and a successful telehealth transformation. It thus paves the way into a new field of skin-conformal tools capable of providing important, high-quality, and high-density information regarding the status of human health.

4.5 Acknowledgements

Chapter 4, in full, is a reprint of the material as it appears in J. R. Sempionatto, M. Lin, L. Yin, E. De la paz, K. Pei, T. Sonsa-ard, A. N. de Loyola Silva, A. A. Khorshed, F. Zhang, N. Tostado, S. Xu, J. Wang, An epidermal patch for the simultaneous monitoring of haemodynamic and metabolic biomarkers. *Nature Biomedical Engineering*. **5**, 737–748 (2021).

4.6 References

1. J. Kim, A. S. Campbell, B. E.-F. de Ávila, J. Wang, Wearable biosensors for healthcare monitoring. *Nature Biotechnology*. **37**, 389–406 (2019).

2. Y. Yu, H. Y. Y. Nyein, W. Gao, A. Javey, Flexible Electronics: Flexible Electrochemical Bioelectronics: The Rise of In Situ Bioanalysis (Adv. Mater. 15/2020). *Advanced Materials*. **32**, 2070115 (2020).

3. Y. Khan, A. E. Ostfeld, C. M. Lochner, A. Pierre, A. C. Arias, Monitoring of Vital Signs with Flexible and Wearable Medical Devices. *Advanced Materials*. **28**, 4373–4395 (2016).

4. C. Wang, C. Wang, Z. Huang, S. Xu, Materials and Structures toward Soft Electronics. *Advanced Materials*. **30**, 1801368 (2018).

5. S. P. Lee, G. Ha, D. E. Wright, Y. Ma, E. Sen-Gupta, N. R. Haubrich, P. C. Branche, W. Li, G. L. Huppert, M. Johnson, H. B. Mutlu, K. Li, N. Sheth, J. A. Wright, Y. Huang, M. Mansour, J. A. Rogers, R. Ghaffari, Highly flexible, wearable, and disposable cardiac biosensors for remote and ambulatory monitoring. *npj Digital Medicine*. **1** (2018), doi:10.1038/s41746-017-0009-x.

6. Y.-D. Lee, W.-Y. Chung, Wireless sensor network based wearable smart shirt for ubiquitous health and activity monitoring. *Sensors and Actuators B: Chemical*. **140**, 390–395 (2009).

7. M. K. Yapici, T. Alkhidir, Y. A. Samad, K. Liao, Graphene-clad textile electrodes for electrocardiogram monitoring. *Sensors and Actuators B: Chemical*. **221**, 1469–1474 (2015).

8. N. Luo, W. Dai, C. Li, Z. Zhou, L. Lu, C. C. Y. Poon, S.-C. Chen, Y. Zhang, N. Zhao, Flexible Piezoresistive Sensor Patch Enabling Ultralow Power Cuffless Blood Pressure Measurement. *Advanced Functional Materials*. **26**, 1178–1187 (2015).

9. C. Dagdeviren, Y. Su, P. Joe, R. Yona, Y. Liu, Y.-S. Kim, Y. Huang, A. R. Damadoran, J. Xia, L. W. Martin, Y. Huang, J. A. Rogers, Conformable amplified lead zirconate titanate sensors with enhanced piezoelectric response for cutaneous pressure monitoring. *Nature Communications*. **5** (2014), doi:10.1038/ncomms5496.

10. C. Wang, X. Li, H. Hu, L. Zhang, Z. Huang, M. Lin, Z. Zhang, Z. Yin, B. Huang, H. Gong, S.

Bhaskaran, Y. Gu, M. Makihata, Y. Guo, Y. Lei, Y. Chen, C. Wang, Y. Li, T. Zhang, Z. Chen, Monitoring of the central blood pressure waveform via a conformal ultrasonic device. *Nature Biomedical Engineering*. **2**, 687–695 (2018).

11. A. J. Bandodkar, W. Jia, C. Yardımcı, X. Wang, J. Ramirez, J. Wang, Tattoo-Based Noninvasive Glucose Monitoring: A Proof-of-Concept Study. *Analytical Chemistry*. **87**, 394–398 (2014).

12. H. Lee, C. Song, Y. S. Hong, M. S. Kim, H. R. Cho, T. Kang, K. Shin, S. H. Choi, T. Hyeon, D.-H. Kim, Wearable/disposable sweat-based glucose monitoring device with multistage transdermal drug delivery module. *Science Advances*. **3**, e1601314 (2017).

13. J. Kim, A. S. Campbell, J. Wang, Wearable non-invasive epidermal glucose sensors: A review. *Talanta*. **177**, 163–170 (2018).

14. H. Lee, Y. J. Hong, S. Baik, T. Hyeon, D.-H. Kim, Enzyme-Based Glucose Sensor: From Invasive to Wearable Device. *Advanced Healthcare Materials*. **7**, 1701150 (2018).

15. J. Kim, J. R. Sempionatto, S. Imani, M. C. Hartel, A. Barfidokht, G. Tang, A. S. Campbell, P. P. Mercier, J. Wang, Simultaneous Monitoring of Sweat and Interstitial Fluid Using a Single Wearable Biosensor Platform. *Advanced Science*. **5**, 1800880 (2018).

16. S. Imani, A. J. Bandodkar, A. M. V. Mohan, R. Kumar, S. Yu, J. Wang, P. P. Mercier, A wearable chemical–electrophysiological hybrid biosensing system for real-time health and fitness monitoring. *Nature Communications*. **7** (2016), doi:10.1038/ncomms11650.

17. Y. J. Hong, H. Lee, J. Kim, M. Lee, H. J. Choi, T. Hyeon, D.-H. Kim, Multifunctional Wearable System that Integrates Sweat-Based Sensing and Vital-Sign Monitoring to Estimate Pre-/Post-Exercise Glucose Levels. *Advanced Functional Materials*. **28**, 1805754 (2018).

18. W. Gao, S. Emaminejad, H. Y. Y. Nyein, S. Challa, K. Chen, A. Peck, H. M. Fahad, H. Ota, H. Shiraki, D. Kiriya, D.-H. Lien, G. A. Brooks, R. W. Davis, A. Javey, Fully integrated wearable sensor arrays for multiplexed in situ perspiration analysis. *Nature*. **529**, 509–514 (2016).

19. H. Gomez, J. A. Kellum, Lactate in Sepsis. *JAMA*. **313**, 194 (2015).

20. M. T. Zanella, O. Kohlmann, A. B. Ribeiro, Treatment of Obesity Hypertension and Diabetes Syndrome. *Hypertension*. **38**, 705–708 (2001).

21. B. M. Y. Cheung, C. Li, Diabetes and Hypertension: Is There a Common Metabolic Pathway? *Current Atherosclerosis Reports*. **14**, 160–166 (2012).

22. M. Epstein, J. R. Sowers, Diabetes mellitus and hypertension. *Hypertension*. **19**, 403–18 (1992).

23. P. Deedwania, Hypertension, Dyslipidemia, and Insulin Resistance in Patients With Diabetes Mellitus or the Cardiometabolic Syndrome: Benefits of Vasodilating β-Blockers. *The Journal of Clinical Hypertension*. **13**, 52–59 (2010).

24. J. Yang, Y. Zheng, X. Gou, K. Pu, Z. Chen, Q. Guo, R. Ji, H. Wang, Y. Wang, Y. Zhou, Prevalence of comorbidities in the novel Wuhan coronavirus (COVID-19) infection: a systematic review and meta-analysis. *International Journal of Infectious Diseases*. **0** (2020), doi:10.1016/j.ijid.2020.03.017.

25. J. R. Halliwill, Mechanisms and Clinical Implications of Post-exercise Hypotension in Humans. *Exercise and Sport Sciences Reviews*. **29**, 65–70 (2001).

26. J. R. Carter, S. F. Stream, J. J. Durocher, R. A. Larson, Influence of acute alcohol ingestion on sympathetic neural responses to orthostatic stress in humans. *American Journal of Physiology-Endocrinology and Metabolism*. **300**, E771–E778 (2011).

27. M. Roerecke, J. Kaczorowski, S. W. Tobe, G. Gmel, O. S. M. Hasan, J. Rehm, The effect of a reduction in alcohol consumption on blood pressure: a systematic review and meta-analysis. *The Lancet Public Health*. **2**, e108–e120 (2017).

28. L. Chen, G. Davey Smith, R. M. Harbord, S. J. Lewis, Alcohol Intake and Blood Pressure: A Systematic Review Implementing a Mendelian Randomization Approach. *PLoS Medicine*. **5**, e52 (2008).

29. R. Maheswaran, J. S. Gill, P. Davies, D. G. Beevers, High blood pressure due to alcohol. A rapidly reversible effect. *Hypertension*. **17**, 787–792 (1991).

30. T. Ohira, T. Tanigawa, M. Tabata, H. Imano, A. Kitamura, M. Kiyama, S. Sato, T. Okamura, R. Cui, K. A. Koike, T. Shimamoto, H. Iso, Effects of Habitual Alcohol Intake on Ambulatory Blood Pressure, Heart Rate, and Its Variability Among Japanese Men. *Hypertension*. **53**, 13–19 (2009).

31. A. Hauke, P. Simmers, Y. R. Ojha, B. D. Cameron, R. Ballweg, T. Zhang, N. Twine, M. Brothers, E. Gomez, J. Heikenfeld, Complete validation of a continuous and blood-correlated sweat biosensing device with integrated sweat stimulation. *Lab on a Chip*. **18**, 3750–3759 (2018).

32. E. Monte-Moreno, Non-invasive estimate of blood glucose and blood pressure from a photoplethysmograph by means of machine learning techniques. *Artificial Intelligence in Medicine*. **53**, 127–138 (2011).

33. Y. Çinar, Blood viscosity and blood pressure: role of temperature and hyperglycemia. *American Journal of Hypertension*. **14**, 433–438 (2001).

34. J. Filipovský, P. Ducimetiére, E. Eschwége, J. L. Richard, G. Rosselin, J. R. Claude, The relationship of blood pressure with glucose, insulin, heart rate, free fatty acids and plasma cortisol levels according to degree of obesity in middle-aged men. *Journal of Hypertension*. **14**, 229–235 (1996).

35. J. R. Mort, H. R. Kruse, Timing of Blood Pressure Measurement Related to Caffeine Consumption. *Annals of Pharmacotherapy*. **42**, 105–110 (2008).

36. M-L. Nurminen, L. Niittynen, R. Korpela, H. Vapaatalo, Coffee, caffeine and blood pressure: a critical review. *European Journal of Clinical Nutrition*. **53**, 831–839 (1999).

37. L.-C. Tai, W. Gao, M. Chao, M. Bariya, Q. P. Ngo, Z. Shahpar, H. Y. Y. Nyein, H. Park, J. Sun, Y. Jung, E. Wu, H. M. Fahad, D.-H. Lien, H. Ota, G. Cho, A. Javey, Methylxanthine Drug Monitoring with Wearable Sweat Sensors. *Advanced Materials*. **30**, 1707442 (2018).

38. B. Ciui, A. Martin, R. K. Mishra, T. Nakagawa, T. J. Dawkins, M. Lyu, C. Cristea, R. Sandulescu, J. Wang, Chemical Sensing at the Robot Fingertips: Toward Automated Taste Discrimination in Food Samples. *ACS Sensors*. **3**, 2375–2384 (2018).

39. R. Y. Asano, M. M. Sales, R. A. Browne, J. F. Moraes, H. J. Coelho Júnior, M. R. Moraes, H. G. Simões, Acute effects of physical exercise in type 2 diabetes: A review. *World Journal of Diabetes*. **5**, 659 (2014).

40. D. Klaric, V. Klaric, Alcohol-Induced Coma, Hypothermia and Hypotension. *Journal of Membrane Science & Technology*. **05** (2015), doi:10.4172/2155-9589.1000137.

41. E. Wilson, W. S. Waring, Severe hypotension and hypothermia caused by acute ethanol toxicity. *Emergency Medicine Journal : EMJ*. **24**, e7 (2007).

42. M. Hillbom, P. Saloheimo, S. Juvela, Alcohol Consumption, Blood Pressure, and the Risk of Stroke. *Current Hypertension Reports*. **13**, 208–213 (2011).

43. M. A. Nystoriak, A. Bhatnagar, Cardiovascular Effects and Benefits of Exercise. *Frontiers in Cardiovascular Medicine*. **5** (2018), doi:10.3389/fcvm.2018.00135.

44. R. H. Fagard, Effects of exercise, diet and their combination on blood pressure. *Journal of Human Hypertension*. **19**, S20–S24 (2005).

45. W. Jia, G. Valdés-Ramírez, A. J. Bandodkar, J. R. Windmiller, J. Wang, Epidermal Biofuel Cells: Energy Harvesting from Human Perspiration. *Angewandte Chemie International Edition*. **52**, 7233–7236 (2013).

46. J. R. MacDonald, Potential causes, mechanisms, and implications of post exercise hypotension. *Journal of Human Hypertension*. **16**, 225–236 (2002).

47. A. Crisafulli, F. Tocco, G. Pittau, L. Lorrai, C. Porru, E. Salis, P. Pagliaro, F. Melis, A. Concu, Effect of differences in post-exercise lactate accumulation in athletes' haemodynamics. *Applied Physiology, Nutrition, and Metabolism*. **31**, 423–431 (2006).

48. P. Kokkinos, Cardiorespiratory Fitness, Exercise, and Blood Pressure. *Hypertension*. **64**, 1160–1164 (2014).

Chapter 5. Summary and future work

5.1 Summary

In this dissertation, some examples of non-invasive glucose monitoring have been demonstrated. The development of non-invasive glucose monitoring devices can potentially enable self-monitoring, point-of-care and avoid the skin-penetration step compared to invasive blood monitoring devices. The principal achievements shown in this dissertation include:

1. The development of a soft wearable microfluidic device that integrated a glucose sensor for extended glucose monitoring and a set of conductive electrodes for the delivery of FDA-approved pilocarpine nitrate for chemical stimulation of sweat on healthy individuals. The device applied 10 min of minimal current to induce the delivery of pilocarpine. The response of the sensor toward glucose changes in the sweat was evaluated during fasting and after food intake. The results displayed by the device showed the sensor was capable of detecting glucose changes before and after food intake.
2. The fabrication of an adhesive patch that included a pair of electrodes for reverser iontophoresis and a three-electrode system for extended glucose monitoring. The results obtained after testing the device on healthy individuals for a period of 8 hrs showed the sensor was capable of keeping its functionality and had no signs of skin irritation. Later the device was tested in diabetic patients, where the sensor detected the increase of glucose concentration in the interstitial fluid throughout 4 hrs.
3. The integration of multiple chemical sensing modalities (glucose, lactate, alcohol and caffeine) alongside a blood pressure sensor. The changes in blood pressure and chemical monitoring were evaluated through different daily activities that included food intake, alcohol intake, caffeine intake, and exercise. The results obtained from different healthy individuals showed that lactate and blood pressure were highly included by performing stationary exercise.

5.2 Future work

The application of non-invasive glucose monitoring devices on a daily basis represents a challenge. For instance, the non-localized detection of glucose as compared to localized glucose detection created a time delay and potential dilution of the glucose concentration measured. Therefore, future work should consider taking into account these potential limitations. In addition, sensing modalities that can take into account the physiological changes in the human body (e.g., temperature and pH) are required to calibrate the glucose sensor's fluctuations due to these physiological variations. Another key factor is the method for assessing the sample, in this dissertation the application of iontophoresis was employed for glucose monitoring. Although this procedure avoided the use of needles or any other skin-penetrating protocol, its extraction and delivery efficiency are dependent on skin permeability and porosity. Therefore, additional modalities that can account for these variations are also the subject of future investigations.